













Universität für Bodenkultur Wien

University of Natural Resources and Life Sciences, Vienna

Reduction and Oxidation dynamics of a fixed bed Chemical Looping combustion reactor, with the usage of ammonia for the reduction

MASTERARBEIT

zur Erlangung des akademischen Grades

Diplom-Ingenieur

im Rahmen des Studiums

Kulturtechnik und Wasserwirtschaft

eingereicht von

Lorenz Untersulzner

Matr. Nr.: 01207527

Department für Materialwissenschaften und Prozesstechnik

Institut für Verfahrens- und Energietechnik

Betreuer:

Univ. Prof. Dipl.-Ing. Dr. techn. Tobias Pröll

Dipl.-Ing. Dr. Florian Zerobin

Wien, Dezember, 2020

Contents

Danksagung

Die folgende Arbeit wurde am Institut für Verfahrens und Energietechnik der Universität für Bodenkultur Wien verfasst. Ein großes Dankeschön geht an den Stellvertretenden Institutsleiter Univ. Prof. Dipl.-Ing. Dr. techn. Tobias Pröll für Koordinierung der Arbeit. Als direkter Ansprechpartner hat er die Arbeit ermöglicht und hatte stets ein offenes Ohr für meine Fragen, welche nicht wenige waren. Ein weiteres Dankeschön geht auch an Dipl. Ing. Dr. Florian Zerobin welche mich die ersten 4 Monate betreut hatte und mir mit hilfreichen Tipps zur Seite stand. Leider beendete ein Berufswechsel unsere Zusammenarbeit.

Meinen Eltern Barbara Weis und Ulrich Untersulzner möchte ich meinen besonderen Dank aussprechen, sie haben mir durch ihre Unterstützung ermöglicht, dort hin zu kommen, wo ich heute stehe. Des Weiteren möchte ich mich bei allen Kommilitonen bedanken, die mich während der Studienzeit begleitet haben. Auch bedanke ich mich bei meinen Geschwistern Johanna und Martha für die Motivation und Unterstützung über die Jahre; sowie allen Freunden und Freundinnen für ihren Beistand und die kreative Freizeitgestaltung.

Abstract

The rising emission of GHG and nitrogen disrupt the natural cycles and bring a variety of problems for humanity. New technologies and ideas are researched to generate and store energy reducing greenhouse gas emissions to encounter these issues. The project Ammonia2HeatStorage tries to combine the Chemical Looping Combustion (CLC) technology and the membrane distillation (MD) technology to find a storage medium for heat by using ammonia as fuel. With this, the supply share of sustainable energy/heat can be potentially increased.

A fixed bed CLC reactor's simulation model allows giving a first impression about the reactor's functionality by loading it with ammonia. The reactor measures 3.6 cm in diameter and 30 cm in length, similar to the pilot plant's geometry at AEE Intec at Gleisdorf/Austria. The reactor uses a copper-based oxygen carrier supported by aluminum oxide. The model uses data from the literature to estimate the reaction kinetics for the solid material. The simulation allows testing with hydrogen and ammonia as fuel as well as the oxidation with air. Furthermore, two different approaches for a cyclic operation are tested.

The influence of the temperature on the reaction dynamics for both fuels and the oxidation reaction is tested. The temperature was varied between 500 and 900°C. The temperature showed little influence on the temperature difference and the heat generated for reduction reactions, as well as on the operation time. Only a small increase for all named parameters was observed. The temperature showed a far more significant influence during oxidation, with a rise of the heat generated from 500°C-900°C by one third. Ammonia did show a good conversion of the OC; yielding only half the heat that hydrogen did for the same experimental setup. The results indicate that ammonia can be used as fuel in fixed-bed CLC for high-temperature heat generation. However, ammonia from MD is a valuable chemical and can be used as fertilizer, reducing conventional production via the Haber-Bosch process, which is very energy demanding. For the cyclic operation, it can be noted that an injection of the fuel and air from opposite sides shows a better result than the injection from the same side.

Kurzfassung

Die steigenden Treibhausgas-Emissionen sowie die Störung des natürlichen Stickstoffkreislaufes führen zu verschiedenen Problemen für die Menschheit. Mit dem Projekt Ammonia2HeatStorage testet die AAE INTEC in Zusammenarbeit mit der BOKU zwei Technologien, die miteinander kombiniert, eine Möglichkeit bieten Ammoniak als chemischen Energieträger zur Hochtemperatur-Wärmeerzeugung und chemischen Wärmespeicherung zu verwenden. Ammoniak soll aus Gärresten der Biogasproduktion oder dem anfallenden Zentratwasser einer Kläranlage mittels Membran Destillation (MD) gewonnen werden. Dieser `grüne´ Ammoniak könnte dazu verwendet werden einen Chemical Looping Combustion (CLC) Reaktor zu laden. Man könnte somit Wärmeenergie über einen längeren Zeitraum ohne Verlust speichern. Dadurch kann man den Versorgungsmix von erneuerbaren Energien und Speichermedien ergänzen.

Der CLC Reaktor wird als Festbett Reaktor (fixed/packed bed reactor PBR) ausgeführt. Um erste Aussagen über die Funktionalität und die Reaktionsdynamiken im Reaktor zu treffen, ist ein Simulationsmodell angefertigt worden. Das Modell erlaubt den Reaktor mit Ammoniak oder Wasserstoff als Brennstoff bzw. Reduktionsmittel und die Oxidation mit Luft zu testen. Das aktive Oxidationsmetall ist Kupfer, welches von Aluminiumoxid gestützt ist. Die kinetischen Daten wurden aus der Literatur entnommen und für das Modell verwendet. Das Modell verwendete ähnliche Geometrien wie die geplante Versuchsanlage bei AEE Intec in Gleisdorf/Österreich, um einen guten Vergleich herzustellen, mit einem Durchmesser von 3.6 cm und einer Länge von 30 cm. Es wurde der Einfluss der Temperatur auf die Reduktionsdynamiken mit Wasserstoff, Ammoniak und die Oxidation mit Luft im Reaktor untersucht. Ammoniak wurde mit Wasserstoff verglichen. Die Simulation wurde auch im zyklischen Betrieb untersucht, dabei wurden zwei verschiedene Szenarien getestet und verglichen.

Die Temperatur wurde zwischen 500°C und 900°C variiert und hatte auf die Reduktionsreaktionen nur einen geringen Einfluss. Dennoch stiegen die Temperatur-differenzen sowie der Energieertrag mit steigender Temperatur, auch die Reaktionszeit wurde verkürzt bei gleichbleibender Umwandlung des Sauerstoffträgers. Bei der Oxidation zeigte die Temperatur einen starken Einfluss, dadurch konnte die produzierte Wärmeenergie zwischen 500 und 900°C um ein Drittel erhöht werden. Der Einfluss der

Temperatur zeigte bei den Experimenten mit Ammoniak Ähnlichkeit mit den Experimenten mit Wasserstoff. Jedoch produzierte Ammoniak im Vergleich zu Wasserstoff nur die Hälfte an Energie und hatte eine deutlich längere Reaktionszeit. Dennoch konnte der Sauerstoffträger vollständig oxidiert werden. Daraus kann man schließen, dass Ammoniak als Treibstoff für einen CLC-Reaktor funktioniert. Die Effizienz ist dennoch deutlich geringer als bei anderen Brennstoffen. Dadurch, dass Ammoniak als Dünger gebraucht wird und die konventionelle Produktion (Haber-Bosch Prozess) extrem energieaufwändig ist, bieten sich andere Brennstoffe besser an. Im zyklischen Betrieb zeigte es sich sehr vorteilhaft Reduktionsgase und Sauerstoff von gegenüberliegenden Seiten einzubringen.

Abbreviations:

GHG	Greenhousegases
RCP	Representative concentration pathways
UNFCCC	United nation framework convention for climate change
IEA	International Energy Agency
WWTP	Waste water treatment plants
CLC	Chemical looping combustion
AEE INTEC	Institute for sustainable technologies
BOKU	University of natural resources and life science
MD	Membrane Technology
OC	Oxygen carrier
MD	Membrane distillation
CLOU	Chemical looping oxygen uncoupling
FBR	Fluidized bed reactor
PBR	Packed bed reactor
atm	Atmospheric pressure
COD	Chemical oxygen demand
BET	Brunauer-emmet-teller
TGA	Termogravimetric analysis

Symbols:

ΔT	temperature difference	K
ΔH_r	difference of the reaction enthalpie	J
H_r	reaction enthalpy	J
cp	heat capacity	J/kgK
X_s	degree of oxidation	-
dx	length increment	m
d	diameter	m
L	length	m
Dax	axial dispersion coefficient	m^2/sec

Lax	axial dispersion heat conductivity	m^2/sec
eps	bed void fraction	-
$n_{mol,tot,in,r}$	molar flow in reduction	mol/s
$n_{mol,tot,in,o}$	molar flow in reduction	mol/s
p	pressure	Pa
ρ	density	-
dt	time steps	s
S_0	enthropie	J/K
R	ideal gas constant	J/Kmol
r_g	layer thickness	m
m	mass	kg
R_0	oxygen transport capacity	-
b	stoichiometric factor in the reduction reaction of metal oxide	mol_{MeO}/mol_{gas}
k_0	reaction constant	$mol^{1-n}\ m^{3n-2}\ s^{-1}$
E	activation energy	J/mol
c	concentration	mol/m^3
V	volumeflow	m^3/s
t	time	s
A	area	m^2
T	temperature	°C
k_{fwd}	forward reaction rate constant	-
Q	heat	J
P	heat generated	W

Indices

s	solids
g	gas
0	initial state
molar	molar
tot	total

red	reduction
ox	oxidation
oc	oxygen carrier

1.Introduction

1.1. Climate change and CO2 correlation

Due to the modernization of societies and economic growth, climate change is a problem to be recognized. The high and steady growth of Greenhouse gases (GHG) released by the combustion of fossil fuels, agriculture and industry cause a rise in GHGs in the atmosphere, leading to temperature and sea-level rise as well as extreme weather phenomena. CO_2 is the primary source of GHG emissions, globally caused mainly by energy and heat production (25 % in 2010), industry (21% in 2010) and transportation (14 % in 2010). Approximatly 95% of emissions derive from fossil fuel combustion. Fig. 1.1 shows CO_2 concentration from 1960 to 2020, which are measured on Mount Maunaloa by the Global Monitoring Laboratory, in black the trendline in red the measured data. [1,2,3]

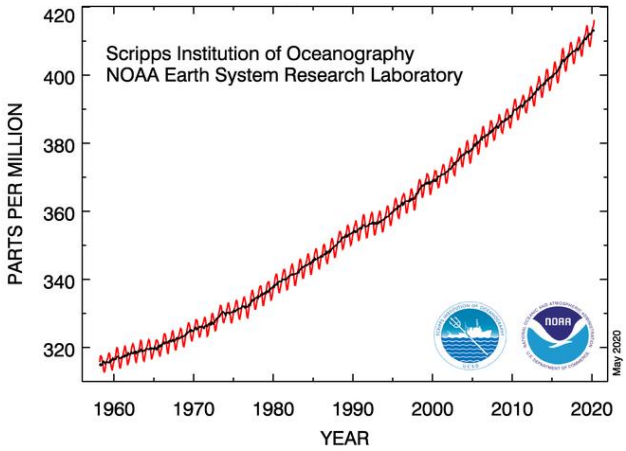

Figure 1.1: Atmospheric CO_2 Concentration on Mount Mauna Loa [4]

There is a steady rise to be observed; the concentration reached 408.54 parts per million in 2019 and is still rising. In the last 800.000 years, concentrations never exceeded 300 ppm. CO_2 has been proven to be a relevant greenhouse gas causing the greenhouse effect to grow stronger. [1,4,5]

The greenhouse effect is a natural phenomenon which provides earth with relatively mild and stable temperatures. The GHG's trap longwave radiation, i.e. infrared light, in the atmosphere so the energy cannot dissipate back into space. However, the rise of GHG's

lead to a rise in the global mean temperature. Different phenomena are related to this, e.g. shrinking of glaciers, a rise in sea levels and of the Ocean Temperature. [1]

The Climate Report 2014 estimates different scenarios for the future through climate models that are calibrated with data from the past. These are based on CO_2 equivalent concentration, which is the sum of all GHGs and mainly encompass CO_2, (76 % in 2010), N_2O, CH_4 and F-gases. According to measured data, in 2011 430 ppm CO_2-eq were estimated, taking into account all relevant GHGs. [1]

The main anthropogenic GHG emission parameters for model calibration are population size, economic activity, lifestyle, energy use, land use patterns, technology and climate policy. Four Representative Concentration Pathways (RCP) show different scenarios for the future. The RCP 2.6 is a stringent mitigation scenario, RCP 4.5 and 6.0 are intermediate scenarios, and RCP 8.5 is a scenario with little to no actions taken. Fig. 1.2 shows the prediction for the CO_2-eq concentration of the models, and Fig. 1.3 shows the impact on the temperature and precipitation on a global scale. [1,3]

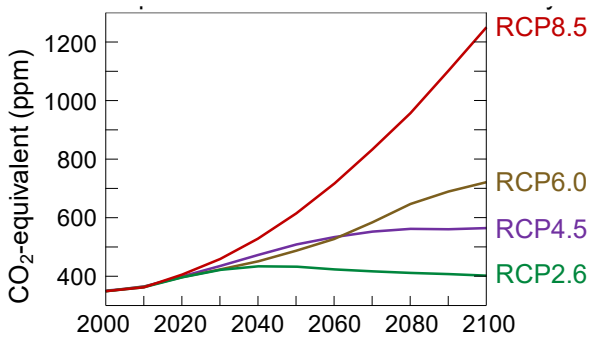

Figure 1.2 : IPCC Representative Concentration Pathways prediction of CO2-eq for the future [4]

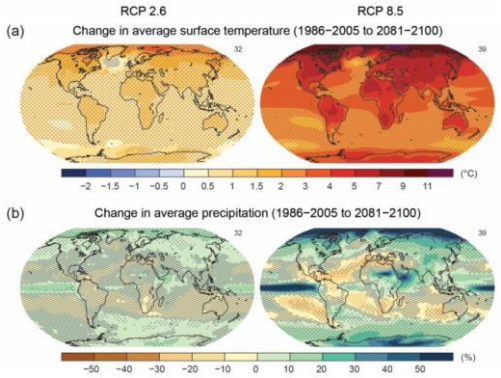

Figure 1.3 : Temperature and Irrigation predictions for RCP 2.6 and 8.5 [6]

Fig.1.3 exemplifies RCP 2.6 and RCP 8.5 and compares the period between 1986 and 2005 with predictions for 2081 to 2100. RCP 2.6 shows a scenario where immediate and radical actions to reduce emissions are taken; RCP 8.5 depicts a scenario of little to no action to achieve this. While there are only moderate changes in the RCP 2.6 scenario, RCP 8.5 predicts temperature differences of up to nearly 9°C and significant changes in the precipitation patterns. These predictions rely upon observations of the past years and are most likely linked to climate change. Which can cause problems, such as a global

temperature rise, warming oceans, shrinking ice sheets, decreased snow cover, sea-level rise as well as an increase in extreme weather events like hurricanes and droughts, leading to major problems for humanity. [1,3,7]

In 2015 the United Nation Framework Convention for Climate Change (UNFCCC) negotiated what is now known as the Paris Agreement, in order to mitigate climate change and to accelerate and intensify the actions and investments needed for a sustainable low carbon emission future. This agreement introduced emission standards so as to achieve certain climate goals, and it has become now of global interest to find new ways to produce power with fewer emissions. [8,9]

The International Energy Agency (IEA) works with governments and industry to create a sustainable energy future. The agency addresses a variety of topics to reduce CO_2 emissions by finding sustainable alternatives, enhancing new technologies and many more. The idea is to create and find alternatives in energy and heat production for a future with less emissions. [10]

1.2. The Nitrogen Cycle

Di-Nitrogen gas (N_2) makes ~79% of the air and is very stable, due to its triple bonding. Consequently, nitrogen has never been a major concern in terms of sustainability. However, led energy-, food production and transportation for humanity to an increase in reactive nitrogen in the environment and therefore to a significant disruption of the natural nitrogen cycle. Reactive nitrogen refers to all other forms of nitrogen except N_2, including oxidized forms (NO, NO_2, N_2O) and reduced forms (NH_3, NH_4). Reactive nitrogen can undergo all different forms and affect all stages of the nitrogen cycle. Reactive nitrogen in the soil can form gases and disturb the atmosphere and vice versa causing various damages in the environment. The primary sources of reactive nitrogen are according to the report `Nitrogen pollution and the European environment` [11, 12, 13]

- **Industrial fixation through the Haber Bosch Process**

  This process produces ammonia by 'fixing' di-nitrogen from the air. It is the primary source for synthetic fertilizers and the leading source for anthropogenic reactive nitrogen, fixing 120 million tons of nitrogen per year in ammonia (NH_3).
- **Combustion of fossil fuels**

  The combustion of fossil fuels releases up to 25 million tons of nitrogen oxides in the atmosphere per year.
- **Fixation due to leguminous crops**

  Legumes fix reactive nitrogen and rise so the productivity of crop fields (40 million tons per year). [11]

Of all industrial sectors, agriculture uses the most nitrogen, either by fixation through legumes or the synthetic fertilizer produced from ammonia won via the Haber-Bosch process. Even though society benefits from it, a lot of the reactive nitrogen is released back into nature through the manure of livestock or human excrements and the combustion of fossil fuels. Additionally, part of the fertilizer leaks into the groundwater and open water due to excessive use. Overloads of reactive nitrogen in water cause a loss in biodiversity and lead to eutrophication. As they form nitrite NO_2 and nitrate NO_3, they also pollute the drinking water by acidification. But not only the water bodies are affected, reactive nitrogen also pollutes the atmosphere, since dinitrogen oxide (N_2O) acts as a very reactive GHG and NO_x molecules attack the ozone layer. It is now a major concern to limit reactive nitrogen from leaking into nature. [11, 12, 13]

Wastewater treatment plants (WWTP) mainly purify reduced nitrogen in order to diminish reactive nitrogen in the environment, transforming it into N_2. Nevertheless, remain high concentration of ammonia in the sewage sludge as well as in the residues of biogas production. This high concentration of ammonia/ammonium lead to long purification time, and costs since the biological treatment request high energy, especially in winter months. The production of 'green ammonia' out of residues of biogas production and centrate water helps reducing purification costs of the wastewater. Moreover, allows it to gain ammonia which doesn´t contribute to further CO_2 emissions, as it is the case for the conventional production and can be used as fertilizer. The reasons why ammonia gains also interest as fuel is explained Section 2.5. [13]

1.2.1. Ammonia 2 heat storage

This work started as a part of project Ammonia2HeatStorage. The institute for sustainable technologies (AEE INTEC) launched this project in cooperation with the University of Natural Resources and Life Sciences, Vienna (BOKU). Since most renewable energy sources are of intermittent nature, storage technologies experience a rise of interest. These storage technologies request high flexibility, a compact design and high energy storage capacity requiring a small volume. These storage mediums shall enlarge the sustainable energy/heat sources and their consistent supply. The idea arose to combine two technologies, the chemical looping combustion (CLC) and membrane distillation (MD), for sustainable heat storage. CLC evolved rapidly in the last two decades and allows for storing energy chemically over long periods without any losses. Compared to other storage technologies, it reaches a high energy density of around 500 kWh/m³. [14, 15,16,]

The operating reactors up to now get loaded using carbonaceous fuels. Within this project, ammonia shall replace conventional fuels and be investigated. The ammonia is extracted via membrane distillation out of centrate water and biogas residues to create an overall sustainable idea. Experiments with the membrane distillation showed already satisfying results. In the course of this project a mathematical simulation model of a fixed bed CLC reactor to explore operation conditions and reaction dynamics was made. This work used this simulation and experimented with ammonia and hydrogen for comparison as fuel. [14,15,16,17]

1.3. Chemical Looping Combustion (CLC)

Chemical looping combustion is a technology, which gained attention in the last two decades. Due to the CO_2 restriction plans, CLC offers a power/heat source with no further CO_2 separation because the flue-gas consists ideally only of H_2O and CO_2. The flue gas is maintained unmixed in the combustion process. This makes it effortless to capture and store the CO_2, to the difference to conventional combustion units, where sophisticated gas separation is necessary. Oxygen carrier (OC) based on metal oxides, e.g., iron (Fe), nickel (Ni), manganese, cobalt (Co), or copper (Cu), are used to react with the oxygen from the air and be reduced afterward with fuel. In this way, the flue-gas remains unmixed, hence

classifying it as **unmixed combustion**.[18] Fig. 1.4 shows the basic principle of a CLC-reactor. It consists of two reactor modules, distinguished by the inlet gas, in air-reactor and fuel-reactor. In the air-reactor reduced forms of the OC are oxidized in an exothermic reaction with air (compounds: N_2, O_2, Ar). The oxidized forms are reduced in the fuel reactor, using biogas (CH_4) or other fuels (synthetic gas, solid coal). The energy-balance depends on the OC, temperature and pressure of the reactor. The reduced OC can be re-oxidized in the air reactor completing a loop, from which the processes´ name derives. Over the years different approaches have been developed and tested; some are detailed in section 2.1. [17,19,20,21]

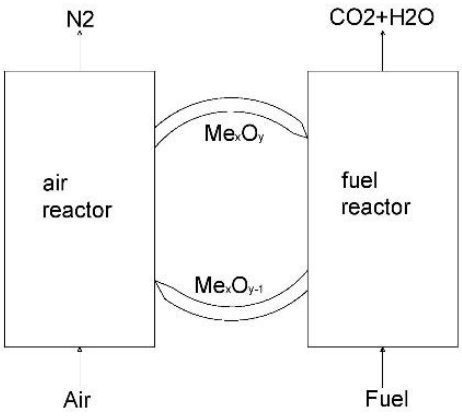

Figure 1.4 : CLC combustion basic principle [22]

In this paper, the CO_2 fixation plays not a crucial role as there is no CO_2 in the exhaust gas. Instead, the fuels Ammonia (NH_3) and Hydrogen (H_2) are tested in the simulation. But because CLC was initially invented as such, it is necessary to explain.

1.4. Research Question

This thesis started as a part of the project Ammonia2HeatStorage. It presents a transient mathematical simulation, available at the institute and adjusted and used for this thesis, of a fixed bed CLC reactor. The model allows modifications of various entry parameters. The oxygen carrier (OC) kinetics described in Garcia Labiano 2004 [23] and Abad 2007 [24] are used for the experiments. This model allows testing and optimizing the operating conditions of a reactor. It also predicts the heat development as well as the breakthrough curve of the gas, taking into account reaction enthalpies and axial diffusion of the gas and heat. Point of observations are:

- The temperature development
- Degree of oxidation of the oxygen carrier
- Conversion of the fuel
- Time of operation
- Heat generated

Central questions for this thesis are:

The influence of the temperature on the model performance

Experiments with H_2 as fuel and air as oxidation agents are conducted to gain information about the model's accuracy. The experiments show the dynamics of the reaction with a copper-based OC in a fixed bed CLC reactor. For the single operation, an adiabatic system is assumed. The operating temperature is varied at 500°C, 600°C, 700°C, 800°C and 900°C. How does the temperature influence the dynamics in the reactor?

The fuel behavior of Ammonia (NH_3)

Ammonia gained importance as a sustainable fuel in the last decade. The Project Ammonia2HeatStorage created the idea to win 'green ammonia' (in a sustainable way) out of wastewater and biogas residues via membrane technology (MD). This ammonia could load the CLC reactor and store heat over long periods. The membrane distillation showed promising results in experiments conducted prior to this work [15]. The high temperatures in

a CLC- reactor (> 500°C), lead to the prediction that ammonia disintegrates immediately to its main constituents at atmospheric pressure as follows: [25]

$2NH_3 \text{ ---> } N_2 + 3H_2$ $\Delta H_r^{700°C} = 101.00$ kJ/mol Eq : 1.1

As shown in Eq. 1.1 H_2 is formed in a 3:2 ratio and can be used as fuel to reduce the oxygen carrier of a CLC-reactor. H_2 has shown good reducing properties forming H_2O and is already tested abundantly as fuel for CLC. Since the nitrogen of the ammonia forms N_2, the flue gas should not have any environmental impact; on the contrary, can it diminish ammonia loads in wastewater. Does the energy output stay high enough since ammonia decomposes endothermically? No test with ammonia as a fuel for CLC are made so far, but the simulation allows a comparison with H_2. How does the temperature influence the reaction dynamics?

Cyclic operation

To better understand the system and gain more profound knowledge about the fixed bed reactor's dynamic behavior, cyclic experiments are conducted using the mathematical model. The system operates alternating a reduction and oxidation process for 10 continuous cycles, giving information about an uninterrupted operating system. A continuous heat removal keeps the reactor almost isothermal. After each reaction, the reactor is purged with N_2. Two scenarios are compared:

- Scenario 1: Injection of fuel/air from the same side
- Scenario 2: Injection of fuel/air from opposite sides

Is there a difference noted in the degree of oxidation? Do the different approaches influence heat generation?

2. Literature review

The following chapter explains the evolution of CLC technology in more detail. Even though this thesis experiments with a fixed bed reactor also the fluidized bed reactors are introduced briefly. The innovation in this work is the usage of ammonia as fuel. Therefore, the chemical ammonia is explained in detail as well as the OC used for the simulation.

2.1. Chemical Looping Combustion

Lewis and Gilliland were the first to introduce the technology in 1954 as a means to produce a pure CO_2 stream. However, since the technology was not very useful for industry and CO_2 had no market, the research of this technology stopped there. Due to a necessary effort to reduce CO_2 emissions in 1987, Ishida [26] investigated an unmixed combustion process which they named chemical looping combustion. During the following years, research was limited until it was proposed as a combustion option for efficient CO_2 capture in 1994. Since then, it has gained more and more importance and now, CLC provides a promising technology to reduce the economic costs of CO_2 capture. Different cycles developed over the years but two main aims have been dominating its research: combustion and H_2 production. As for this work, only the combustion is relevant, a brief differentiation of the current combustion technologies will follow below. [19, 22, 27]

The aggregate state of the fuel mainly serves to distinguish the variants of the CLC process. Initially, CLC discussed the combustion of gaseous fuels. Nevertheless, solid fuels' combustion started gaining interest because of the lower costs and their abundant availability. In the beginning, mainly, coal was used in experiments. Nowadays, the interests have shifted towards biomass as a negative emission technology if combined with energy-efficient CO_2 capture and storage. In 2012, the Chalmers University of Technology in Sweden started experimenting with liquid fuels such as kerosene or refinery oil. However, these technologies are still at the very beginning of their development and will therefore not be mentioned further. [27, 28]

The CLC-reactors can be categorized by the type of fuels as follows: [19,29]

- **Gaseous fuel combustion**

CLC describes gaseous fuel combustion, where the fuel, e.g., natural gas, synthetic gas, reacts directly with the oxygen-carrier. The most prominent gaseous fuels are hydrogen (H_2), methane (CH_4), carbon monoxide (CO), and gas mixtures of the named.

- **Solid fuel combustion**

Syngas-CLC: A combustion of solid fuel with the previous gasification. This means that solid fuels are first gasified to produce syngas, which then operates with the OC. It requires pure oxygen for the gasification and can be described as indirect solid fuel combustion.

In-situ gasification CLC (iG-CLC): The iG-CLC describes a process where the OC reacts with the gasification product of solid fuel (e.g., coal). The gasification happens directly in the reactor itself.

CLOU: In this process, the OC first releases gaseous oxygen, which, in a second step, reacts with the fuel in a similar to conventional combustion process within the fuel reactor. The OCs need particular characteristics, as they have to react with oxygen in the air reactor and then release it in the fuel reactor. The OC needs a suitable equilibrium of partial pressure of the gas phase. [19, 30]

The bed regime inside the reactor can further categorize the CLC plants. Up to now, the majority of the existing CLC plants worldwide use two interconnected reactors with a **fluidized bed** regime. This fluidized-bed circulates between the reactor at high temperatures (< 900°C), melting the OC. In the first reactor, called fuel reactor, the fuel (e.g., CH_4) reduces the metal oxides and absorbs the oxygen, whereas the OC is burnt, oxidized, in the air reactor, as is shown in the Eq. 2.1 and Eq. 2.2. These reactor types are favorable for large-scale powerplants and were first introduced as the technology of circulating fluidized bed systems. Due to its usage in other fields, such as solid fuel combustion, this a well-established technology. The CLC-powerplants producing more than 10 kWh are listed in table 2.1:[19]

Table 2.1: List of operating CLC units over 10kWth (state: 2011) [19]

Location	Unit size [kW_{th}]	Configuration	Fuel	Oxygen-carrier	Operation time [hours]
Gaseous fuels					
Chalmers University of Technology *Sweden*	10	Interconnected CFB[a]-BFB[b]	n.g.[d]	NiO,Fe_2O_3	1350
Institute of Carboquimica, ICB-CSIC *Spain*	10	Interconnected BFB-BFB	CH_4	CuO	200
IFP-Total, *France*	10	Interconnected BFB-BFB-BFB	CH_4	NiO	n.a[c]
Xi'an Jiaotong *University of China*	10	Interconnected pressurized CFB-BFB	Coke oven gas	Fe_2O_3/CuO	15
ALSTOM Power Boilers *France*	15	Interconnected CFB-BFB	n.g.	NiO	100
Korean Institute of Energy Research *Korea*	50	Interconnected CFB-BFB	CH_4,CO, H_2	NiO, CoO	28 /300
Technical University of Vienna *Austria*	120 CLC 140 CLR	DCFB	CH_4, CO, H_2	NiO, ilmenite	>90 /20
Solid fuels					
Chamers University of Technology *Sweden*	10	Interconnected CFB-BFB	Coal, petcoke	Ilmenite	90
Southeast University *China*	10	CFB- spouted bed	Coal, Biomass	NiO, Fe_2O_3	130
Ohio State University *USA*	25	Interconnected Moving bed Entrained bed	Coal	Fe_2O_3	n.a
ALSTOM Windsor, *USA*	65	Interconnected CFB-CFB	Coal	$CaSO_4$	n.a
Darmstadt University of Technology *Germany*	1 MW_{th}	Interconnected CFB-CFB	Coal	Ilmenite	operational 2011
ALSTOM Windsor *USA*	3MW_{th}	Interconnected CFB-CFB	Coal	$CaSO_4$	operational 2011

a) CFB (circulating fluidized bed) b) BFB (bubbling fluidized bed) c) n.a. not available d) n.g. natural gas

The main problems faced with a circulating fluid bed reactor (CFBR) are sintering of the OC, a carbon deposition at high temperatures as well as poor airtightness among fluidized beds. The gas-solid separation between gaseous reaction products and fine OC particles is challenging and the reactor's setup itself is complex. As the machine continually operates at very high temperatures, it would also be inappropriate to frequently start and stop the reactor, which a medium to small scale boiler often requires. Furthermore, the attrition of the OC is formidable due to the harsh operating conditions of the process. [31]

Generally, the chemical reactions in the reactor can be described as follows:

$$(2n + m)\ Me_xO_y + C_nH_{2m} \text{ ---> } (2n + m)\ Me_xO_{y-1} + nCO_2 + mH_2O \qquad \text{Eq : 2.1}$$

$$2Me_xO_{y-1} + O_2 \text{ ---> } 2Me_xO_y \qquad \text{Eq : 2.2}$$

Me_xO_y and Me_xO_{y-1} are the metal oxides, and C_nH_{2m} in Eq. 2.1 provides the fuel which leads to a reduction of the metal with the production of water and carbon dioxide. Eq. 2.2 shows the oxidation in the air reactor, where the reduced metal is oxidized again. [27]

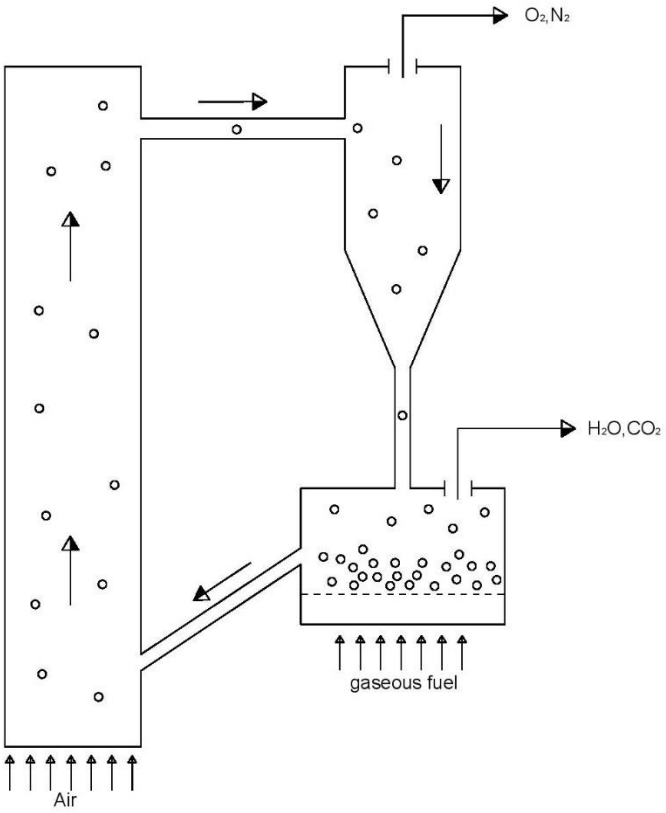

Figure 2.1 : Concept of an interconnected fluidized bed reactor [28]

Figure 2.1 depicts the concept of an interconnected fluidized bed reactor. The metal oxide circulates through the fuel- and air-reactor, creating two flue gas streams at high temperatures. Constituents of the flue gas depend on the fuel used for the reduction process. This thesis models a fixed bed reactor, but the concept remains more or less the same with the difference that the particles remain solid and do not circulate between two reactor batches, as shown in Fig. 2.2.

2.1.1. Fixed (Packed) Bed Reactor

Fixed bed or packed bed (PBR) CLC- reactors have gained more interest in recent years. Some primary studies from Noorman [32] have shown their feasibility, but the community did not draw much attention to PBR systems compared to fluidized bed reactors (FBR). The PBR consists only of one reaction tube, a heater and a pressure shell. Fig. 2.2 shows the concept of a PBR. The CLC exhibits reduction, oxidation, heat removal and reactor purging (to prevent gas mixture) in turns within the same reactor batch. [33]

The reaction is fundamentally dynamic. At operating conditions forms the gas a reaction front and a heat front in the reactor. Thanks to the different velocities, the reaction front is faster than the heat front, storing the heat after the oxidation in the reactor and allowing the generation of a stream with constant temperature and mass flow during the heat removal phase. But to generate a continuous stream of hot air during all processes, two or more reactor modules should work parallel as recommended in Spallina [34]. Where the particles are stationary, and the gas flow switches periodically.[34, 35]

The main advantage of a fixed bed reactor is its compact design, which leads to fewer capital costs. Moreover, it avoids the separation of the gas and the solid phase at the outlet and does not require the circulation of the bed material, which opposes vast technical challenges. The utilization of the OC is higher due to the larger difference in the degree of oxidation between the oxidized and reduced forms, using the OC's full potential. In contrast, in a fluidized bed, the OC is only partly reduced or oxidized. To implement the CLC technology in a conventional power plant, it is necessary to operate on high pressure and temperature. Thanks to the compact design, it is significantly easier to operate on high pressure for fixed bed reactors in comparison to the FBR. [32, 34, 36]

Some problems with PBR include temperature and concentration fluctuations of the flue gas, due to the different processes occurring in the same reactor. It also yields the risk of the gas fingering through the bed not using the full potential of the OC. Furthermore, the inlet gas needs to be at operating temperatures, causing technical challenges to the gas piping system for in- and outlet gas and an energy loss through the gas heating modules. Using an indirect heat exchanger, using the hot flue gas to heat the inlet gas, can decrease this problem. If the inlet gas temperature is not high enough, the OC does not react with

sufficiently fast kinetics. Hamers [37] proposed two different OCs, one highly reactive at the beginning, such as copper and a second one that is suitable to operate on very high temperatures, with better mechanical and chemical stability (e.g. iron-based OC). To make sure that no fuel or by-products may slip through the reactor, a sophisticated control-system needs to be installed at the gas outlet. [35,37,38]

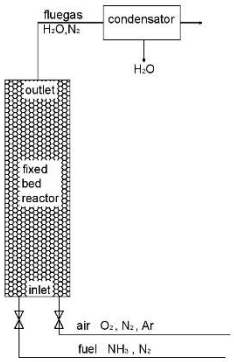

Figure 2.2 : Concept of a fixed bed reactor (PBR)

As we can see in Fig. 2.2, the reactor consists of a tube with two gas inlets, one for the fuel (in this case ammonia) and one for the air. The flue gas ideally consists only of water and N_2, so that the steam can be condensed leaving a pure N_2 outlet gas stream. This work compares the reactivity of a copper-based OC in a single batch reactor module using two different fuels - H_2 and NH_3. The energy output depends highly on the OC. More detailed explanations and properties of the OC are given in the following section.

2.2. The oxygen carrier (OC)

The oxygen carrier is the centerpiece of the chemical looping system. In the past 20 years, research groups put much effort into finding suitable OCs. OCs are based on chemical reactive metal-oxides such as nickel, iron or copper. The main characteristics of an OC can be described as follows: [39]

The **reaction kinetics** which determines the selectivity of the reaction with the fuel and air towards the desired endproducts. A high reactivity for a full conversion of the OC from oxidized to reduced state and vice versa is achieved. The reactivity also determines the amount of bed inventory needed. More extensive bed inventories require bigger plants and

increase the construction costs of the reactor. Moreover, high reaction enthalpies (H_r) are aimed during oxidation and reduction with relatively low oxygen concentrations. [19, 40]

The **oxygen transport capacity (R_0)** describes the maximum amount of oxygen that can be transferred by the OC per cycle. Very low capacities lead to significant circulation rates and contribute to many redox cycles that pose much stress on the OC. (Table 2.3)

Since the reactor modules are operating under high temperatures, they demand a high **mechanical and chemical stability of the OC,** as well as resistance towards fragmentation and attrition and a high melting point. There are small differences in the required characteristics for fixed and fluidized bed reactors.

Moreover, the **costs** and **environmental impact** should be as low as possible, and the OC readily available. If possible the OC material should be further nor toxic or hazardous since the OC needs to be replaced occasionally. The research interest has shifted from synthetic produced OCs towards appropriate materials in natural ores e.g. ilmenite or industrial waste for economic reasons. [41]

Since the chemical looping should operate during long periods, the OC must keep its properties after many redox- cycles, requiring **high cyclic stability.**

These characteristics create the foundation for the evaluation of appropriate OCs**.** The first experimental tests were made with nickel-, iron and cobalt-based OCs by Ishida and coworkers.[26,42] Studies followed with manganese and copper based oxides and $CaSO_4$. Consequently, pure metal oxides can never fulfill the criteria listed above: the harsh operating conditions lead to mechanical weakness, sintering tendency and a decrease of the chemical reactivity after repeated redox cycles due to agglomeration. Heat tolerant inert materials are added to support the metal oxides. The most prominent are Al_2O_3, TiO_2 or yttria-stabilized zirconium, SiO_2, ZrO_2, kaolin, sepiolite, bentonite, or hexa aluminate. Up to now most studies have concentrated on synthetically produced nickel-, copper-, iron-, and manganese-based OCs. In the last decade, ilmenite, a natural ore, gained interest in the field because it showed good OC properties and is cheaply available. [43, 44, 45, 46]

Different synthesizing methods have developed over the past years in order to achieve the best effects, as the preparation method greatly influences the physicochemical properties of the OC. It can provide a better pore structure and give the OC a higher mechanical and

chemical strength by increasing the resistance to attrition as well as diminishing agglomeration problems. Moreover, the chemical reactivity can rise and have a favorable effect on the oxygen transport capacity. Different synthesis methods of OCs have emerged and various approaches are proposed in the available literature. This work uses OCs prepared with impregnation. [29, 44, 45, 46]

In comparison to the OCs used in a fluidized bed, the particles in a fixed bed reactor must be much bigger. Due to the thermal and chemical expansion, there are strong mechanical forces at work and the OCs need to support the mechanical stress posed upon their weight during repeated redox-cycles. Disintegrating leads to large pressure drops and further contributes to a poor overall performance of the reactor. [45, 47]

This work tests a copper-based OC because of the high reaction rates during both reactions. The support material of the OC is aluminum oxide (Al_2O_3). The papers published by Garcia Labiano [23] and Abad [24] describe the physical and kinetic parameters of OCs, which form the parameters for the mathematical model of this work. [19]

Table 2.2 : Reaction enthalpies of different OC with various fuels and oxygen (0°C/atm) [19]

Redox-system	**ΔH_r kJ/mol gas or C**				
	H2	O2	CH4	CO	C
$CaSO_4$ / CaS	-1.6	-480.5	158.6	-42.7	86.9
Co_3O_4 / Co	-14.3	-455.1	107.9	-55.4	61.6
Co_3O_4/CoO	-45.5	-392.7	-16.8	-86.6	-0.8
CoO / Co	-3.9	-475.9	149.5	-45	82.4
CuO / Cu	-85.8	-312.1	-178	-126.9	-81.4
CuO / Cu_2O	-100.4	-282.8	-236.6	-141.6	-110.7
Cu_2O / Cu	-71.1	-341.4	-119.5	-112.3	-52.1
$CuAl_2O_4$ / Cu-Al_2O_3	29.3	-542.2	282.2	-11.8	148.7
$CuAlO_2$ / Cu-Al_2O_3	-47.3	-389.1	-24.1	-88.4	-4.4
$CuAl_2O_4$ / $CuAlO_2$	105.9	-695.4	588.5	64.7	301.9
Fe_2O_3 / Fe_3O_4	-5.8	-472	141.6	-47	78.4
Fe_2O_3 / FeO	38.3	-560.3	318.4	-2.8	166.8
Fe_2O_3-Al_2O_3 / $FeAl_2O_4$	-56.8	-370	-62.3	-98	-23.5
Fe_2TiO_5 / $FeTiO_3$	-14.6	-454.4	106.5	-55.8	60.9
Mn_2O_3 / MnO	-53.3	-377.1	-48	-94.4	-16.4
Mn_2O_3 / Mn_3O_4	-140.4	-202.8	-396.6	-181.6	-190.7
Mn_3O_4 / MnO	-9.7	-464.3	126.3	-50.8	70.8
NiO / Ni	-2.1	-479.4	156.5	-43.3	85.9
$NiAl_2O_4$ / Ni-Al_2O_3	-1.6	-480.4	158.6	-42.8	86.9

2.2.1. The copper-based oxygen carrier

Copper is a reddish, extremely ductile chemical element, naturally found in the free metallic state in nature. It can be a primary mineral in basaltic lavas or located as a reduced form in carbonates, chlorides sulfides or arsenides. Additionally, it is combined in many minerals. It is an excellent conductor of heat and electricity. Its atomic weight is 63.55 g/mol, and its density at 20°C counts 8.96 g/m³. Under atmospheric pressure, the melting point lies at 1,083°C and the boiling point at 2,567 °C. It shows his excellent oxygen carrier properties as it takes the oxygen transport role in mollusks and crustaceans' blood. It is one of the most used metals worldwide, especially by the electrical industry. The conventional way to attain copper is by smelting or leaching. It forms different types of alloys, the most famous probably being bronze. By forming alloys, it combines both metals' properties, leading to a wide variety of usage. [48]

The copper-based oxygen carrier seemed very promising due to high reaction enthalpies during the oxidation and reduction processes for different fuels and its high reactivity. Consequently, it can diminish the energy loss caused by the decomposition of ammonia during the reduction. Furthermore, it is one of the 'cheaper' synthetic materials with an estimated cost of around 3000 €/t OC, compared to nickel and cobalt, and has a lower environmental impact. However, compared to natural ores and iron, it is rather expensive. [31, 39]

Copper has one of the highest oxygen transport capacities compared to other pure metal oxides, such as shown in table 2.3. Depending on the percentages of the support material, these values can change. Lastly, it shows an excellent conversion rate of 100 % with the fuel hydrogen, as stated by Jerndal [50].

The reaction equations in the reactor with H_2 as fuel and O_2 are given as follows with reaction enthalpies given under atmospheric pressure:

For the Reduction:

$CuO + H_2 \rightarrow Cu + H_2O$ $\quad \Delta H_r^{700°C} = -96.99$ kJ/mol Eq : 2.3

For the Oxidation

$Cu + 0.5\ O_2 \rightarrow CuO$ $\quad \Delta H_r^{700°C} = -150.70$ kJ/mol Eq : 2.4

Even though the copper-based oxygen carrier showed high reactivity with all used preparation methods and support materials, only the performance of those prepared by impregnation resulted in satisfying chemical and mechanical stability after multiple redox-cycles. The used support materials are SiO_2, TiO_2, or γ-Al_2O_3. Apart from co-precipitation with Al2O3, other preparations do not achieve the same results, showing a decay of reactivity and mechanical properties after repeated redox-cycles. In combination with Al_2O_3, copper partly forms $CuAl_2O_4$, but this doesn´t further affect the reaction as it reduces at similar rates as CuO. [23,24, 19, 37]

Table 2.3 : Oxygen transport capacity of the pure metal oxides [40]

System	R_0 (-)
NiO/Ni	0.2142
CuO/Cu	0.2011
CuO/Cu_2O	0.1006
Fe_2O_3/FeO	0.1002
Mn_3O_4/MnO	0.0699
Fe_2O_3/Fe_3O_4	0.0334

Some problems with the copper-based OC include the low melting point, which leads to agglomeration, especially in FBRs. Since the achieved temperature difference defines the overall efficiency, the energy output is limited to this circumstance. To raise the resistance of copper-based OCs, they only contain a small part (max. 20%) of reactive metal. Operating temperatures should also not exceed 800°C in the fuel reactor, even though 500 W and 10 kW FBR units are already operating successfully [51] with 15% Cu and y-Al_2O_3 based OC-particles using syngas and methane as fuel. Another point worth mentioning is that CuO decomposes to Cu_2O at high temperatures and low oxygen availability. Therefore parts of O_2 are also seen in the flue gas during reduction reactions, yet these do not limit the reactivity. [23,24 ,19, 37]

2.3. Fuel hydrogen and ammonia NH_3

To reduce CO_2 emissions, fossil fuels need to be replaced by environmentally friendly and sustainable fuels. Hydrogen (H_2) seems a promising substance to achieve this, as it has a high energy density (gross calorific value (GCV) = 141.7 MJ/kg) and is environmentally

compatible. However, it does bring problems with storage and transportation. H_2 has a density at 0°C and atmospheric pressure of 89.87 g/m³ and is 14 times lighter than air. It diffuses faster than any other gas, even though gaseous H_2 has an extremely high heat capacity (cp_{H2} = 14.4 kJ/kgK). The high flammability and the formation of water as the end product make it an outstanding candidate for an alternative fuel. However, it implies complicated safety issues as it is very volatile and has a very low flashpoint. H_2 burns with an invisible flame and presents explosion danger in the presence of air at high concentrations. [25,52,5325,54]

Due to its low volumetric density, it results in rather low energy content compared to other fuels, which further leads to storage problems, given that it's low compressibility prohibits to economically store large amounts. Storage units operate at 200 bar to store 14 g/L of H_2 in gaseous form. Higher density can be achieved in liquid form with a density of 71 g/L but at a temperature of -253°C. This results in storage costs of 1.97 $/kg-$H_2$ for 15 days. [52,55]

Another approach is the indirect storage of hydrogen in chemicals like ammonia (NH_3), methane (CH_4) or methanol (CH_3OH). From these options, NH_3 provides the only carbon-free chemical. In its liquid form, NH_3 stores 108g of hydrogen/L and its storage and transport is far more economical than for H_2 (storage costs for NH_3 are 0.09 $/kg-$H_2$ for 15 days). NH_3 is the most synthesized chemical worldwide. Therefore, the infrastructure for transportation and storage is readily available and well established. It is mainly stored at 10 bar and room temperature or liquefied at -35 °C, with a high energy density (GCV = 22.5 MJ/kg) comparable to that of gasoline. Figure 2.3 compares the storage capacities of liquified NH_3, liquified H_2, and compressed H_2 and also gives the gross heating value at 0°C and atm for the given amount. The density for liquid ammonia is 603 g/L. [52,55,56]

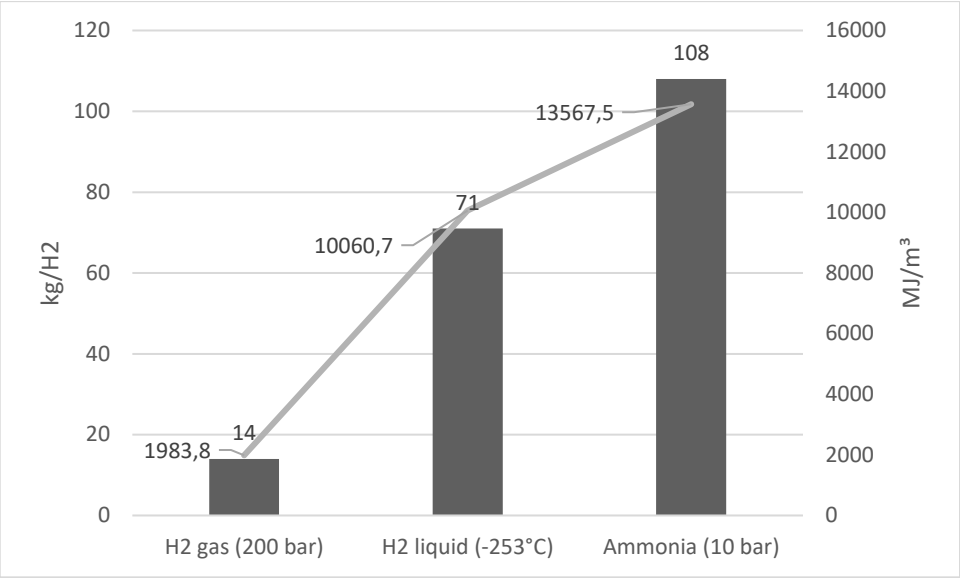

Figure 2.3: Hydrogen Storage capacities (gH_2/L) and gross calorific value MJ/m^3

Furthermore, it can be considered as a non-flammable substance during transportation due to its very low flammability. Ammonia is lighter than air and can dissipate immediately in the atmosphere. Besides, it is easily detected through its characteristic smell. Some problems faced with ammonia as an energy vector are:

- Carbon-free synthesis of ammonia
- Power generation from small to utility-scale size
- Public acceptance through safety regulations and appropriate community engagement
- Economic viability for the integration of technologies and green production of ammonia [52, 53, 57]

Ammonia has a trigonal pyramidal shape, with the nitrogen surrounded by hydrogen atoms and two free electrons attached to it. It is a colorless gas with a penetrating odor and a density of 0.73 kg/m^3 at atmospheric pressure and 25°C. Its boiling point is at -33.55 °C (239.8 K), and its freezing point at -77.65 °C (195.5 K). Because of its low reactivity, the combustion is challenging. But taking into account that a CLC reactor operates at high temperatures, ammonia should decompose to H_2 and N_2 in an endothermic reaction, as the reaction equation shows. [58]

$2NH_3 \dashrightarrow N_2 + 3H_2$ $\Delta H_r^{700°C} = 101.00$ kJ/mol Eq : 2.5

Fig.2.3 shows the ideal gas equilibrium constant of ammonia in dependency to the temperature calculated with the Gibbs free enthalpy for standard pressure. The result shows a 'complete' decomposition to N_2 and H_2 at 250 °C at atmospheric pressure. In literature, 99% decomposition of ammonia at 600 °C is confirmed. [25]

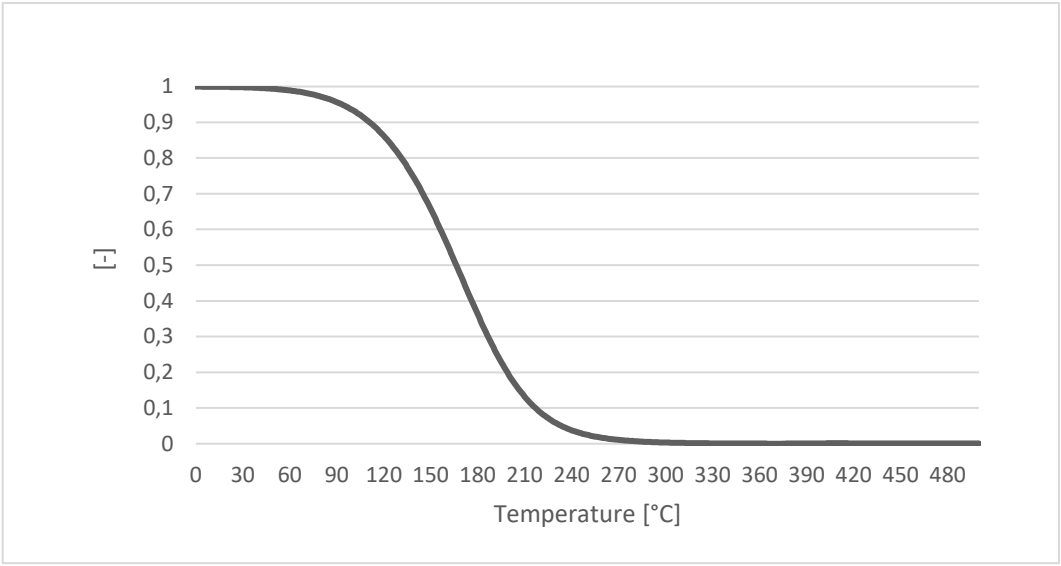

Figure 2.4 : Partial pressure equilibrium constant of ammonia using the Gibbs free enthalpy according to the NASA polynomials.

Despite its toxicity, ammonia seems feasible as a fuel and, hence, the distribution and storage infrastructure already exists. The production and distribution are mature technologies that already produce around 100 million tons of ammonia each year. It is used primarily for the production of fertilizer (80% of total amount of ammonia) but also in the production of polymers, paper, pharmaceutics and energy concepts. [53,58]

Currently, 90 % of ammonia is produced via the Haber Bosch process. This process reacts H_2 and N_2 under high pressure and temperature (400-500 °C and 100-200 bar) using an iron-based catalyst to ammonia. The hydrogen production for ammonia synthesis requests a high amount of energy from fossil fuels. The Haber-Bosch process needs 3-5% of the world's natural gas for H_2 extraction and 1-2 % of the world's energy reserves. This leads to high CO_2 emissions during the whole process, contributing 1.5 % of the global CO_2 emissions annually. Taking this into account, ammonia needs a more sustainable way of production to be considered a sustainable fuel. One idea is its production via the Haber Bosch process using sustainable energy sources to operate. Other methods are in development, with three main approaches reviewed by Li [59]. This work proposes a

synthesizing method to produce ammonia out of the centrate water and biogas residues in a wastewater treatment plant, such as in the course of the project Ammonia2HeatStorage. The next section explains this approach briefly [53, 59, 60, 61]

2.4. From waste to fuel

As explained in the introduction, reactive nitrogen leads to various problems in the environment. The reactive NH_4* Ammonium is a primary product of human excrements and consequently, high concentration of it can be found in wastewater. Biological denitrification is a reliable method for cleansing the water and is currently used in most wastewater treatment plants. This biological treatment needs a specific ratio between the chemical oxygen demand and nitrogen (COD/N). Via two steps, nitrification and denitrification, ammonia is transformed into N_2 and released into the atmosphere. These biological processes have a high energy demand as the best temperatures for bacteria lies at around 20 °C. Therefore, and especially in winter, WWTPs need the energy to heat the water in their pools. In the last decade's biogas production out of sewage sludge in combination with biomass from other sources, e.g. agriculture and food production, help WWTPs generate power for self-sustainment, as it is one of the most crucial energy consumers that are managed by municipalities. [62, 63, 64, 65]

Due to the rising production of biogas, a seemingly environmentally friendly energy source, fermentation residues arise. These residues contain constituents worthy of recycling. Depending on the feed of the biogas production, the residues contain different percentages of constituents. High percentages of N-NH_4, nitrogen in the ammonium form, make it attractive for agricultural use as fertilizer. Law restrictions in the overuse of nitrogen fertilizer has led to the search for different usages. Up to now, advanced residues were refed in the wastewater treatment process, causing high concentrations of nitrogen in the wastewater and purification periods that are too long. This refeed causes high processing costs and graver environmental impact given that the denitrification process emits small amounts of N_2O in the atmosphere, a very reactive GHG with rising importance. *Project En Reeco Treat* tried to gain ammonia through a membrane distillation out of centrate water (i.e. water won by compressing sewage sludge) to reduce wastewater concentrations. [15, 64, 66]

Membrane distillation was initially invented for the desalination or purification of seawater and freshwater; it is an energy-saving alternative to other separation techniques such as reverse osmosis or distillation. The installation consists of a porous, hydrophobe membrane, through which gaseous molecules can defund. The fluid feed is in direct contact with the membrane. Surface tensions prohibit the feed from leaking through and creating a liquid-gaseous interface at the pores. The driving force is a vapor pressure difference between the feed and permeates side. Moreover, it is necessary to have a sufficient temperature difference between both sides. The efficiency depends less on the maximum temperature than on the temperature difference. [15, 67]

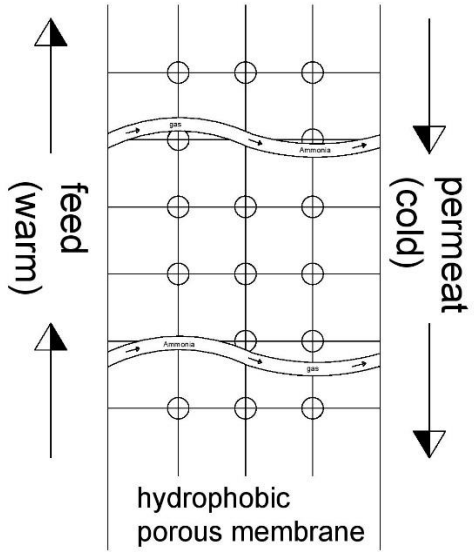

Figure 2.5 Concept of membrane distillation

Figure 2.4 shows the concept behind membrane distillation. *Project en Reeco Treat* extracted ammonia with an energy consumption of 17kWh$_{th}$ per kg NH_4-N with membrane distillation plate modules. The distillation allows a separation rate of 60 %. The ammonia can be used in the CLC process. The report proposes adding sulfuric acid in order to gain the endproduct ammonia sulfate $(NH_4)_2SO_4$, an already valuable endproduct (0.8€/kg) which finds usage as fertilizer or for industrial purposes after reforming. This opens up the question if ammonia is sustainable fuel since 'green ammonia' can reduce the production of conventional ammonia. [15]

3. Methodology

For this thesis, a mathematical model of a reactor available at the institute is the basis of calculation and results discussed. The simulation is implemented in the software Matlab and also performs in the free software Octave Gnu. It predicts the behavior of a CLC fixed bed reactor and gives insight into the gas movement in the reactor. Moreover, it shows the heat development inside the system and the conversion of the OC. The simulation gives the possibility to test ammonia and hydrogen with an oxygen carrier to find the best operating setup, without the need for immediate practical testing. This thesis concentrated tests on a copper-based OC, but to ensure the quality of results, the comparison with practical experiments is necessary. [68]

All models propose an abstraction of real processes and system and can give essential information about:

- Design and scale-up
- Process control
- Optimization
- Mechanistic understanding
- Evaluation and planning of experiments
- Troubleshooting and diagnostics
- Determine quantities that cannot be measured directly
- Simulation instead of costly experiments
- Feasibility studies to determine potential [68]

For this thesis, the major points of interests of the simulation are:

- The duration of the operation (time)
- The degree of oxidation $\mathbf{X_s}$ after a single operation and repeated cyclic operation
- Gas breakthrough curve
- The heat development in the reactor, and the amount of heat generated
- Feasibility of the fuel ammonia $\mathbf{NH_3}$, and comparison with the fuel hydrogen $\mathbf{H_2}$

The calculation is based on a dynamic solution of a 1-dimensional mass and energy balance via partial differential equations. The approach follows an explicit Euler scheme; further explanations give Section 3.5.

3.1. System Parameters

The tubular reactor measures 3.6 cm in diameter and 30 cm in length and is divided into 41 spatial nodes (volume segments) for calculation shown in Fig 3.1. Each volume segment measures a length of 7.317 mm, which corresponds with the length increment **dx** for the calculation. The length compared to the constructed pilot plant is reduced from 6 m to 0.3 m to shorten the calculation time. The volume inside the reactor corresponds to 12.214 l. Is the reactor filled with the oxygen carrier the void fraction remains 40% of the total volume, counting 4.886 l. Fig. 3.1 shows the operational setup based on a pilot plant projected for the practical experiments of the AMMONIA2HEATSTORAGE project, constructed at the TU Graz. The reactor operates at atmospheric pressure. The model takes into account the axial dispersion (D_{ax}), assumed with 0.001 m²/s, of the gas, as well as the axial dispersion (L_{ax}) of the heat conductivity, counting 1 m²/s. The values for the simulation are listed in table 3.1.

Table 3.1: Parameter for the simulation

parameters	**value**	**unit**
diamerter ***d***	3.6	cm
lenght **L**	30	cm
axial dispersion coefficient $\mathbf{D_{ax}}$	0.001	m²/s
axial dispersion heat conductivity λ_{ax}	1	m²/s
bed void fraction ε	40	%
specific heat capacity of solid $\mathbf{cp_s}$	1275	J/kg
molar flow in reduction $\mathbf{n_{mol,tot,in,red}}$	1.15E-4	mol/s
molar flow in oxidation $\mathbf{n_{mol,tot,in,ox}}$	2.738E-4	mol/s
pressure **p**	1	bar
apparent density ρ_s	1800	kg/m³
length increment **dx**	7.317	mm
time steps **dt**	0.02	s

The timesteps **dt** of the calculation is 0.02 seconds. To reduce the result matrix dt for results is increased to 10 seconds for the reduction with hydrogen and the oxidation. The reduction with ammonia took notably longer; therefore, the dt of the results is 60 s.

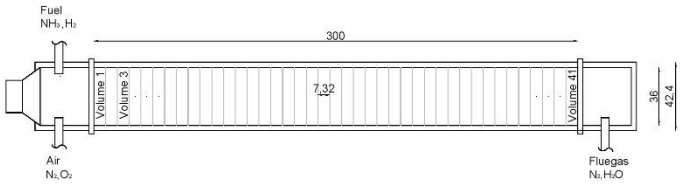

Figure 3.1: Process design of the reactor used in the simulation

3.2. NASA Polynomials

In chemistry and chemical engineering, the knowledge of thermodynamic properties is essential to find a solution for a wide variety of problems. These properties can be calculated with the knowledge of the chemical equilibrium compositions. The Nasa Lewis research centre developed over 50 years ago computer programs that can calculate complex chemical equilibriums and thermodynamic properties. Early versions of the program from Gordon and McBride 1976 [69] achieved wide acceptance and are in continuous updating and revisions since. For this work, relevant, where the molar heat capacity (Cp), entropy (S_0) and enthalpy (H) of different materials (solid phase and gas phase in the system). These functions can be expressed as a function of the temperature, in the form of polynomials with 5 and 6 coefficients, respectively. The constants are already available for a vast number of materials in the gaseous, liquid or solid phase. The species contain two sets of coefficients, one for the temperatures from 200-1000 K and the other

from 1000-5000 K. These coefficients are only correct for isobaric conditions. The heat capacity is calculated as follows in Eq. 3.1. [70]

$$\frac{Cp(T)}{R} = a_1 + a_2 \cdot T + a_3 \cdot T + a_4 \cdot T + a_5 \cdot T \qquad \text{Eq : 3.1}$$

The enthalpy is calculated as follows in eq. 3.2:

$$\frac{H*(T)}{R \cdot T} = a_1 + \frac{a_2}{2} \cdot T + \frac{a_3}{3} \cdot T^2 + \frac{a_4}{4} \cdot T^3 \cdot \frac{a_5}{5} \cdot T^4 + \frac{a_6}{T} \qquad \text{Eq : 3.2}$$

And the Entropie after eq. 3.3:

$$\frac{S_0(T)}{R} = a_1 \cdot lnT + a_2 \cdot T + \frac{a_3}{2} \cdot T^2 + \frac{a_4}{3} \cdot T^3 + \frac{a_5}{4} \cdot T^4 + a_7 \qquad \text{Eq : 3.3}$$

3.3. Cu/CuO physical and kinetic properties

First material related studies of a copper-based OC were made in 2004 by F.Garcia-Labiano[23] and Abad et al. 2007[24], where the aim was to obtain the kinetics to describe the redox reaction for a CLC reactor with fluidized bed using CH_4, H_2 and CO_2 for reduction and air (O_2) for the oxidation. This work uses the OC kinetics obtained from the named study. Aldrich Chemical Co. produced the particles by impregnation, with 10 % wt content of copper supported by aluminum oxide Al_2O_3.

Table 3.2: Physical properties by Abad et al. 2007 [24]

		Cu10Al
CuO	%	10
Al_2O_3	%	90
ρ_s	kg/m³	1800
ρ_{molar} Cu	mol/m³	140,252
ρ_{molar}CuO	mol/m³	80,402
r_g Cu	m	2.30E-10
r_g CuO	m	4.00E-10
porosity	%	57
$R_{0,lim}$	%	2
specific surface area BET	m² / g	41.3

Tests of Labiano showed that the active surface coincides with the material's specific surface area, concluding that the active material is covering the inert material fully with a thin layer also inside the pores. Labiano obtained the specific surface area through the Brunauer-Emmet-Teller (BET) method, measured by the physisorption of N_2. The

thermogravimetric analysis (TGA) determines the oxidation and reaction kinetics of the OC. The exact setup of the TGA is explained further in Labiano[23]. The OC material gets crushed, the OC gets heated up (m_{oc} 15mg) and is oxidized and reduced in terms. The Test showed for all tested fuels (CH_4, CO and H_2) and air at 1073 K (800°C) excellent rapid conversion rates of the OC.

The OC has a plate-like geometry with a particle size of 0.17 mm. The physical properties are listed in table 5. ρ describes the material's apparent density, while ρ_{molar} the molar density is. ρ_{molar} depends on the state of oxidation of the OC. R_{oc} describes the oxygen transport capacity and is calculated as follows:

$$R_{oc} = \frac{m_{Ox} - m_{Red}}{m_{Ox}} \qquad \text{Eq : 3.4}$$

Where m_{ox} describes the oxidized molar mass and m_{red} the reduced molar mass. The variable r_g describes the layer thickness. The molar density and layer thickness are changing during a redox cycle according to the mass transfer of oxygen using the shrinking core model. The degree of oxidation for reduction ($X_{s,r}$) and oxidation ($X_{s,o}$) calculates according to the following eq 3.5 and 3.6.

$$X_{s,r} = \frac{m_{ox} - m_{red}}{m_{ox} \cdot R_{oc}} \qquad \text{Eq : 3.5}$$

$$X_{s,o} = 1 - X_{s,r} \qquad \text{Eq : 3.6}$$

The change of the degree of oxidation of the OC in time follows eq.3.7

$$\frac{dX_r}{dt} = \frac{b \cdot k \cdot C^n}{\rho_{mol} \cdot L} \qquad \text{Eq : 3.7}$$

The kinetic constant follows an Arrhenius type dependency with temperature.

$$k = k_0 \cdot e^{-\frac{E}{R \cdot T}} \qquad \text{Eq : 3.8}$$

[24, 23]

The supporting inert material is alumina oxide (Al_2O_3); only 10 % of the weight content of the OC remains active metal-oxide, as shown in table 3.2. Alumina has a high melting point of 2,072 °C at atmospheric pressure. The porosity of the OC particle is 57 %. [23,24, 37]

Table 3.3 : Reduction oxidation kinetic properties [23,24]

$CU_{10}AL$		H_2	O_2
K_0	$mol^{(1-n)} \cdot m^{(3n-2)} \cdot s^{(-1)}$	1.00E-04	4.70E-06
E	kJ/mol	33	15
N		0.6	1

The kinetic properties gathered from Abad and Labiano assume uniform size OC. k_0 describes the preexponential factor of the chemical rate constant, E the activation energy and the reaction Order is given by n. [23,24,22]

3.4. The core of the simulation model

The following chapter shows the core of the simulation available at the institute. The following chapter describes the mass balance and energy balance with the corresponding boundary conditions for inlet and outlet.

Table 3.4: Variables used to create the mathematical model

Figure	Description
V	Volume flow
C	Concentration
A	Area
D_{ax}	Axial diffusion
t	Time
x	Length
Λ_{ax}	Axial dispersion of heat conductivity
T	Temperature
C_g	Heat capacity gas
C_s	Heat capacity solids
r	Reaction constant

For the Mass balance:

The calculation is based on a partial differential equation approach for a dynamic spatial problem description. Using a discretization poses a solution to the problem by

implementing the finite difference method. It uses an explicit integration algorithm to solve. The problem can be described according to Fig. 3.2

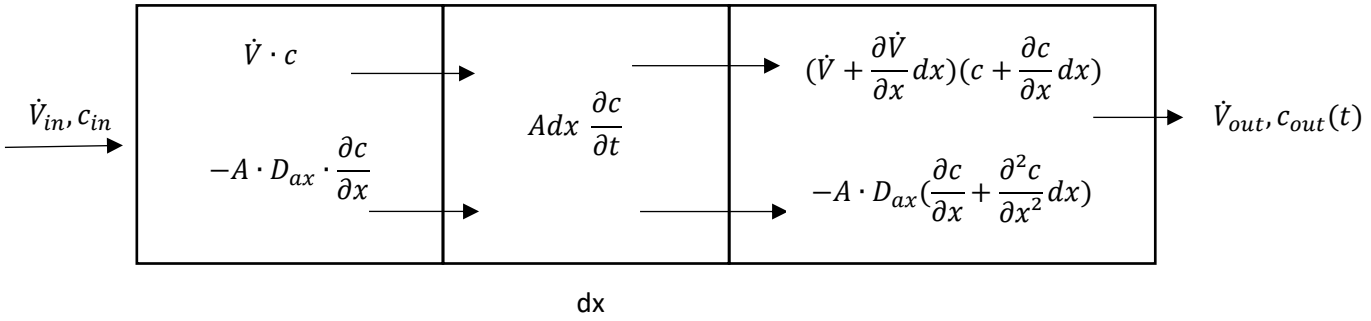

Figure 3.2: Scheme of the mass balance assumption for the calculation

where equations 3.9 and 3.10 describe the material balance equation

$\dot{V} \cdot c$ Eq : 3.9

$-A \cdot D_{ax} \cdot \frac{\partial c}{\partial x}$ Eq : 3.10

Eq 3.10 describes the axial dispersion assumed constant and is expressed according to Fick's law. As the spatial distribution is given, the concentration change over time (dc/dt) is looked for. Figure 3.2 shows the general considerations for the gas movement in the reactor, leading to equation 3.11 after some algebraic transformation. [71]

$\frac{\partial c}{\partial t} = D_{ax} \cdot \frac{\partial^2 c}{\partial x^2} - \frac{dv}{A} \cdot c - \frac{V}{A} \cdot \frac{\partial c}{\partial x}$ Eq : 3.11

The method of finite differences is applied to get the concentration of the following timesteps. Thanks to the explicit approach, it can be calculated straight forward after Eq 3.12. With the limitation, that too big timesteps contain the risk of instability. The ratio between dx/dt needs to be very low. [72]

$\frac{c_{l+1} - c_l}{\Delta t} = (\frac{D_{ax}}{\Delta x^2} + \frac{V}{2A\Delta x}) c_{k-1} + (\frac{-2D_{ax}}{\Delta x^2} - \frac{dv}{Ax}) c_k + (\frac{D_{ax}}{\Delta x^2} - \frac{V}{2A\Delta x}) c_{k+1}$ Eq : 3.12

As the calculation is a function of second order and the variables at the borders are not defined, it requires boundary conditions for in- and outlet. The model considers the reactor to be closed on both sides. At the inlet it is formulated as follows.

Boundary condition inlet:

$$\dot{V}_{in}, c_{in} \rightarrow \left| \begin{array}{l} \dot{V} \cdot c \\ -A \cdot D_{ax} \cdot \frac{\partial c}{\partial x} \end{array} \right.$$

$$V_1 = V_{in}$$

For k=1 is $c_{k-1} = c_0$.

$$c_0 = c_2 - \frac{2\Delta x}{AD_{ax}}(V_1 c_1 - V_{in} c_{in}) \qquad \text{Eq : 3.13}$$

This leads to the equation for concentration change during dt by inserting eq 3.13 in 3.12 and can be calculated.

The boundary condition outlet:

$$\frac{\partial^2 c}{\partial x^2} \equiv 0$$

for k=n then $c_{k+1} = c_{n+1}$

$$c_{n+1} = 2c_n - c_{n-1} \qquad \text{Eq : 3.14}$$

Then inserting again in eq 3.12 it can be calculated straight forward.

The Heat balance

The heat balance follows an identical mathematical approach to the mass balance. Of course, the formula changed. It is based on a partial differential equation for a dynamic spatial problem description.

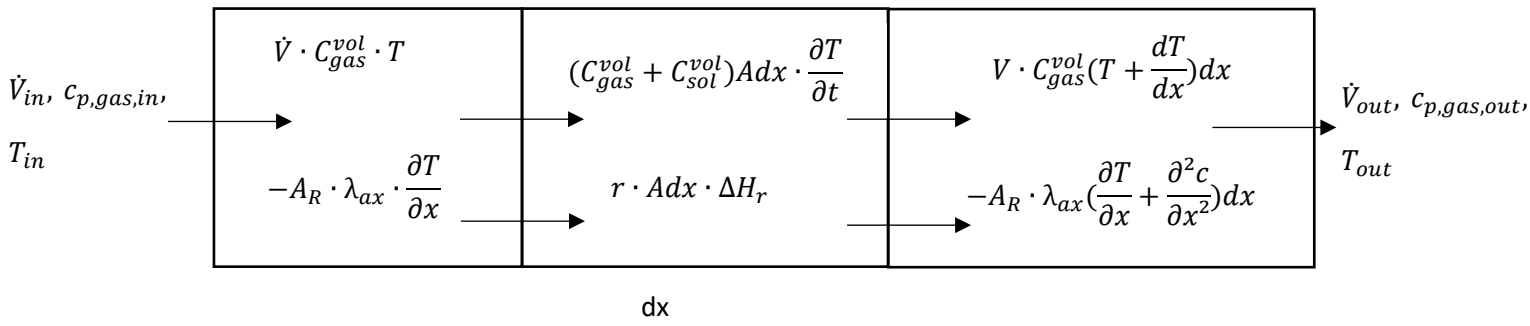

Figure 3.3: Scheme of the mass balance assumption for the calculation

The mol stream is linked with the heat capacity of the gas and the temperature T_{start}. Described by equation 3.15

$$\dot{V} \cdot C_{gas}^{vol} \cdot T$$ Eq : 3.15

Further influence gives the axial dispersion of heat conductivity according to the thermal conduction described by Fourier, expressed according to Eq 3.16: [73]

$$-A_R \cdot \lambda_{ax} \cdot \frac{\partial T}{\partial x}$$ Eq : 3.16

Figure 3.3 shows the general considerations for the heat development in the reactor, leading to the equation 3.17, and solved after the heat change dT/dt.

$$\frac{\partial T}{\partial t} = -\frac{V \cdot C_{gas}^{vol} \cdot \frac{\partial T}{\partial x}}{C_{ges}^{vol} \cdot A} - \frac{\lambda_{ax}}{C_{ges}^{vol}} \frac{\partial^2 T}{\partial x^2} + \frac{r \Delta H_R(T)}{C_{ges}^{vol}}$$ Eq : 3.17

$$\frac{T_{l+1} - T_l}{\Delta t} = \left(\frac{\lambda_{ax}}{C_{ges} + \Delta x^2} + \frac{\dot{V} C_{gas}}{2 C_{gas} A \Delta x}\right) T_{k-1} + \left(\frac{-2\lambda_{ax}}{C_{ges} \Delta x^2}\right) T_k + \left(\frac{\lambda_{ax}}{C_{ges} \Delta x^2} - \frac{\dot{V} C_{gas}}{2 A C_{ges} \Delta x}\right) T_{k+1} + \frac{r \cdot \Delta H_r}{C_{ges}}$$ Eq : 3.18

As the calculation is a function of second-order and follows an explicit scheme, it requires boundary conditions for in- and outlet. The mathematical approach is similar to the mass balance. At the inlet it is formulated as follows.

$$\dot{V}_{in}, c_{P,gas,in}, T_{in} \Big| \begin{array}{l} \dot{V} \cdot c_p \cdot T \\ \\ -A \cdot \lambda_{ax} \cdot \frac{\partial T}{\partial x} \end{array}$$

Leading to the T_0 which can be inserted in Eq. 3.18:

$$T_0 = T_{k-1} = T_2 - \frac{2\Delta x \cdot \frac{1}{2}(V_1 C_{p1} + V_{in} C_{Pin})}{A \lambda_{ax}} (T_1 - T_{in})$$ Eq : 3.19

Boundary condition outlet

$$\frac{\partial^2 T}{\partial x^2} \equiv 0$$

By inserting 3.20 in equation 3.18, Eq. 3.20 dT/dt can be calculated straight forward.

$$T_{n+1} = 2T_n - T_{n-1}$$ Eq : 3.20

The result gives a 3-dimensional diagram as shown in Fig. 3.4.

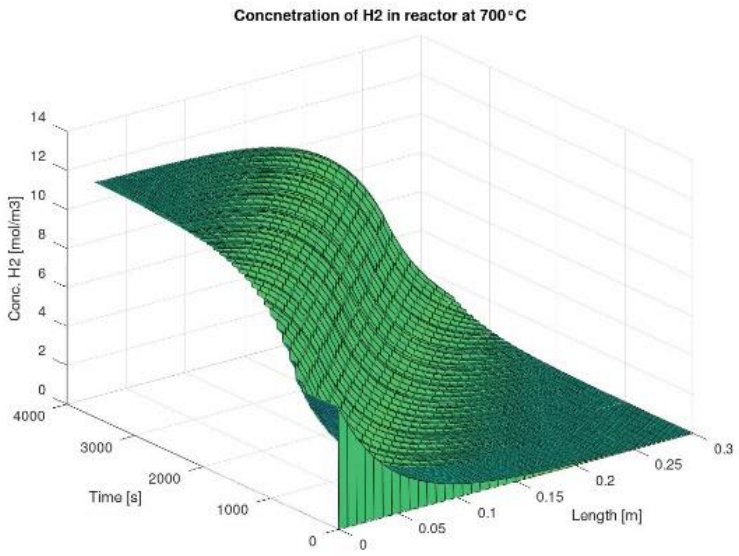

Figure 3.4 : Example of results by the simulation as 3d plot

3.5. Thermodynamics

This work examines the reduction of copper with H_2 and NH_3. Furthermore, the oxidation with air. The reactions occurring in the simulation are briefly summarized below. The reaction enthalpies (ΔH_r) are given for atmospheric pressure and given temperature:

$CuO + H_2 \rightarrow Cu + H_2O$ $\Delta H_r^{700°C} = -96.99$ kJ/mol Eq : 3.21

For the Oxidation

$Cu + 0.5\ O_2 \rightarrow CuO$ $\Delta H_r^{700°C} = -150.70$ kJ/mol Eq : 3.22

Reduction with ammonia

$2NH_3 \text{ ---> } N_2 + 3H_2$ $\Delta H_r^{700°C} = 101.00$ kJ/mol Eq : 3.23

$CuO+H_2 \text{ ---> } Cu + H_2O$ $\Delta H_r^{700°C} = -96.99$ kJ/mol Eq : 3.24

4. Evaluation

This work examines the reaction dynamics of a fixed bed CLC reactor with the fuels H_2 and NH_3 for reduction and air for oxidation in a single operation, where the single operation defines the assumption of a fully oxidized/reduced OC at the start of the operation and is oxidized/reduced one time. The solid bed material remains the copper-based OC for all

calculations and the pressure is kept constant at 1 bar for all simulations. The influence of the reactor temperature on the reaction time and conversion of the OC are examined closely. These simulations make it possible to observe the concentration of the various gases in the different volume elements over time and the distribution over the whole reactor length over time.

The single operation assumes an adiabatic process, meaning no heat loss or transfer to the outside of the system occurs. This represents ideal circumstances, which are not the case in actual performances over more cycles. Therefore, cyclic tests were investigated by reducing and oxidating the reactor in terms. After purging the system with N_2, the procedure is repeated 10 times. To limit the temperature, rise in the reactor, continuous extraction of power is made.

Even though copper does not exhibit the best properties for an oxygen carrier, mostly because of its low melting point, it has excellent conversion rates and reacts rapidly. Moreover, fixed bed reactors operate at temperatures below 1000 °C, keeping it an interesting candidate for this application. Furthermore, it was also chosen because of it's exothermic behavior for both reactions. [36]

4.1. Reduction with hydrogen

The studied model simulates the gas's reaction dynamics in the reactor for different temperatures in the range of 500 °C to 900 °C. Hydrogen reduces the OC under exothermic conditions producing H_2O. The simulation assumes a fully oxidized OC for the start of the operation a fully oxidized OC. A constant fast reduction is desirable. It is a closed adiabatic system, meaning no heat loss or transfer to the outside is occurring. The simulation stops when the flue gas composition reaches the critical concentration c_{crit} of the fuel, which corresponds to 10% of the inlet fuel stream. Since the fuel is heated up and valuable. The fuel constitution is assumed 100 vol% hydrogen. The reactor is filled with nitrogen at the start of the operation.

In the following diagrams, the first run with the fuel hydrogen at an inlet gas temperature of 700 °C is discussed. The fuel is fed in Vol.1 and diffuses in all directions through the

system. The mol flow rate of the fuel is 1,15E-04 mol/sec. After initializing the reaction, the residence time of the N_2 in the reactor is a few seconds, as depicted in Fig. 4.1. The curve marked by circles shows the N_2 concentration in the first volume segment, while the curve marked with stars the last (41). After 10-seconds, the N_2 concentration is already around zero mol/m³ in the first volume. After 30 seconds, the concentration hits nearly zero mol/m³ in the last section. Furthermore, the graph illustrates very well that c_{max} (maximal molar concentration) of the gas in the reactor is 12.359 mol/m³ at a temperature of 700°C and atmospheric pressure.

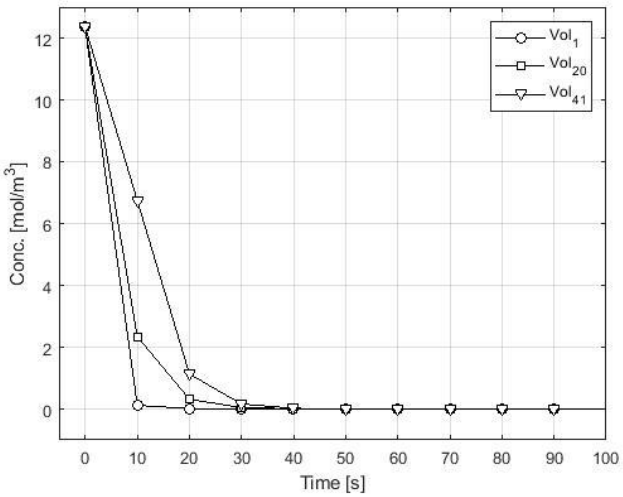

Figure 4.1: Concentration of N_2 during the reduction with H_2 at 700°C in Vol. 1 (o), Vol.20 (□) and Vol 41(▽)

Figure 4.2 depicts the concentration of H_2 at all volume segments and highlights Vol. 1, 20 and 41 of the reactor over time. The calculation stops after 2960 seconds (~50 min) when the exhaust gas's hydrogen concentration surpasses c_{crit} of 1.236 mol/m³, corresponding to 10 % of the inlet gas concentration. Because of the discretization, the concentration shows bumps in Fig. 4.2 and for all graphs illustrated over time since the timesteps are far smaller than the length difference. In Figure 4.2, the concentration rises after complete reduction of the OC. After 50 seconds, the H_2 concentration starts rising in Vol.1; this correlates with the degree of oxidation (X_s) of the volume, which reaches 0 % by this time. Figure 4.3 illustrates the distribution of H_2 in the reactor at t_{start} after 1800 s and at t_{end}. The distribution shows the gas concentration over the reactor length and shows an even distribution at t_{end} over the whole reactor length.

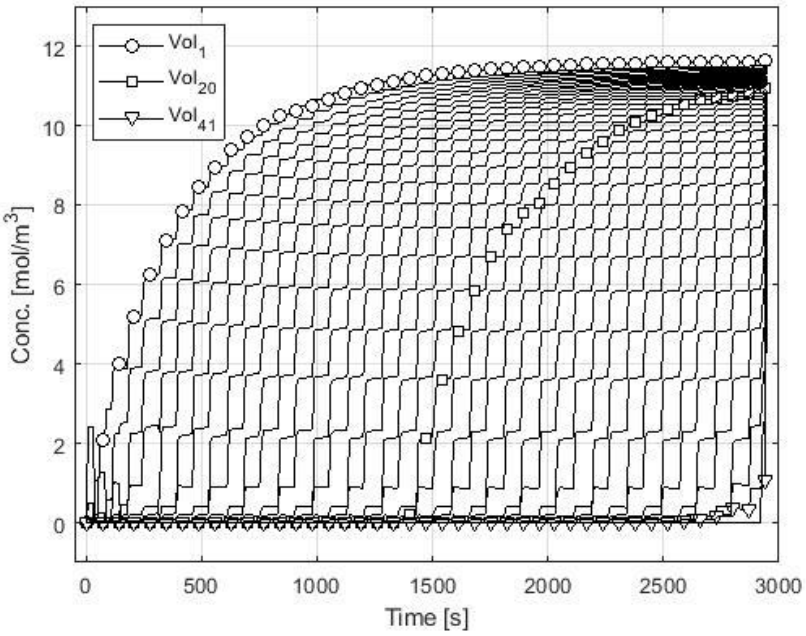

Figure 4.2: Concentration of H_2 at 700 °C over time at Vol.1 (o), Vol. 20 (□) and Vol. 41(▽) the remaining (-)

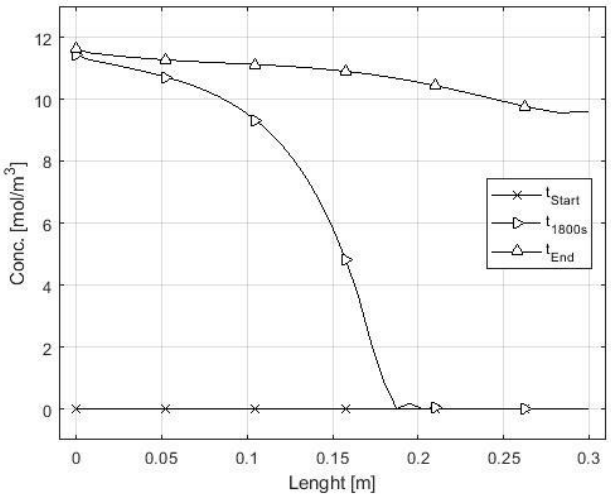

Figure 4.3: Distribution of H_2 at 700°C over the length at t_{start}(x), t_{1800} (▷) and t_{end}(△)

Fig. 4.4 shows the degree of oxidation of the volume segments, where each line represents one segment. The degree of oxidation is a dimensionless value and ranges from 1-0, where 1 represents a fully oxidized OC and 0 a fully reduced one. The first volume reduces entirely after 50 seconds, confirming the correlation of the concentration rise of H_2 with the degree of oxidation. The reactor reaches a complete reduction after the operation. This reduction is very uniform and reduces a volume every 50-70 seconds. The hydrogen reacts with the oxygen of the OC and forms H_2O as the result of the reaction. This reaction proceeds rapidly, underlining the excellent reactivity of copper with H_2.

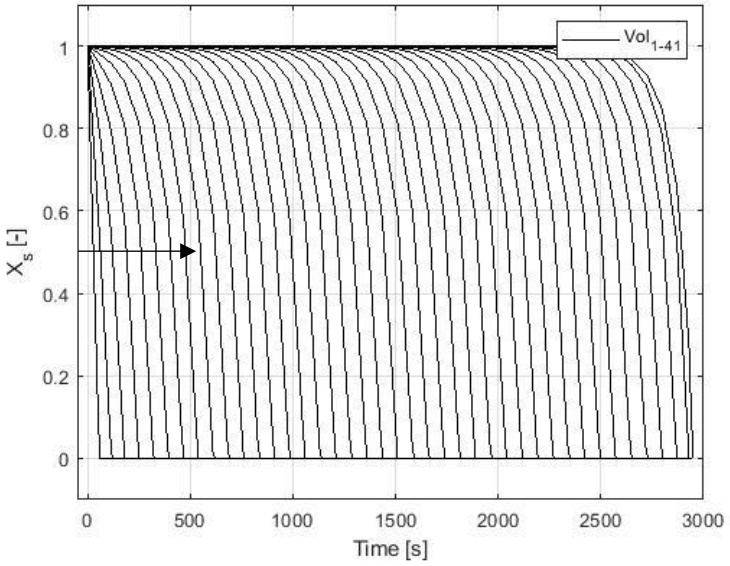

Figure 4.4: Degree of oxidation of all volumes over time (-)

The relation between the concentration of H_2O and H_2 is illustrated in Figure 4.5 in the volume segment 20. The H_2O concentration is high at low H_2 concentrations. H_2 reduces the OC immediately, leading to the formation of H_2O. As soon as the OC of the prior volumes is fully reduced, the H_2 concentration starts rising, pushing the water steam out.

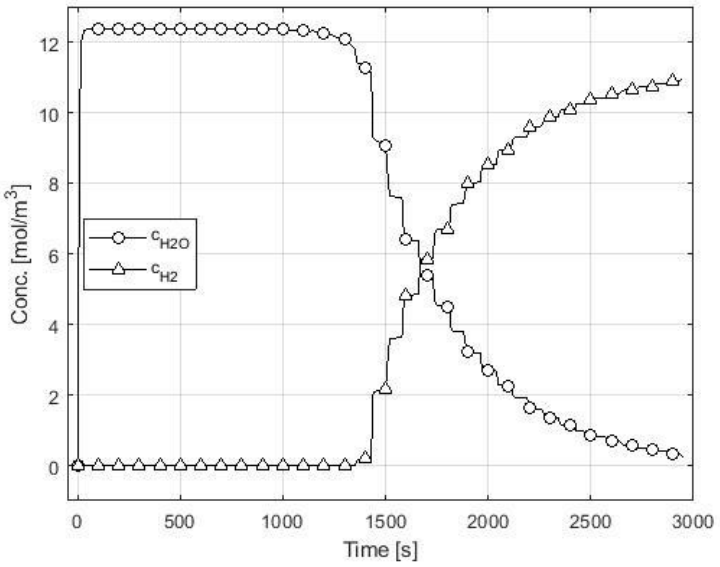

Figure 4.5: Concentration of H_2 (△) and H_2O(o) in Vol. 20 over time at 700°C

Figure 4.6 illustrates the concentration of H_2O at volume 1, 20 and 41. It depicts high concentrations of H_2O from the start of the operation, as the H_2 is converted to water steam and rushes through the reactor. The distribution depicted in Figure. 4.7 underlines these

observations and shows very well that the steam is pushed out by the mol flow of the fuel gas. The fuel gas shows excellent conversion, and the model seems to depict the interactions between OC and fuel very well. At t_{start} c_{H2O} is 0 and as soon as the operation starts, H_2O is formed and fills the reactor.

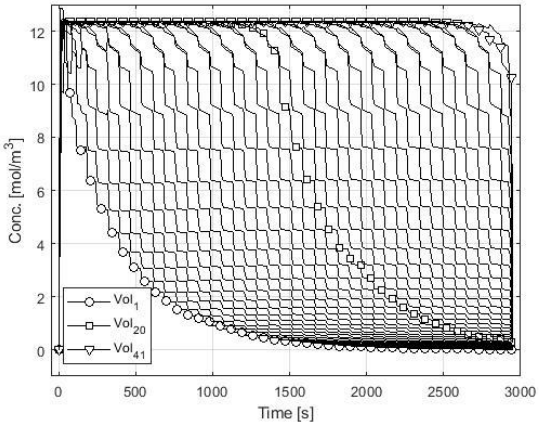

Figure 4.6: Concentration of H_2O over time in Vol.1 (o), Vol.20(□) and Vol.41(▽) the remaining (-) at 700°C

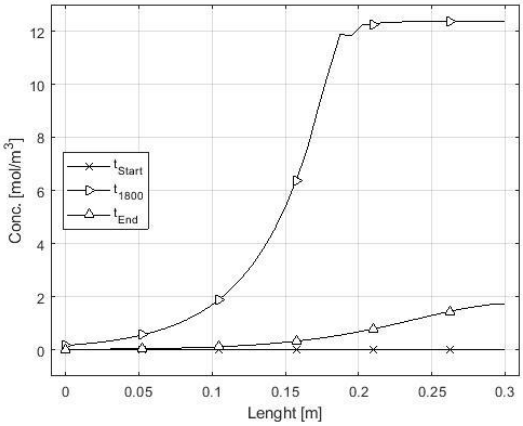

Figure 4.7: Distribution of H_2O in the reactor at t_{start}(*), t_{1800} (▷) and t_{end}(△) at 700°C

Figure 4.8 illustrates the heat development over time in the reactor. The temperature rises to a maximum of 806.4 °C, reaching a maximal temperature difference of 106.4°C. The OC reacts fast, and after 70 seconds, the first volume reaches its maximum temperature. After the peak, the temperature drops slightly around 7 °C. The temperature decreases slowly afterward until the end of the operation. The reactor heats up more in the reactor's rear part, reaching nearly the same T_{max} throughout Vol 10-41. Figure 4.9 shows the temperature distribution at the end of the reaction. It depicts the temperature decrease in the first volume elements nicely after the reaction is finished. The temperature in the rear part stays constant with a little rise at the end.

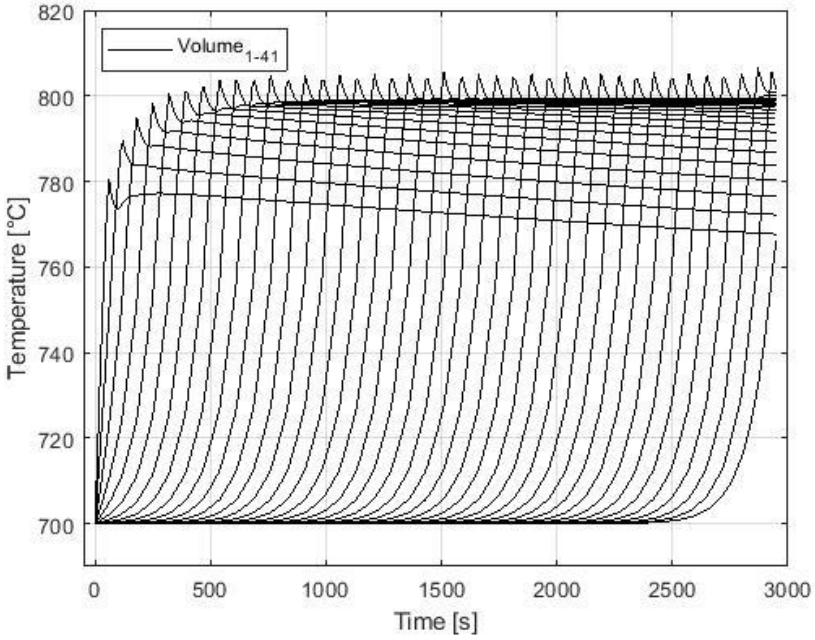

Figure 4.8: Heat development over time in all volume segments (-) at 700°C

Figure 4.10 illustrates the degree of oxidation and the heat front. As soon as the OC starts reacting the temperature rises.

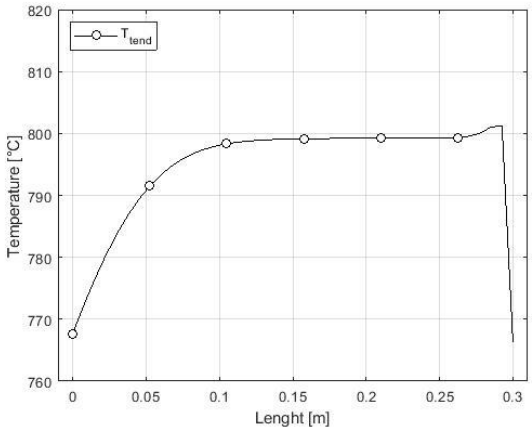

Figure 4.9: Heat distribution (o) in the reactor at t_{end} 700°C

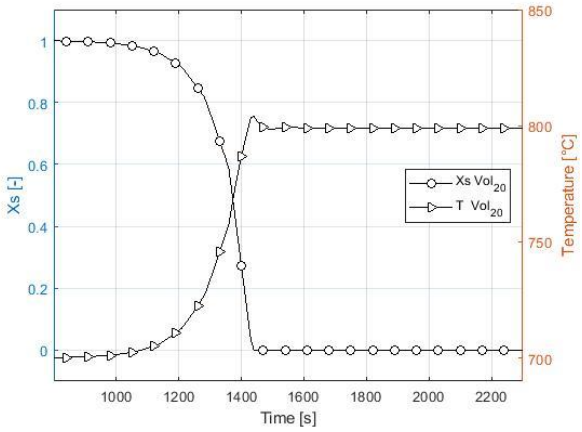

Figure 4.10: Degree of oxidation (o) and heat front (▷) in Vol. 20 at 700°C

Comparing the concentration of H_2 with the temperature over time in Figure 4.11, shows the concentration of H_2 rise as soon as the OC is fully reduced correlating with the temperature reaching its maximum.

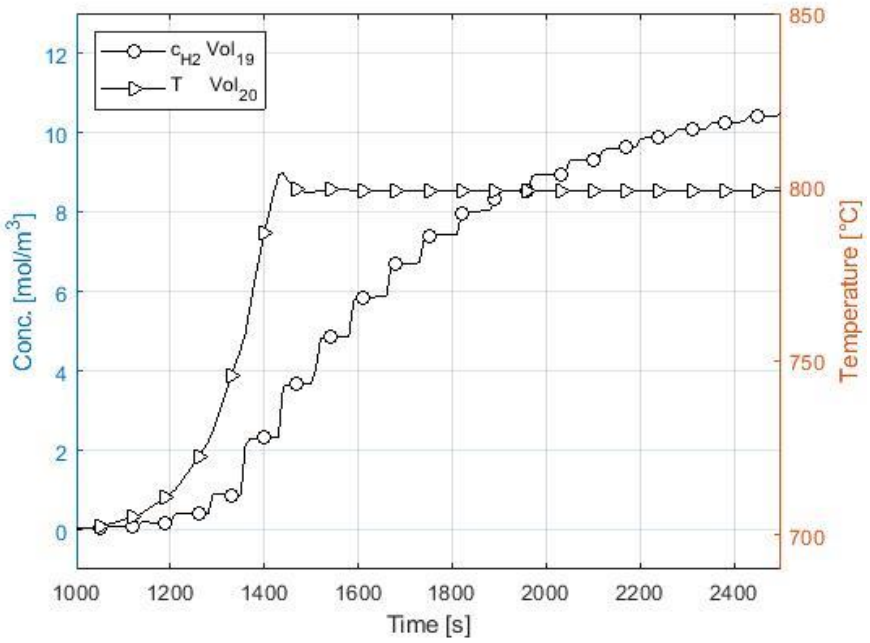

Figure 4.11: Gas front (o) and heat front (▷) in Vol. 20 at 700°C

4.1.1. Comparison of reduction with H_2 for different temperatures

For comparison, the reaction of a single operation was repeated for the different temperatures named above and shown in table 4.1. The settings in the reactor remained the same., listed in table 3.1. For the evaluation, significant issues are:

- the time of operation
- the breakthrough curve as well as the conversion rate, which provides essential information about reactivity and efficiency of the reactor.
- The temperature development, which gives further important information about energy output optimally aiming at a high-temperature difference

Table 4.1 summarizes some basic information about the different simulations.

Table 4.1: Overview of the experiments with general information for the reduction with H_2

	Comparison of reduction with H_2 for different temperatures				
Temperature [C°]	500	600	700	800	900
Concentration [mol/m³]	15.6	13.8	12.4	11.2	10.3
time of operation [s]	3030	2990	2960	2930	2910
dT max [°C]	103.2	103.9	106.4	107.4	108.9

Figure 4.12 depicts the comparison of the concentration of H_2 in Volume 1 over time. The maximum molar concentration in the reactor rises with lower temperatures according to the ideal gas equation and is listed in Table 4.1. Even though the experiments with a higher inlet gas temperature exhibit a reduction of the operation time and achieve a slightly higher maximal temperature rise, all conducted experiments reach a full reduction of the OC at the end of the operation.

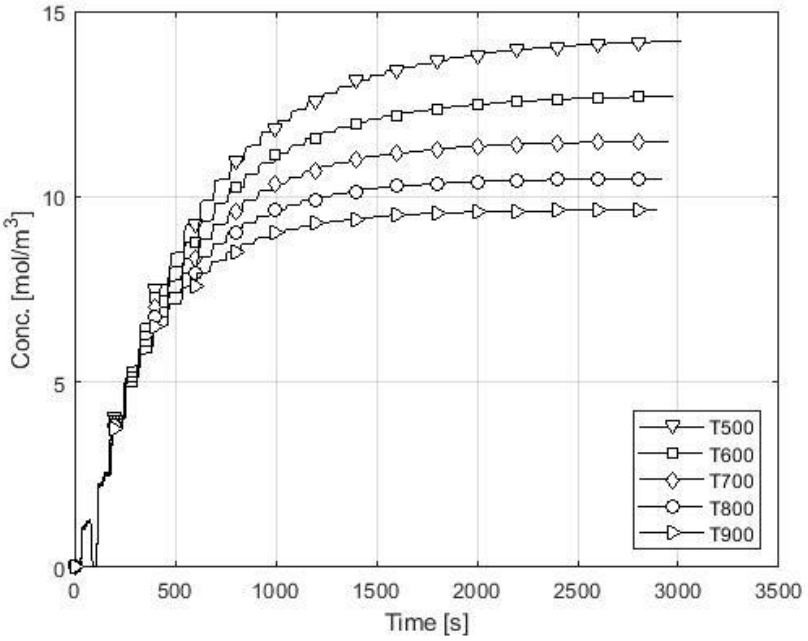

Figure 4.12: Comparison of the concentration during reduction with H_2 for the different [500°C (▽), 600°C (□), 700°C (◇), 800°C (o), 900°C (▷)]

Figure 4.13 illustrates the distribution in the reactor at two different time steps, after 1000 s and 2000 s. Lower temperatures show a steeper breakthrough curve but a slower conversion of the OC. After 2000 seconds for the experiments from 600-900 °C, nearly no difference is noted.

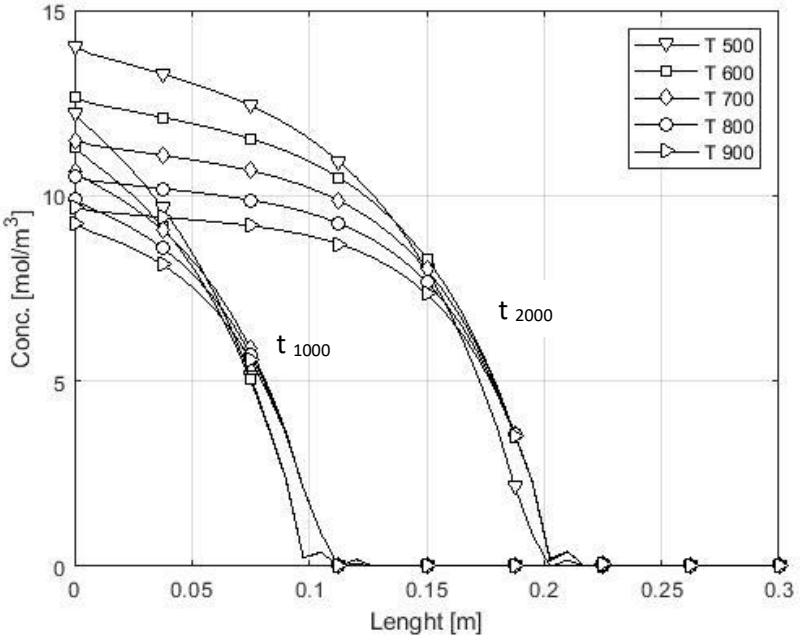

Figure 4.13 Distribution of H_2 in the reactor after 1000 and 2000 seconds [500°C (▽), 600°C (□), 700°C (◇), 800°C (o), 900°C (▷)]

Figure 4.14 shows the degree of oxidation of the OC in volume 30. The reduction front is very similar for all experiments. The velocity of the front rises with the temperature. With a difference between 500-900°C of approx. 100 seconds.

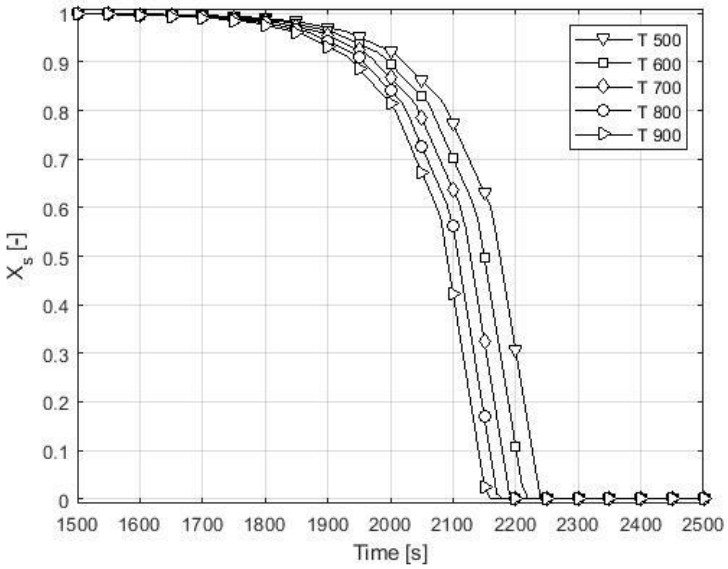

Figure 4.14 Degree of oxidation for different Temperatures at Vol.30 [500°C (▽), 600°C (□), 700°C (◇), 800°C (o), 900°C (▷)]

Fig. 4.15 illustrates the temperature difference in Vol.7. It shows that higher inlet gas temperatures reach a higher temperature difference. After 2000 seconds, the difference counts ~406 °C between experiment T_{500} and T_{900}.

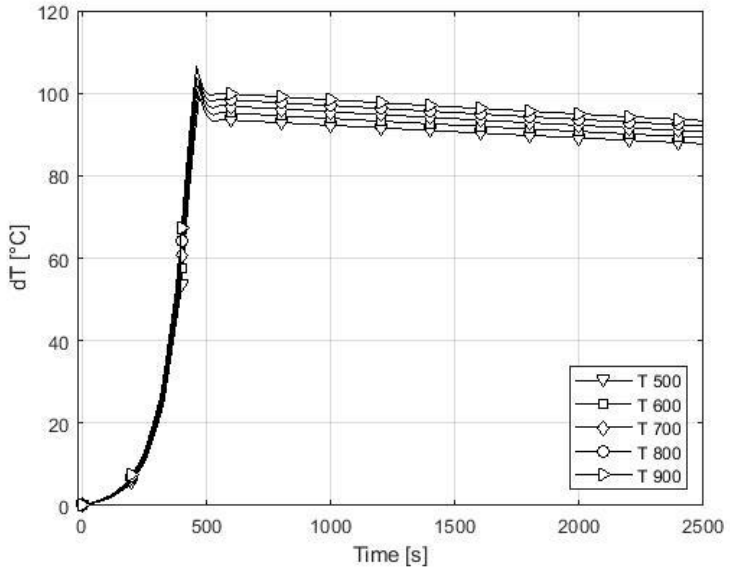

Figure 4.15: Temperature difference at Vol. 7 during reduction with H_2 for different Temperatures [500°C (▽), 600°C (□), 700°C (◇), 800°C (o), 900°C (▷)]

4.2. Oxidation with air

The oxidation of the OC is discussed next. This chapter evaluates a single oxidation process at 700°C. The OC is fully reduced, and the reactor is filled with N_2 at the beginning of the reaction. The oxidation stops if the outlet gas reaches c_{crit} 10 % of the inlet gas concentration of air to prohibit a significant loss of heated air. For the single-cycle adiabatic conditions are assumed.

The gas constituents are relevant for the oxidation process. The reactor should operate with air for economic reasons. Since copper is highly reactive and various studies already showed some good results [31,32,47,74] no problems are expected considering only 21vol % of air is O_2. The air has an oxygen and nitrogen ratio of 21% to 79%; the simulation neglects other prominent constituents like argon and carbon dioxide. The mol flow is 2.73E-04 mol/s, which is notably higher during oxidation, mainly because of the higher reaction rate constant k_0 of O_2 and the lower volumetric concentration, so the operation time remains similar. The concentration in the reactor at 700 °C remains 12.39 mol/m³ according to the ideal gas equation. After 3500 seconds (~59 min), the experiment reaches c_{crit} at the outlet,

leading to the reaction's termination. During combustion, the oxygen absorbs onto the OC, leaving only N_2 as flue gas.

Figure 4.16 displays the O_2 concentration propagation in all volume segments highlighting (1, 20,40 and 41) over time. The concentration is higher in the first volumes. As the reactor heats up, lower concentrations of oxygen are reached, which range between ~2-2.4 mol/m³. The breakthrough curve of the gas is steep as desired. After 60 seconds, the concentration rises, correlating with the full oxidation of the first segment, it takes 70-100 seconds to reduce a volume segment, with a rise the further the reaction proceeds. The boundary condition lead to some errors in the last volume segment. Vol. 40 reduces partly after Vol 41. Therefore, a second condition for terminating the reaction is considered, where the concentration in Vol.40 must be higher than in Vol.41, additionally to reaching c_{crit}. Fig. 4.17 depicts the distribution of O_2 in the reactor at selected points in time. It shows an even distribution with a steep reaction front moving through the reactor.

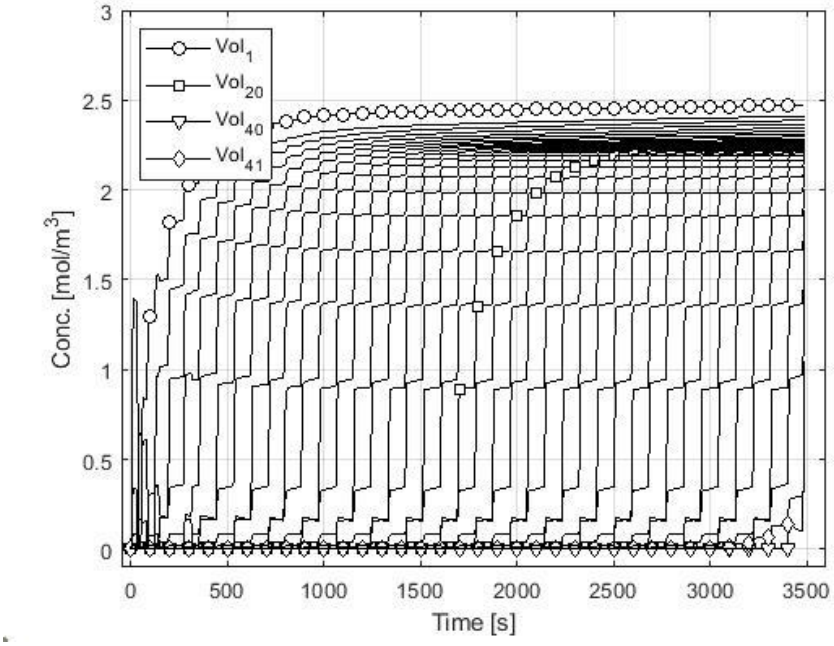

Figure 4.16: Concentration O_2 at 700 °C in Vol. 1(o), Vol.20(□), Vol.40 (▽), Vol.41(◇) and the remaining (-)

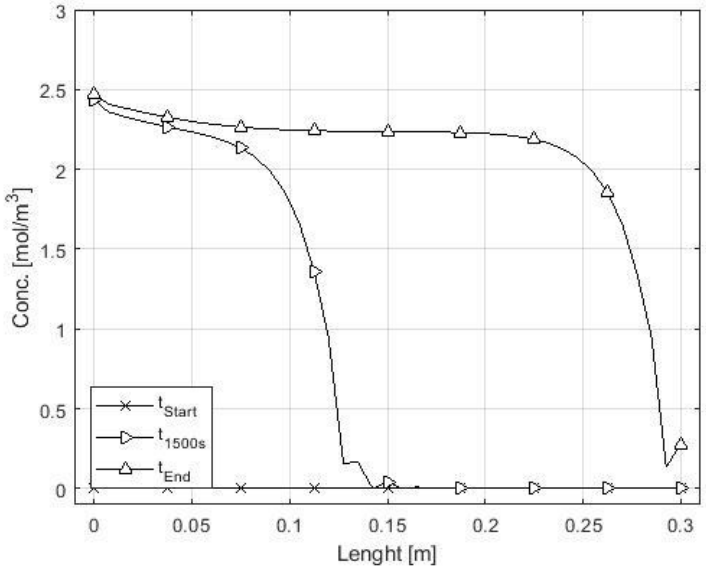

Figure 4.17: Distribution O_2 over the length at t_{start}(x), t_{1500} (▷) and t_{end}(△)

The N_2 concentration drops shortly after the start of the experiment since the reactor is filled with 100% N_2 at t_{start}. Figure 4.18 depicts c_{N2} and shows an initial drop in Vol.1 but rises immediately since the O_2 is absorbed. Figure 4.19 shows the concentration at three time steps (t_{start}, after 1500 seconds (25 min) and at t_{end}) over the reactor's length. The concentration diminishes over the length due to the temperature differences. The reaction front is steep. The minimal concentration thought never drops below 8 mol/m³; since 79 vol% of air remain N_2.

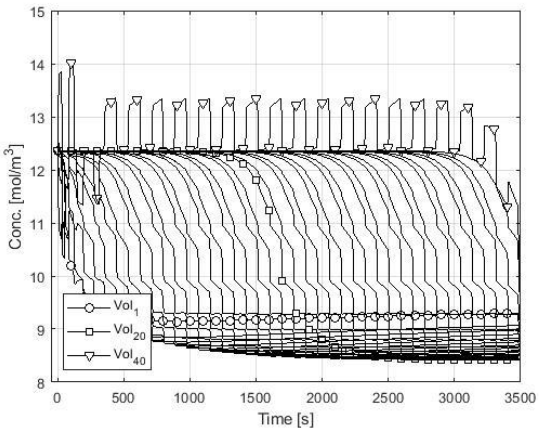

Figure 4.18: Concentration N_2 over time Vol. 1(o), Vol.20(□), Vol.41 (▽) and the remaining (-)

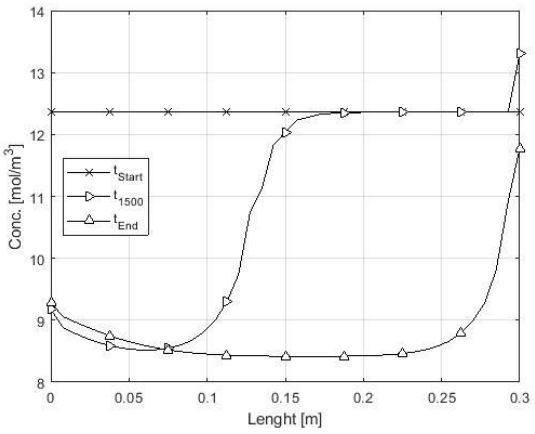

Figure 4.19: Distribution of N_2 in the reactor t_{start}(x), t_{1500} (▷) and tend(△)

Figure 4.20 illustrates the concentration of O_2 and N_2 in Vol.15. It shows the relation between the concentrations. Equilibrium in Vol 15 is reached after approx. 1800 seconds.

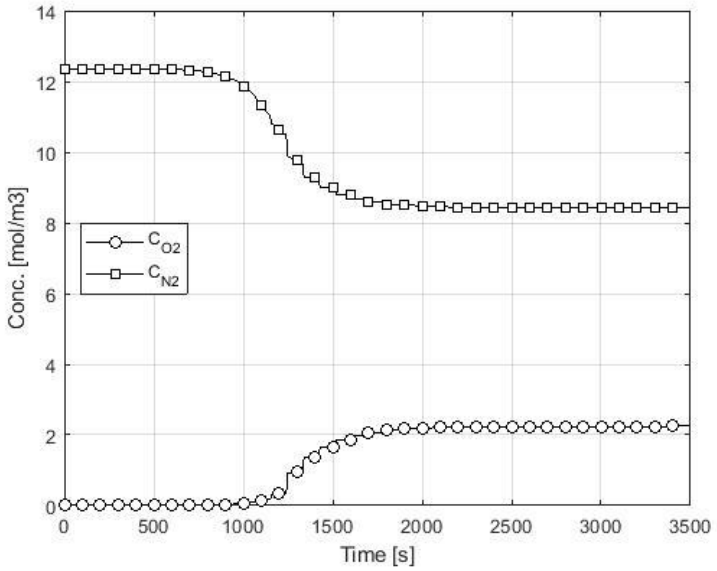

Figure 4.20: Concentration of O_2 and N_2 at Vol. 15 at 700 °C O_2 (o) and N_2 (□)

Figure 4.21 depicts the degree of oxidation of the different volume segments. The reaction stops after 3500 seconds, leaving 1 segment partly oxidized. Vol.1 is fully oxidized after 60 seconds. The simulation shows a uniform conversion.

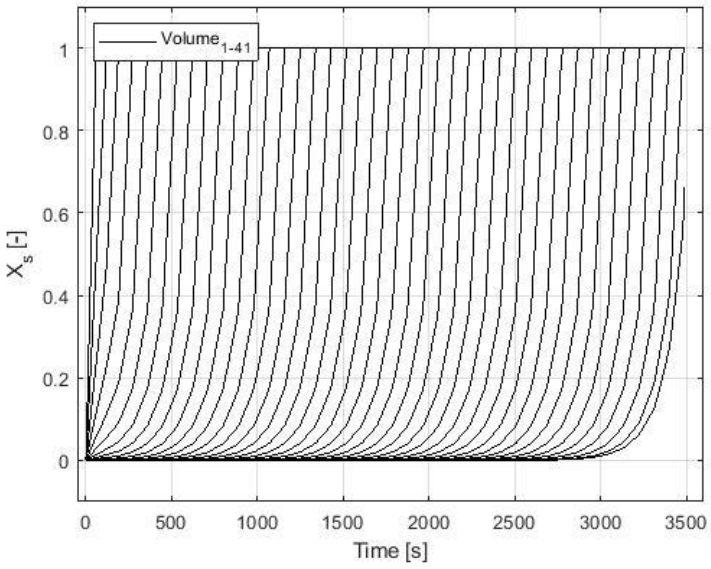

Figure 4.21: Degree of oxidation of all volume segments

As shown in Fig. 4.22, the reactor reaches its maximum temperature after 60 seconds in Vol.1 at 823.18 °C, since the axial heat dispersion influences the OC. The first volume heats

up less than the following. Maximal temperature is reached in Volume 12 after 990 seconds at 865.48 °C. After the oxidation, the temperature declines slowly but notably, especially the front part of the reactor shows a decrease of around 90 °C.

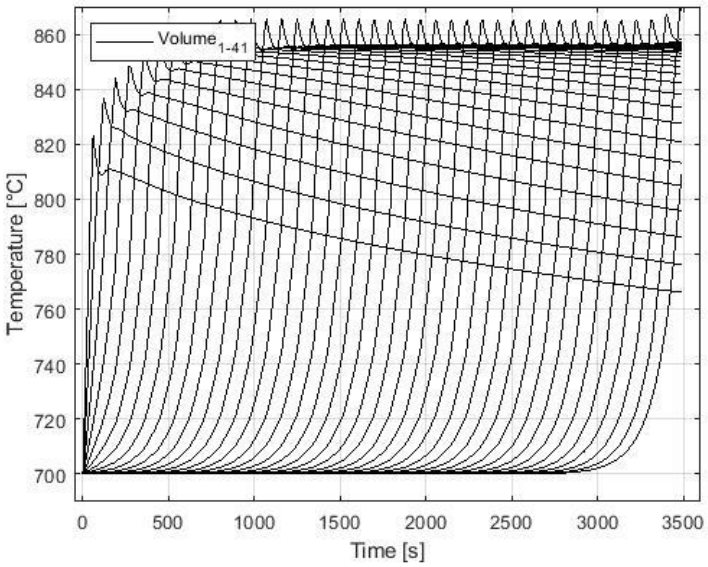

Figure 4.22: Temperature development of all Volume segments over time

Fig.4.23 depicts the heat distribution in the reactor at t_{end}, where the front part of the reactor shows a temperature difference of ~80°C to the rear part, although the temperature difference between Vol.1 and Vol.40 at their respective maximum counts ~46 °C. At the end of the reaction, the system reaches a mean temperature of 848.98°C. Figure 4.24 shows the heat front and gas front, the concentration starts rising as soon as the OC is reduced, and the segment reaches maximal temperature.

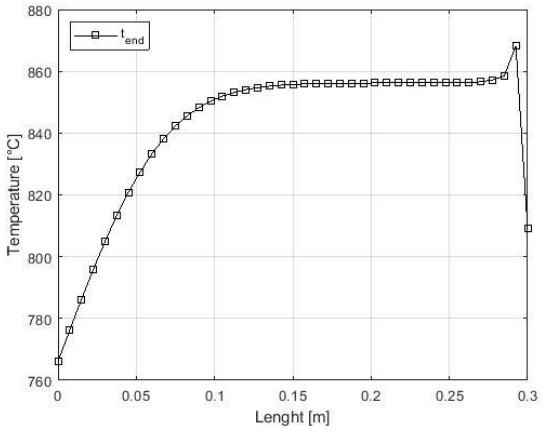

Figure 4.23: Temperature distribution at t_{end} in the reactor

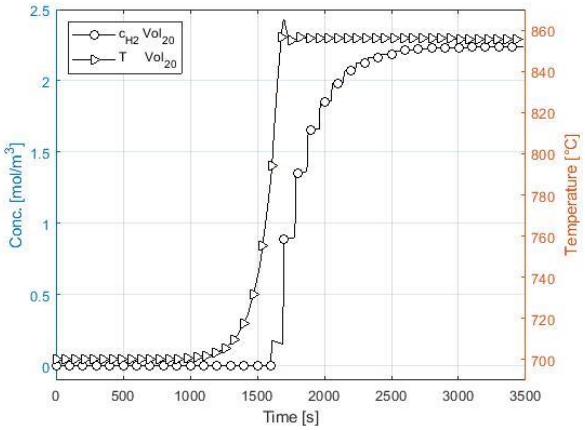

Figure 4.24: Gas front(o) and heat front (▷) in at Vol.20 over time

4.2.1. Comparison of oxidation with air for different temperatures

The single simulation was repeated for different reactor temperatures, ranging from 500-900°C, to understand the temperature's influence on the reaction dynamics. The temperature was varied in the same steps as for the reduction with H_2. Apart from the temperature, the entry parameters remain the same as discussed in chapter 3. The points of observation are listed 4.1.1. For oxidation, air is used as the oxidizing agent, consisting of two components. The concentrations of the gas component based on the temperature in the reactor are listed in Table 4.2, with the time of operation and the maximal temperature difference achieved.

Table 4.2: Overview of the experiments with general information for the oxidation with air

	Comparison of reduction with O2 for different temperatures				
Temperature [C°]	500	600	700	800	900
max. Concentration [mol/m³]	15.6	13.8	12.4	11.2	10.3
max. Concentration O2 [mol/m³]	3.27	2.89	2.60	2.35	2.15
max. Concentration N2 [mol/m³]	12.3	10.9	9.8	8.9	8.1
time of operation [s]	4360	4110	3420	3100	3020
dT max [°C]	180.84	178.67	167.44	164.20	163.20

The concentration of the gas rises with lower temperature due to the ideal gas equation. Figure 4.25 illustrates the concentration in Vol.41. The comparison shows a faster-moving reaction front at higher temperatures without worsening the breakthrough curve.

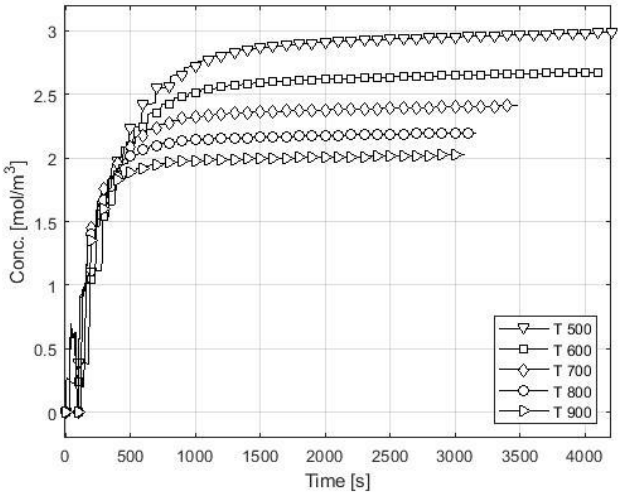

Figure 4.25: Concentration of oxygen in Vol. 2 at temperature [500°C (▽), 600°C (□), 700°C (◇), 800°C (o), 900°C (▷)]

The distribution in Figure 4.26 at the timesteps 1000 s and 2000 s underline these observations. The longer the reaction, the more difference can be noted in the distribution of c_{O2}

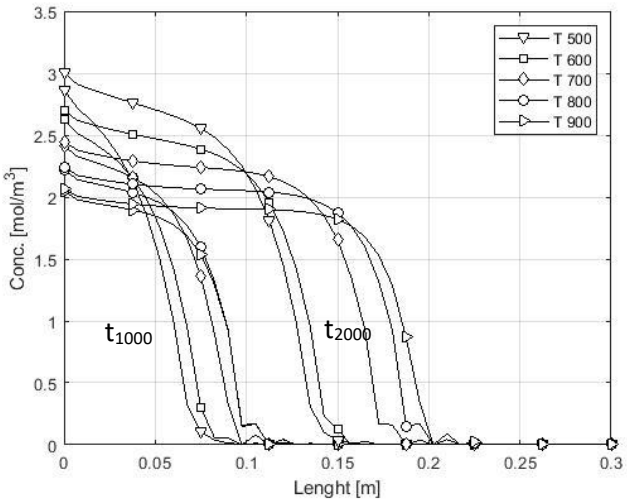

Figure 4.26: Distribution of c_{O2} for different temperatures at t_{1000} and t_{2000} [500°C (▽), 600°C (□), 700°C (◇), 800°C (o), 900°C (▷)]

Figure 4.27 illustrates the degree of oxidation for the different temperatures. Lower temperatures show a slower conversion of the OC— however, it does not influence the breakthrough curve and the conversion rate. A stronger gap between 600-700 °C can be observed. Over 800°C little differences are noted. Between 500-900°C, a difference of approx. 1000 seconds is noted

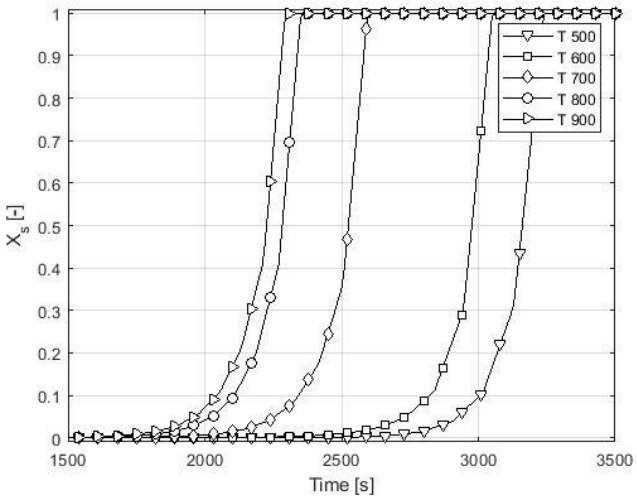

Figure 4.27: Degree of Oxidation at Vol. 30 for different temperatures OC [500°C (▽), 600°C (□), 700°C (◇), 800°C (o), 900°C (▷)]

The higher temperature difference reaches the simulation at lower starting temperatures, even though not a big difference is noted. (Figure 4.28) Due to the faster reaction, the heat

front moves faster through the reactor, shown in Fig. 4.29, where the temperature distribution after 1500 seconds is depicted for the investigated temperatures.

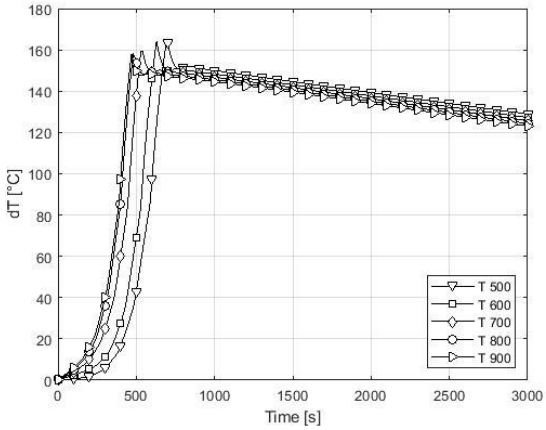

Figure 4.28: Temperature difference at Vol.20 [500°C (▽), 600°C (□), 700°C (◇), 800°C (o), 900°C (▷)]

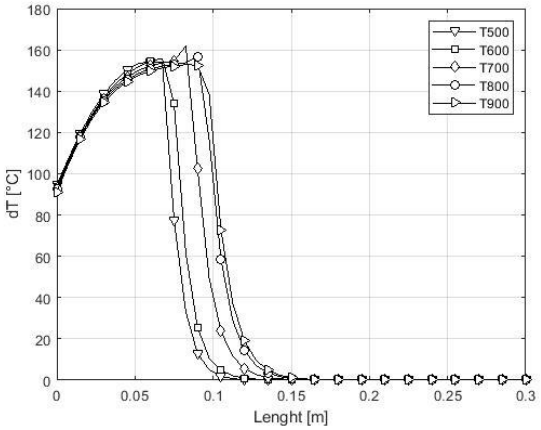

Figure 4.29: Temperature difference at t_{1000} OC [500°C (▽), 600°C (□), 700°C (◇), 800°C (o), 900°C (▷)]

Figure 4.30 shows the temperature distribution at the respective t_{end} for all temperatures. It illustrates lower temperatures for the lower operating temperature at the front part of the system, but a higher temperature at the rear part.

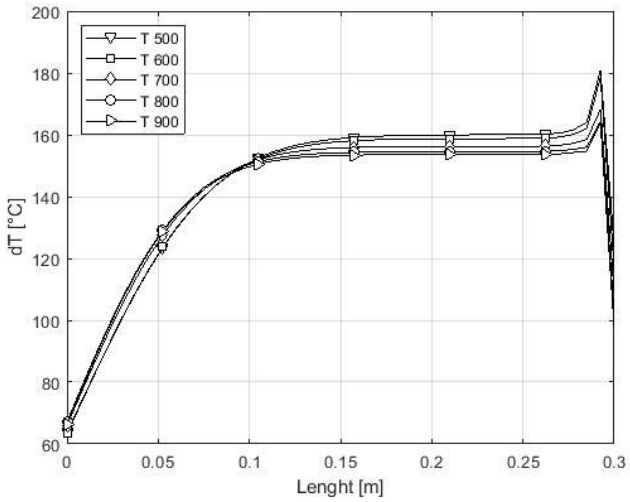

Figure 4.30: Temperature difference at t_{end} for temperatures [500°C (▽), 600°C (□), 700°C (◇), 800°C (o), 900°C (▷)]

4.3. Reduction with NH_3

The simulation showed satisfying results for reduction with H_2 and oxidation with air. The reduction of a single cycle operation with ammonia as fuel was simulated next. Starting conditions are a fully oxidized OC and a reactor filled with dinitrogen gas. The reactor temperature for the diagrams in this section is 700 °C. Further simulations were conducted with temperatures of 500°C, 600°C, 800°C and 900°C. The observation concentrated on the formation of H_2, depending on the decay of ammonia, the breakthrough curves of the hydrogen gas, as well as the formation of H_2O. Further, essential points are the analysis of the developing heat, as well as the degree of oxidation reached. The hydrogen concentration formed in the reactor was taken to get the critical concentration corresponding with 10% of the hydrogen concentration after the decomposition of ammonia. Hydrogen can reach a maximum concentration of 6.2 mol/m³ at 700°C.

The decomposition of ammonia (NH_3) happens immediately in the reactor. The reaction equilibrium at 600 °C and 1 bar with ideal thermodynamic assumptions predict an ammonia decomposition 99.9 mol % to H_2 and N_2. To reach a 100% decomposition much higher temperatures or catalysts are needed, such as ruthenium or nickel. To simplify the reaction a nearly complete decomposition is assumed in the reactor. It behaves as a first-order reaction. [25]

The mol flow is the same as for the fuel H_2 with 1.15E-04 mol/sec. The fuel composition consists of 50 vol% ammonia and 50 vol% water steam. A mixture of gases is chosen; otherwise, too high energy losses due to the endotherm decomposition of ammonia are expected. Also, the planned pilot-plant will operate with a fuel mixture. The hydrogen concentration reaches its critical amount of 0.62 mol/m³ in the exhaust gas after 4320 seconds (72 min), leading to the stop of operation. Dt of the results is 60 seconds as the operation and the calculation took notably longer than the reduction with pure hydrogen and the oxidation.

The forward reaction rate constant (kfwd) describes the reaction velocity of NH_3 towards the products N_2 and H_2 until the system reaches equilibrium for a given temperature and pressure. The decomposition's reaction rate has a significant influence on the results as it

influences the velocity of the decomposition of ammonia. The first test assumes a kfwd of 1, which in subsequent tests is varied to 0.2, 0.5 and 1.2 to observe the scale of influence and choose the most appropriate.

Figure 4.31 illustrates the NH_3 distribution in the reactor. It demonstrates the influence of the reaction rate constant. With a reaction rate value of 0.2 NH_3 does not decompose completely. 0.167 mol/m³ reach the outlet at a system length of 30 cm. The temperature has only a small influence since the equilibrium for ammonia is already near zero at temperatures around 250 °C according to the equilibrium calculation shown in Fig. 2.3. The time 1200 s was chosen randomly because the decomposition is not affected by the time.

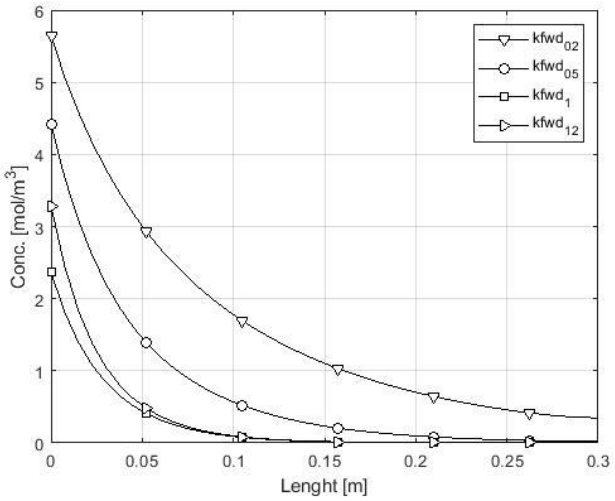

Figure 4.31: Concentration of NH_3 at 1200 sec for different kfwd [kfwd 0.2 (▽), kfwd 0.5 (o), kfwd 1 (□), kfwd 1.2 (▷)

According to the higher rate constant, the decomposition increases as well. A great change is observed until kfwd 1.0, where 90% of ammonia decomposes within the first 10 cm. Raising the rate constant further seems not to make decisive changes. This led to the decision to use the kfwd of 1.0 for further simulations. The concentration reaches nearly zero after 10 cm, where only a small part of ammonia remains. Moreover, it is unclear if the OC acts as a catalyst accelerating the decomposition, as no test with copper could be found in the literature.

Fig. 4.32 illustrates the concentration of N_2 in the reactor at a temperature of 700°C. It shows the drop of the N_2 concentration, as it gets pushed out after starting the operation in a few seconds. C_{N2} counts 12.36 mol/m³ prior to the initializing of the feed at 700 °C and 1 bar. c_{N2} immediately drops to 1.27 mol/m³. The concentration rises again, as shown in

Fig. 4.33, because the decomposition of NH_3. After that, the concentration remains stable at around 2 mol/m³ and is influenced solely by the temperature. C_{N2} remains similar in the different volume segments, having the lowest concentration in the first, as there is still the most ammonia present.

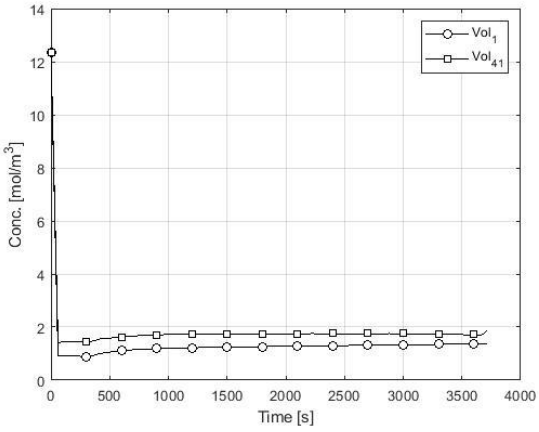

Figure 4.32: Concentration of N_2 in Vol. 1 (o) and Vol. 41(□)

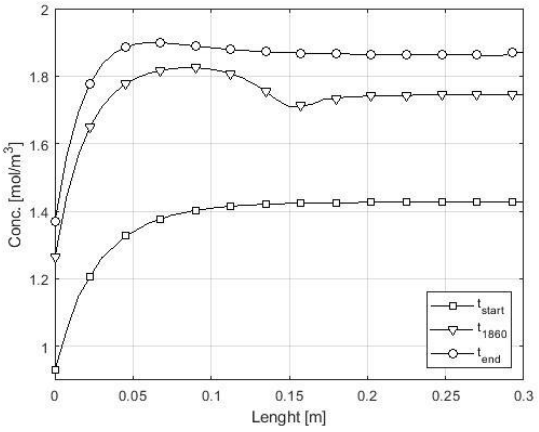

Figure 4.33: Distribution of N_2 in the reactor t_{start} (□), t_{1800}(▽) and t_{end}(o)

H_2 acts as the reducing agent and appears after the decomposition of ammonia. This reaction order illustrates the distribution graph of Figure 4.35 showing c_{H2} over the length at different timesteps (t_{start}, at t_{2160} and t_{end}). The H_2 gets formed out of the NH_3 according to the reaction and reacts immediately with the OC forming H_2O. Figure 4.34 illustrates c_{H2} at 4 different volumes. The maximal concentration possible is 6 mol/m³ due to the mixture of the fuel with water steam. In the first volume only a small amount of H_2 appears, leading to a long time until the OC is fully reduced. The maximum amount of H_2 concentration in vol. 1 reaches 3.8 mol/m³., ~2 mol/m³ less than the maximum in the reactor not influenced by c_{NH3}.

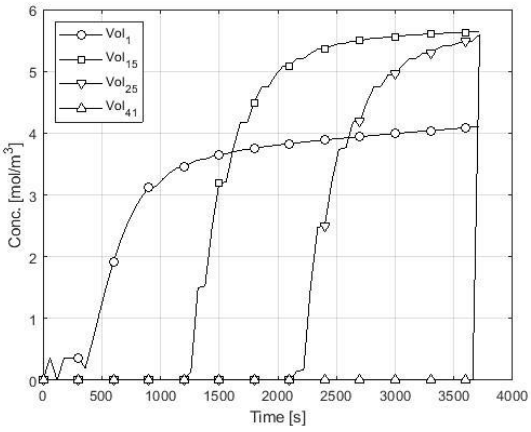

Figure 4.34: Concentration of H_2 700°C at Vol.1(o), Vol.15(□), Vol.25(▽) and Vol.41(△)

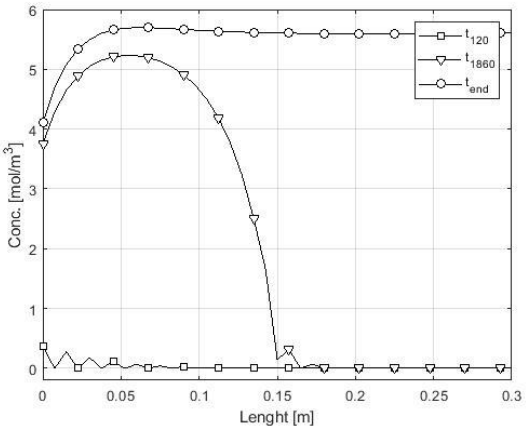

Figure 4.35: Distribution of H_2 at 700°C at t_{start}(□), t_{1800} (▽)and t_{end}(o)

The concentration of H_2O undergoes different changes. As shown in Figure 4.36 at the inlet the concentration is 6.9 mol/m³ as it makes 50% of the fuel. The concentration rises with the reduction of the OC since H_2 forms H_2O as a result. The concentration decreases after the OC is fully reduced, and the partial pressure of H_2 rises. The distribution illustrated in Figure 4.37 shows the c_{H2O} rise to 11 mol/m³, sharing the available volume with the present nitrogen. At later time steps we see a decrease of the H_2O concentration to 4 mol/m³—the ratio of the substance's changes. The fuel ratio H_2O/NH_3 is 1:1, as NH_3 decomposes in a ratio of 2:4, meaning the ratio between the substances changes for H_2O:N_2:H_2 to 1:0.5:1.5. According to the new ratio the maximal amounts in the reactor change to ~6 mol/m³ for H_2, ~4mol/m³ for H_2O and ~2 mol/m³ for N_2. Therefore, the distribution at t_{end} highlights a decrease in the concentration in the anterior part of the system. It is not immediate since the hydrogen c_{H2} is not available in the first volume elements.

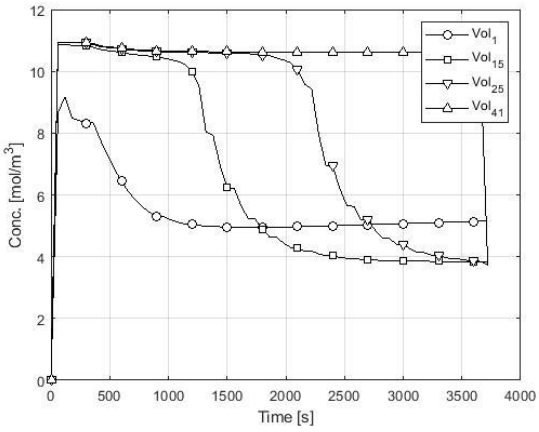

Figure 4.36: Concentration of H_2O at 700°C at Vol.1(o), Vol.15(□), Vol.25(▽) and Vol.41(△)

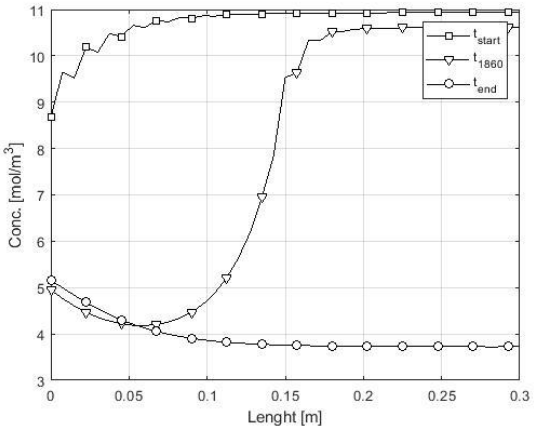

Figure 4.37: Distribution of H_2O at 700° at t_{start}(□), t_{1800} (▽)and t_{end}(o)

The example of Vol.20 depicts the interaction of the 3 gases over time in Figure 4.38. The reaction curve is steep, meaning a uniform breakthrough of the gas.

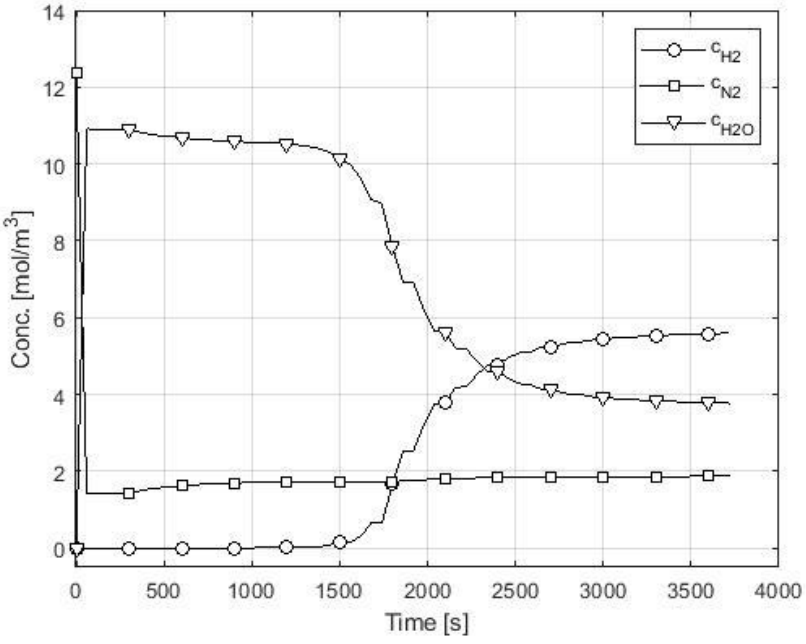

Figure 4.38: Concentration of H_2 (o):H_2O(□):N_2(▽) at Vol. 20 700°C

Fig. 4.39 shows the degree of oxidation of the OC of the different volume elements. The first Vol. reduces completely after 360 seconds. The prior decomposition has little influence on reducing the OC and reaching full reduction after ~63 min. The reactor reaches the c_{crit} when all the OC is reduced.

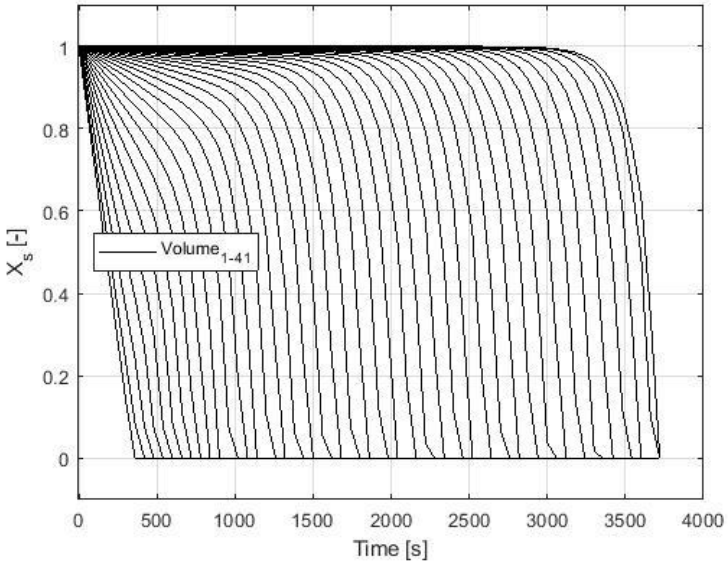

Figure 4.39: Degree of oxidation of the OC at 700°C of all volume elements

Fig. 4.40 shows the heat development of Vol.1-41. A strong temperature decline after the reduction in the first Vol. elements reflects the endothermic decomposition of ammonia. The reduction of the OC leads to a rise in temperature, with a maximal temperature rise of 109.89°C. The temperature rises during the reduction in average around ~100°C per element. The temperature is influenced strongly by the decomposition of ammonia. Figure 4.41 shows the distribution of the temperature at t_{end}. The front part of the reactor cools down to 642 °C while the rear half of the reactor shows a temperature rise to ~ 800 °C. The mean temperature of the reactor at the t_{end} is 766 °C.

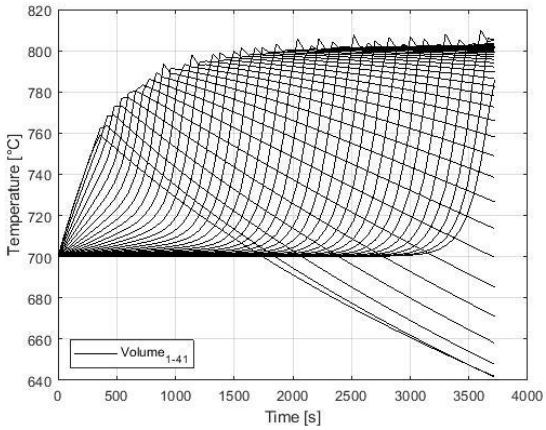

Figure 4.40 Temperature change over time of all volume elements

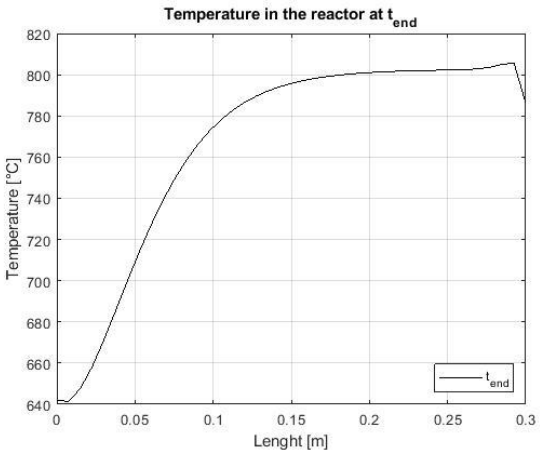

Figure 4.41: Temperature distribution at t_{end}

4.3.1. Comparison of reduction with NH_3 for different temperatures

For a better understanding of the dynamics, the experiments were repeated for the temperatures 500°C, 600°C, 800°C and 900°C. It is important to note here that a fixed rate of ammonia decomposition to nitrogen and hydrogen was assumed, as discussed in Figure *4.31* above. All other settings remain the same to create a good comparison and understand the influence the temperature has on the system. Important points of observation are:

- The degree of oxidation
- The heat development
- The time of the experiment

Table 4.3 summarizes some general information about the experiments conducted.

Table 4.3: Overview of the experiments with general information for the reduction with NH_3

	Comparison of reduction with NH3 for different temperatures				
Temperature [C°]	500	600	700	800	900
max. Concentration [mol/m³]	15.6	13.8	12.4	11.2	10.3
max. Concentration H2 [mol/m³]	7.8	6.9	6.2	5.6	5.0
max. Concentration H2O [mol/m³]	5.3	4.7	4.2	3.8	3.6
max. Concentration N2 [mol/m³]	5.3	4.7	4.2	3.8	3.6
time of operation [s]	3840	3780	3780	3720	3720
dT max [°C]	108.40	107.21	109.89	111.87	111.80

Figure 4.43 illustrates the distribution of the H_2 gas after 3600 seconds in the reactor. According to the ideal gas equation, the concentration is higher at lower temperatures. The distribution curve concords with this theory. The reaction proceeds similarly fast for all temperatures, except for 500°C.

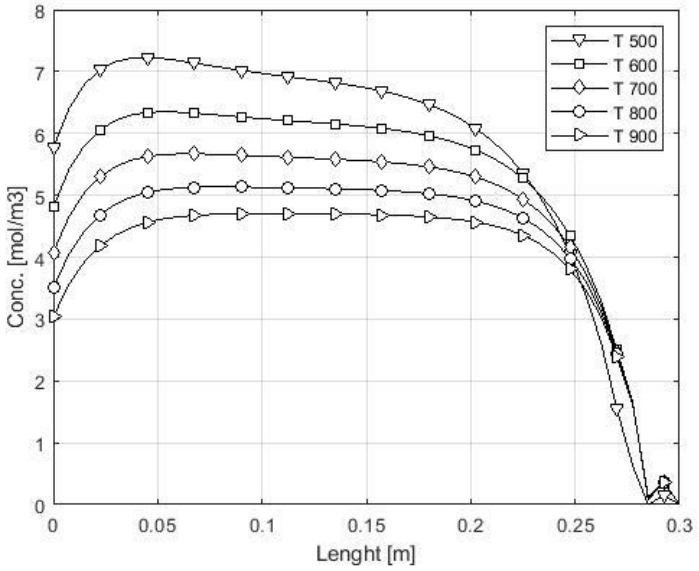

Figure 4.42: Distribution of H_2 for the different Temperatures at 3600 [500°C (▽), 600°C (□), 700°C (◇), 800°C (o), 900°C (▷)]

Figure 4.44 shows the difference in the degree of oxidation in Vol. 30 for all tested temperatures. The reduction proceeds faster for higher temperatures, although it varies only around 60 seconds. The breakthrough curve remains similar for all temperatures.

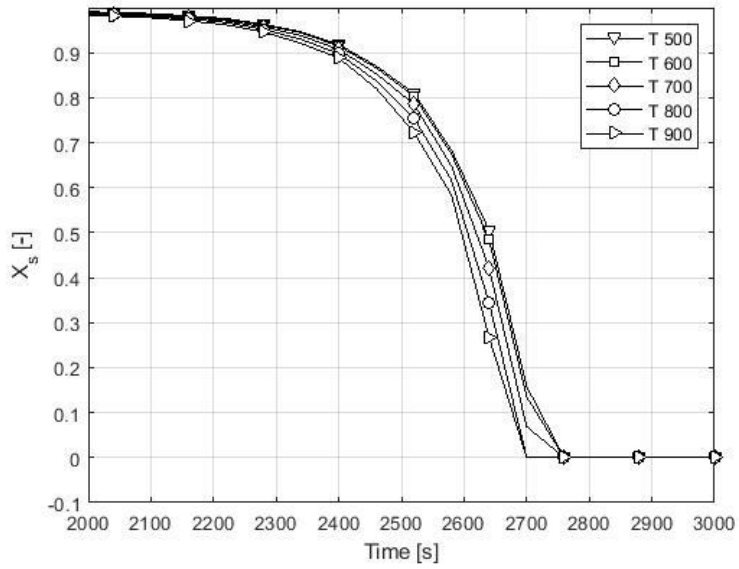

Figure 4.43: Degree of oxidation of volume 30 for different [500°C (▽), 600°C (□), 700°C (◇), 800°C (o), 900°C (▷)]

Figure 4.45 depicts the temperature difference during the experiment in Vol.7. A slightly higher temperature difference could be achieved with higher operating temperatures. The difference between operations at 500 and 900 °C is around 5 °C during reduction. Figure 4.46 illustrates the temperature difference distribution at t_{end}. Operating temperatures of

900 °C reach around 5 °C more in the whole reactor than the operating temperature of 500 °C.

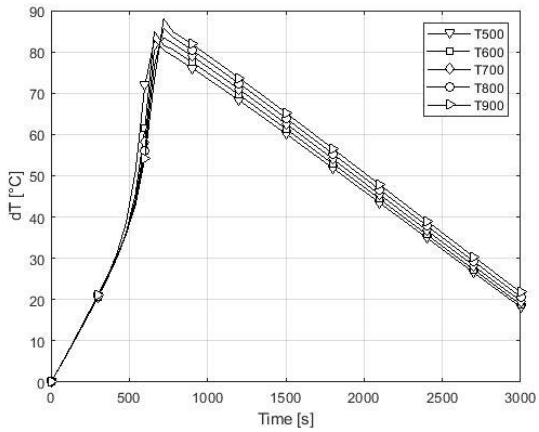

Figure 4.44: Temperature difference at Vol.7 for [500°C (-), 600°C(·), 700°C(·-), 800°C(-), 900°C(·)]

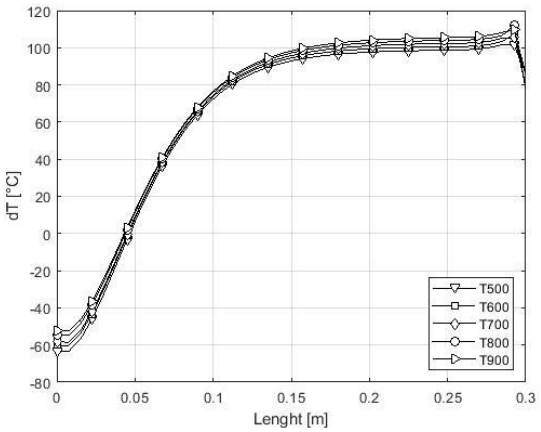

Figure 4.45: Temperature difference at t_{end} for [500°C (-), 600°C(·), 700°C(·-), 800°C(-), 900°C(·)]

4.4. Cyclic operation

The single operation gives a first impression of the reaction dynamics. To test the system properly, it needs to operate in a continuous experiment. More cycles were simulated continuously, where the degree of oxidation and the temperature were transferred as starting conditions for the next run. The starting conditions of the cyclic experiments were a fully oxidized OC. The fuel used for the reduction was hydrogen (100 vol %) and for oxidation air. The reactor was reduced and oxidized in 10 cycles, 10 times reduced, and 10 times oxidized. As seen in the prior experiments, it is crucial as one cycle does not lead to full oxidation. Hence it is very likely that the operation time diminishes while operating in cycles. After an undefined number of cycles, the reactor should reach an equilibrium, where the duration of one cycle, as well as the degree of oxidation, remain stable.

As for both reactions the OCs of the rear parts in the reactor remain unused, two different scenarios are considered.

- Injection of fuel and air from the same side
- Injection of fuel and air from opposite sides

The idea behind this is to achieve better utilization of the OC with the injection from opposite sides. For the cyclic tests, it was essential to extract the generated heat; otherwise, the reactor reaches far too high temperatures and distorts the results. An isothermal process is aimed at, meaning a constant mean temperature in the reactor. This approach correlates better with reality, where a stable temperature of the reactor is desired. The heat is removed over the whole reactor length continuously. In a practical test, a thermoelectric generator could be used or a water tank producing steam as a way to remove heat from the system. The heat calculates using the specific heat capacity as follows:

$$Q = dT \cdot m_{OC} \cdot cp_s \qquad \text{Eq : 4.1}$$

DT describes the temperature difference, mOC the mass of the oxygen carrier and cp_s is the solid material's heat capacity. In agreement with the first law of Joule, the power can be calculated as follows.

$$P = \frac{Q}{t} \qquad \text{Eq : 4.2}$$

The simulation allowed extracting a certain amount of power continuously to maintain the same mean temperature at the end of each operation. For heat removal, the values from Table 4.4 were assumed. The mass of the OC is calculated through the volume of the reactor and the OC density.

$$m_{OC} = V \cdot (1 - e_{bed}) \cdot \rho_{OC} \qquad \text{Eq : 4.3}$$

The heat capacity of solid bed inventory counts 1275 J/kg K, which is derived from the heat capacities of aluminum oxide and copper, also used in the prior experiments. For dT the mean temperature was calculated at the end of the reaction of the single operations.

Table 4.4 : Parameter and corresponding values for the calculation of generated power

m_{OC}	0.3298	kg
cp	1275	J/kgK
dT_{ox}	139.62	K
dT_{red}	94.45	K
t_{red}	2500	s
t_{ox}	3500	s
Q_{ox}	58707.41	J
Q_{red}	39714.49	J
P_{ox}	16.77	Watt
P_{red}	15.89	Watt

The power extracted during oxidation is only 1 Watt higher even though the temperature difference is around 45°C, but since the reaction time for the reduction is shorter, results in the given values for P. Both approaches are presented in the following section.

4.4.1. Cyclic experiment scenario 1

The experiment started with a reduction of a fully oxidized OC. 100 vol % hydrogen is used as fuel and air (21 vol% O_2 and 79 vol% N_2) for oxidation. The mol streams remained the same such as for the single operation. During reduction, a mol stream of 1.15E-04 mol/s is used and for oxidation 2.738E-04 mol/s. The OC, as well as the geometry of the system, remained the same explained in section 3. The removed power changes for reduction and oxidation, according to Table 4.4. The scenario concept is exemplified in Figure 4.47.

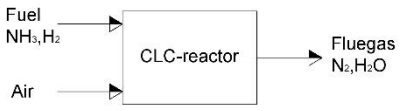

Figure 4.46: The concept of cyclic operation injection from fuel and air from the same side

Figure 4.48 shows the degree of oxidation of the last two volume elements since all others completely oxidate and reduce in 1 cycle. While Vol.41 reduces entirely but oxidates only half the OC, does Vol.40 only shows partial oxidation and reduction for all cycles with the usage of ~ 80-90% of the OC. The cycles start with a full oxidized OC and are reduced first. The break condition for operation remains c_{crit} (10% of inlet concentration) of fuel/air at the outlet. The reactor is purged with nitrogen after every cycle. The operation time decreases after every cycle. Since not all of the OC is transformed fully, c_{crit} is reached faster as in single operation experiments. While the first reduction takes 2810 sec to complete, the last reaction takes 2700 sec. The oxidation takes significantly more time, 3600 seconds for the first cycle and 3630 for the last. The whole experiment (10 cycles) needs 63580 seconds to finish, approximately 17.5 h.

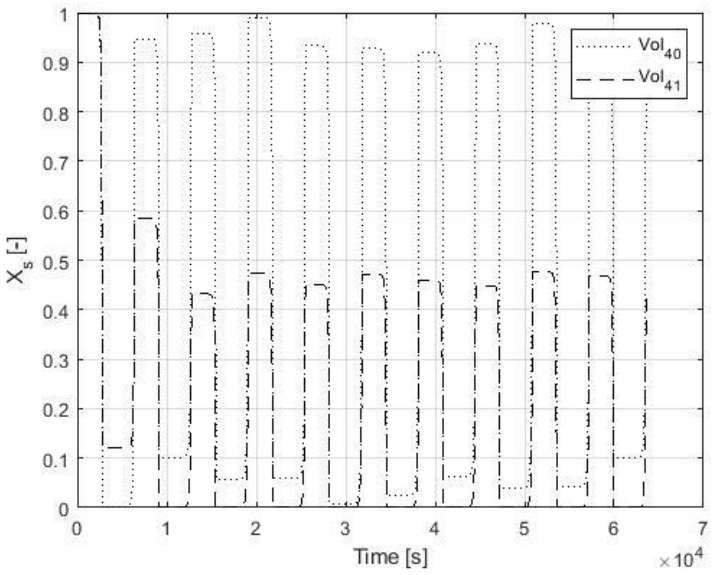

Figure 4.47: Degree of Oxidation of Volume 40 - and Vol 41 -- segments over time

While the reduction diminished operation time over the cycles, the oxidation showed a slight increase. One cycle takes ~106 min to complete. Figure 4.49 illustrates the temperature development over time in all volumes. A slight decrease in the mean temperature of around 2 °C is noted after every cycle. As the OC reacts, the temperature rises due to the exothermic reaction. The heat is continuously removed during the operation over the whole reactor length, leading to a continuous decrease of temperature if no reaction is occurring.

The mean temperature shows a decline after 10 cycles of 21 °C. We can see a slight increase in the temperature of around 5°C during the oxidation during one cycle, while during reduction, the temperature diminishes approx—6 °C. The reactor reaches the highest and lowest temperatures during oxidation.

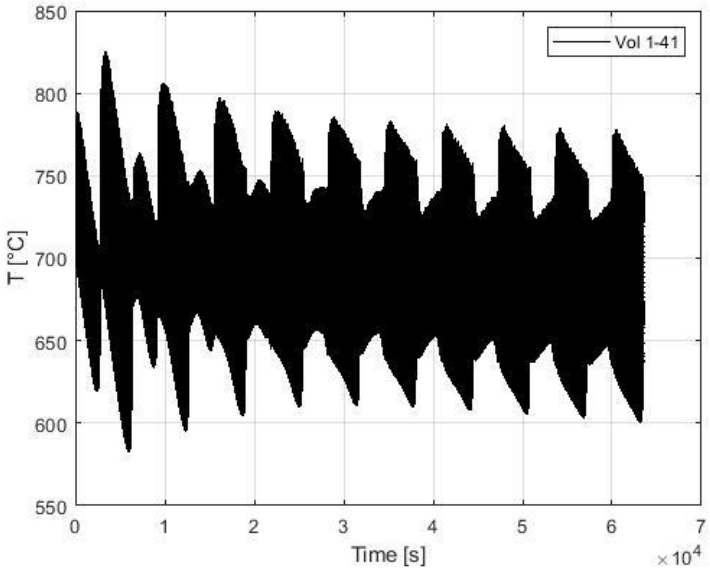

Figure 4.48: Temperature change over time of the 10 cycles of all Volume segments

Let's compare the temperature development in Vol. 1 illustrated in Figure 4.50 with Vol.41 in Figure 4.51. It shows that Vol. 1 heats up at the beginning of each operation, while the temperature in Vol.41 sinks first and heats up as soon as the reaction front reaches the volume. The mean temperature is higher at Vol. 1. Moreover, both diagraphs illustrate a temperature shift four times per cycle.

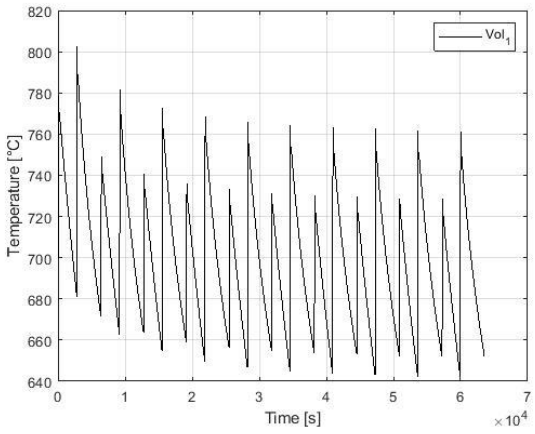

Figure 4.49: Temperature development in Vol.1 over 10 cycles

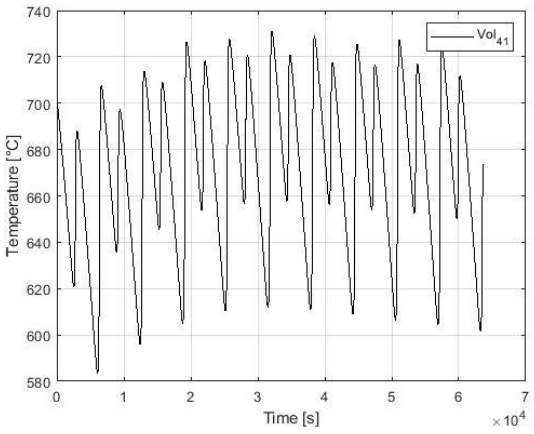

Figure 4.50: Temperature development in Vol.41 over 10 cycles.

Figure 4.52 gives a closer view of the degree of oxidation during the oxidation and reduction at the respective last cycle. The OC is reduced to 99.9 % during reduction, shown with the solid line marked by circles. A little part of Vol.40 seems to not be fully reduced. The oxidation shows that a significant part of the OC at the end of the reactor unused. 50 % of the Vol.41 and about 5% of Vol. 40.

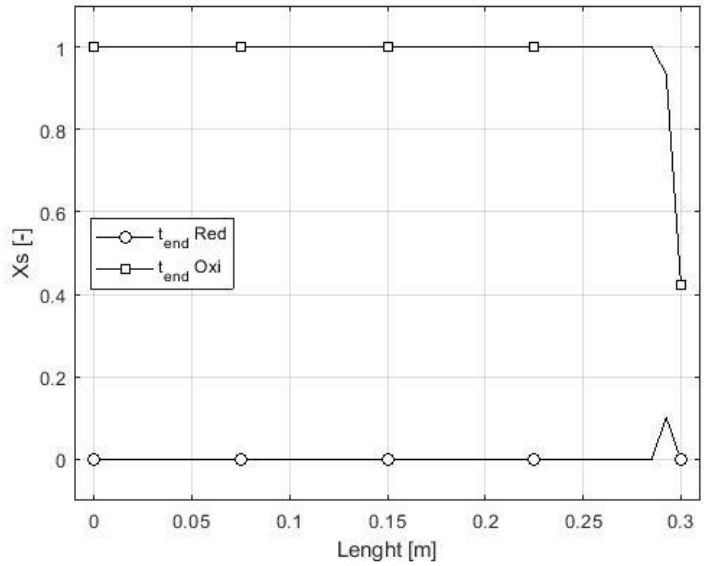

Figure 4.51: Degree of Oxidation at t_{end} (·) of Oxidation and t_{end} (-) of reduction of the last cycle

4.4.2. Cyclic experiments scenario 2

The cyclic experiments are repeated for an injection of the fuel and air at opposite sides. Figure 4.53 illustrates the concept. Better usage of the OC is expected with this approach, even though for practical experiments, it poses various technical issues, as the piping system is needed on both sides as well as a control system, to observe the flue gas concentrations.

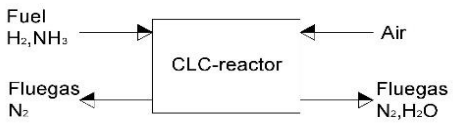

Figure 4.52: Concept of cyclic operation injection from fuel and air from the same side

To create a fair comparison, apart from the injection site, the entry values and heat removal remain the same, as listed in Table 4.4. The cycle starts again by reducing a fully oxidized OC. The fuel gets injected in Vol. 1 while the oxygen is introduced into Vol. 41. Figure 4.54 shows the degree of oxidation of the first two and the last volume element since all others completely oxidate and reduce in 1 cycle. While the Vol.1 and Vol.2 do not oxidate, Vol.41 does not reduce entirely. In Vol. 1, only half of the OC oxidates, while Vol.2 over 90% with little variations. Also, Vol.41 reduces nearly completely (< 90 %), showing notable differences between the cycles. There were few changes to observe during the operation time, though a steady increase is noted, leaving the assumption that it did not find equilibrium. While the reduction seems stable after 2810 seconds, the oxidation shows a steady increase and rises from the first to the last cycle by 30 seconds to a total of 3630 sec. A significant difference, though, can be noted for the oxidation and reduction time. The whole experiment took 64250 seconds, around 17.9 h; one complete cycle took ~107 min.

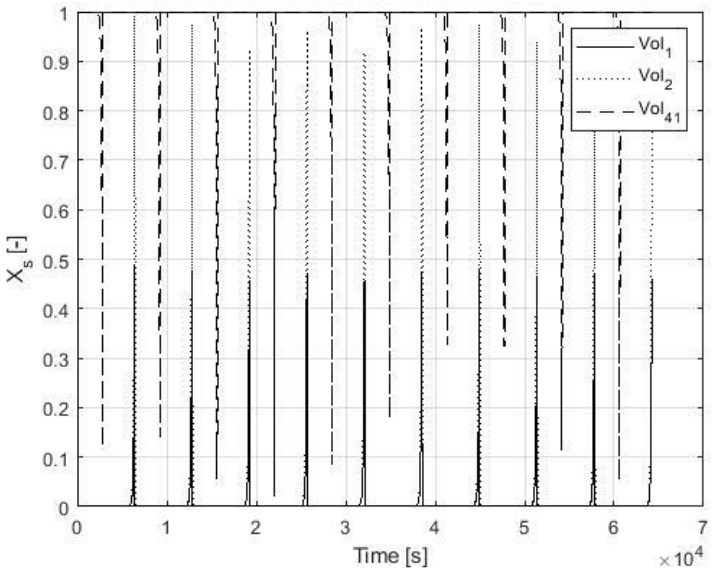

Figure 4.53: Degree of Oxidation of Vol.1(-), Vol.2(·) and Vol.41(--) over time

Figure 4.55 shows the heat development over 10 cycles of all volumes. The overall mean temperature shows a decrease of ~14 °C after the experiment. The different operations can be identified immediately. After oxidation the mean temperature rises around 6°C, the reduction shows a temperature decrease after each operation. Surprisingly, the reactor reaches its maximal temperature after 5 cycles during the reduction reaction. Since the

oxidation reaction terminates in the front part, the reactor immediately heats up again, resulting in the highest temperature.

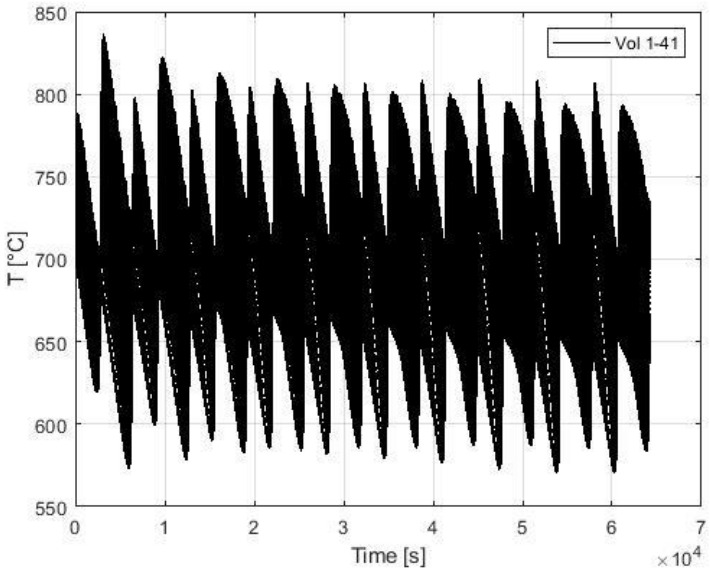

Figure 4.54: Temperature development of all volume elements over 10 cycles.

Figure 4.56 illustrates that the temperature distribution, especially after the reduction, shows a strong decrease after many cycles in the reactor's rear part. The first cycles show a more equilibrate temperature in the reactor, while after 7 cycles a temperature difference of ~20°C between the front and rear part of the reactor is noted.

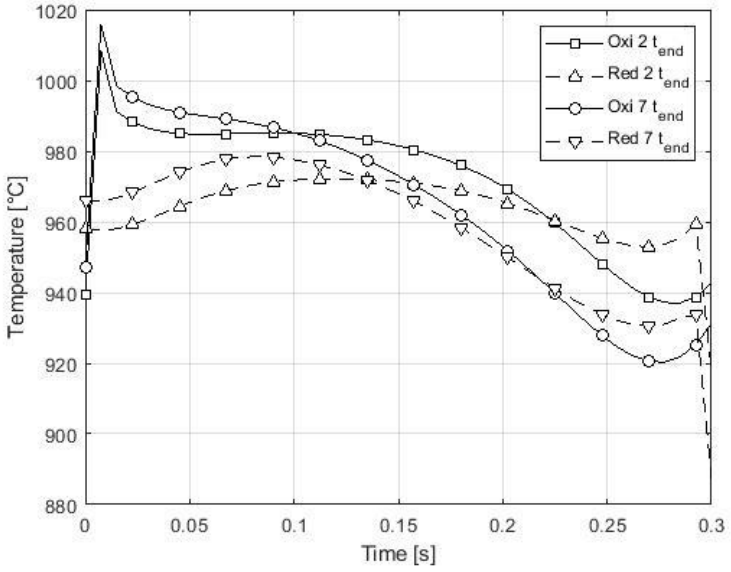

Figure 4.55: Comparing the temperature distribution of both reactions at t_{end} of cycle number 2 and 7

When comparing the temperature in Vol. 1 in Figure 4.57 with Vol. 41 illustrated in Figure 4.58, little differences in the patterns can be seen. Nonetheless, the mean temperature in Vol. 1 shows a little increase, Vol. 41 shows a small decrease. The temperature shows two shifts of temperature in one cycle.

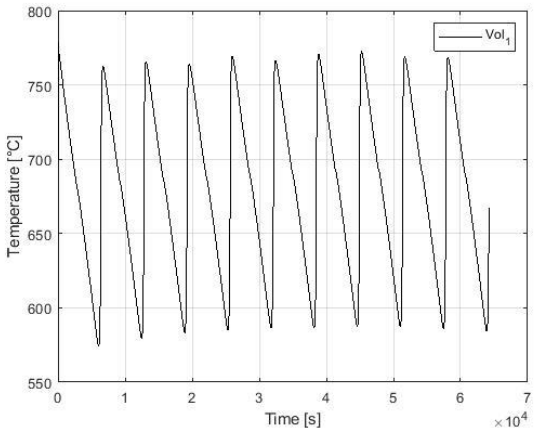

Figure 4.56: Temperature development over 10 cycles at Vol.1

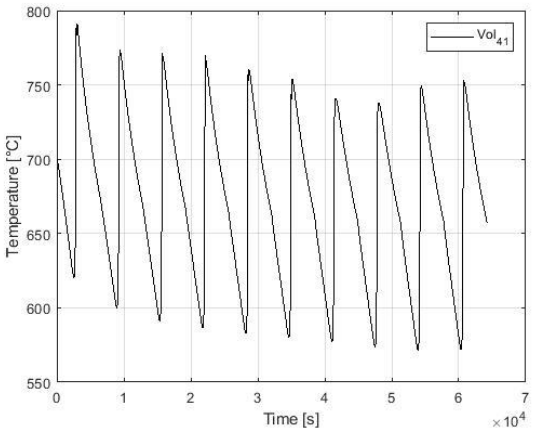

Figure 4.57: Temperature development over 10 cycles at Vol.41

Figure 4.59 illustrates the degree of oxidation at t_{end} of the reduction and over the reactor's length. It affirms the better conversion of the OC during reduction. Only 5 % of the OC are not reduced. In contrast, the oxidation leaves a notably larger part of OC unreacted, around 50% in the last volume and ~5 % in the second to last.

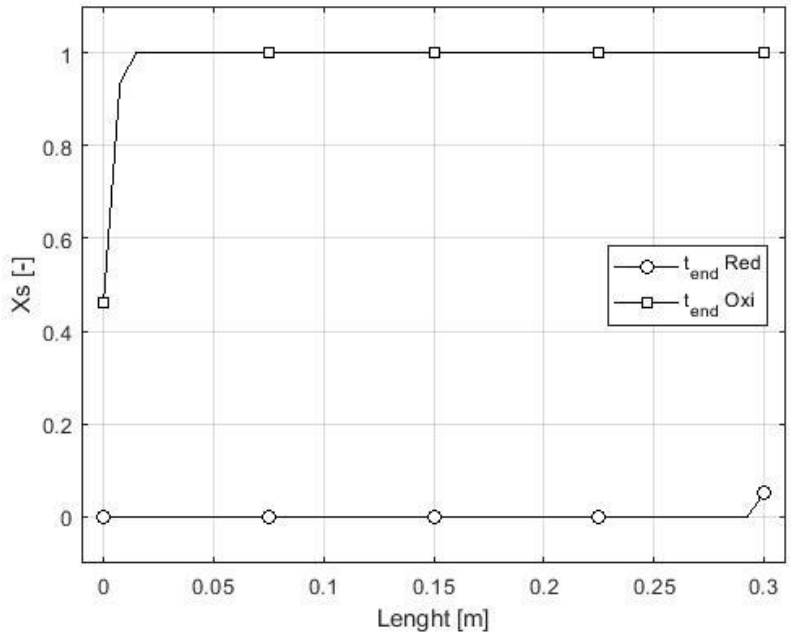

Figure 4.58: Degree of oxidation of oxidation (·) and reduction (-) at t_{end} ot the last cycle

5. Discussion

The next chapter summarizes the results obtained and compares different temperatures as well as the efficiency between both fuels used. These results allow predictions about conversion rate, duration and heat development for a practical test. The reactor model assumes small proportions; this leaves some uncertainties about upscaling the system even though it gives an excellent first impression of the reaction dynamics.

5.1. Reduction with Hydrogen H_2

The reduction of copper-based OC with hydrogen is tested abundantly in prior studies because of copper's high reactivity, even though only one active CLC reactor over 10kW is in operation with a copper-based OC. The institute of carbochimica in Spain uses a fluidized bed regime on copper-based OC and CH_4 as fuel.[19] CH_4 has much higher reaction enthalpies than H_2. The excellent conversion properties of H_2 and the simplicity in the reaction were the main reasons for the testing. Moreover, it allows a good comparison to the reduction with ammonia since the reducing agent is always hydrogen.

First experiments were done at an inlet fuel gas temperature of 700°C. The enthalpies for the reduction count 96.99 kJ/mol. The model worked fine and reflected the kinetics predicted by Abad okay [24]. The theoretical approach (all of the OC reacts) assumes a rise of 96.99 °C, while the model predicts a rise of ~94 °C. Satisfying results obtained were the conversion of the fuel as well as the reduction of the OC. These correlate well with the literature and confirm the accuracy of the simulation. The simulation shows an even usage of the OC as well as the distribution of temperature. c_{crit} is reached after full conversion of the OC. For the single operation, the inlet gas temperature was varied to understand the influence and allow a suggestion for practical experiments. The temperature does influence the reaction slightly. The breakthrough curves of the gas, as well as the conversion of the OC, show similar results for all temperatures, even though higher operating temperatures lead to a higher temperature difference.

Table 5.1: Summary of the results of the single operation with H_2 as fuel for different temperatures

Comparison of reduction with H_2 for different temperatures					
Temperature [C°]	500	600	700	800	900
Heat [J]	38285.5	38956.6	39619.4	40240.2	40831.7
Tmean [°C]	591.3	692.9	794.5	895.9	997.3
time of operation [s]	3030	2990	2960	2930	2910
dT max [°C]	103.23	103.86	106.40	107.41	108.90
P [Watt]	12.64	13.03	13.38	13.73	14.03

Moreover, the starting temperature has a significant influence on the operation time. The reduction of the reactor with fuel at 100 vol % H_2 took ~50 min. The time varies for the different temperatures of about 5 min on this small scale.

To conclude, the gas breakthrough curve is equal for all temperatures. Higher temperatures lead to a slightly stronger increase in temperature and reduce the reduction time. The gas and reactor need to be heated up more, which results in higher energy input.

5.2. Oxidation

To hold the costs of operation low, air is used for the oxidation of the CLC reactor. For the model, the air constituents are 21 vol % oxygen and 79 vol % nitrogen, neglecting the other, most prominently Ar and CO_2. The reactor produces most of the heat during oxidation as the reaction enthalpy is - 150.70 kJ/mol and around 53.71 kJ/mol higher than for reduction. The temperatures are varied in the same manner as for the reduction with H_2. This test assumes a wholly reduced OC in an adiabatic system. The oxidation takes longer than the reduction.

The air temperature for the first experiment was 700°C. The Oxygen carrier does not oxidate completely after one experiment. The outlet signal is not reliable; therefore, a second break condition is added, that c_{crit} was only valid if the X_s of Vol 40 was higher than that in Vol. 41.

The same temperature variation was tested as for the reduction. The time of operation decreases strongly; while the operation at 500 °C took ~73 min, it takes 50 min at a temperature of 900°C. On the contrary to the reduction with H_2, the temperature

difference decreases with higher temperatures. The maximal temperature rise occurred at a temperature of 500 °C. Also, the mean temperature is higher (~5°C) for lower temperatures. Since the gas moves slower, the heat can diffuse and heat the solid material in contact. The heat generated nonetheless remains significantly higher for high temperatures due to the shorter operation time.

Table 5.2 : Summary of the results of the single oxidation for different temperatures

Comparison of reduction with O2 for different temperatures					
Temperature [C°]	500	600	700	800	900
Heat [J]	60261.78	59875.86	58567.10	58294.44	57887.55
Tmean [°C]	643.66	742.74	839.62	938.97	1038.00
time of operation [s]	4360	4110	3500	3170	3090
dT max [°C]	180.84	178.67	167.44	164.20	163.20
P [Watt]	13.82	14.57	16.73	18.39	18.73

This contradicts the observations made by Abad [23,24], who measured a greater influence on the reduction reaction. However, were the test made with a TGA, which measures only a small part of OC. The gas propagation is similar even for reduction, achieving 99% oxidation of the OC. The reactor does heat up very fast at the beginning of the reactor and during reduction underlining copper's high reactivity.

5.3. Reduction NH_3

For the prior discussed experiments, different literature for comparison and kinetics are available. Ammonia poses a new fuel for investigation. The idea derives from the Project Ammonia2Heat, with the idea to utilize ammonia obtained out of sewage sludge and biogas residues. The considerations taken for the thermodynamics are explained in prior sections. Ammonia decomposes in an endotherm reaction reducing the energy output. The observations make clear that ammonia is not as efficient as pure hydrogen. But since it can diminish the WWTP's purification costs, it poses a possible available alternative to load a CLC reactor.

The first experiments consider a fuel temperature of 700°C. The model assumes a 99 % conversion of ammonia within the first 10 cm. Practical test must confirm these

assumptions since most experiments use a catalyst for the decomposition. The experiments took around 3800 seconds (~ 70 min). The additional time compared to the reduction with H_2 also arises due to the mixture of fuel with steam (ratio NH_3:H_2O = 50:50). This choice was made to limit the temperature loss at the front part of the reactor. Vol.1 at the example of 700 °C reduces nearly four times slower than the reduction with H_2, in 420 seconds. Because of the low concentration of the reacting agent in the first volume element, ammonia needs to decompose first. The mean temperature at the end of the reaction rises ~65°C, 30 °C less than during reduction with H_2. After an initial increase due to the reduction reaction, heat loss prevails according to the endotherm decomposition in the reactor's front part. A heat front moves with the reaction through the reactor. The reactor heats up similarly to the reduction with H_2, with the explained difference at the front. However, a higher absolute maximum is reached with ammonia as fuel. This can be explained according to the longer reaction time and the axial heat dispersion.

The reduction was repeated for the same temperature variations as the oxidation and reduction with H_2. The temperature shows a similar dependency on the starting temperature as the reduction with H_2, meaning an increase of mean temperature and dT_{max}, as well as a decline of operation time. However, the temperature shows less influence on the operation time for NH_3. The reaction takes 64 min for 500°C to reach c_{crit}. It takes 14 min longer than the reduction with H_2. This proves the functionality of the model also for ammonia, although it shows a minor efficiency. The reaction time also decreases for higher temperatures, with a difference of 120 seconds (2 min).

Table 5.3: Summary of the results of the single operation with NH_3 as fuel for different temperatures

Comparison of reduction with NH_3 for different temperatures					
Temperature [C°]	500	600	700	800	900
Heat [J]	26372.39	27085.50	27664.38	28398.46	28964.75
Tmean [°C]	562.87	664.57	765.95	867.70	969.05
time of operation [s]	3840	3780	3780	3720	3720
dT max [°C]	108.40	107.21	109.89	111.87	111.80
P [Watt]	6.9	7.2	7.3	7.6	7.8

Without copper as OC and a high reaction enthalpy for reduction, it is questionable if ammonia is feasible, as the temperature could decrease too much. Ammonia seems to

work as a reducing agent for practical experiments. Still, the question remains if ammonia decomposes under high temperatures completely as assumed, which could be guaranteed by using a catalyst. Nickel could pose a promising candidate since it is a widely used and known catalyst and is also tested abundantly as OC for CLC. The advantage of copper is the strong exotherm reactivity during reduction, which nickel does not have.

Since ammonia is a very requested chemical for agriculture as fertilizer, it seems wasteful to use it as fuel. Producing green ammonia can reduce the very energy-demanding production of conventional ammonia production via the Haber Bosch Process, contributing to high emissions on a global scale. Nevertheless, long term storage mediums are an additional option in the sustainable energy/heat supply mix. Furthermore, as explained in section 2.5, ammonia gained interest as a storage medium for H_2. But it is still at the very beginnings, and the effectiveness is questionable. [52] But if the fertilizer market is saturated or the law restrictions don't allow further nitrogen fertilizer usage, it can be an interesting option to limit high concentration in the groundwater and find usage for ammonia.

5.4. Comparing the results of the experiments for the single operation

To create a better overview between the single operations, they are compared in the operation time, the temperature difference at t_{end} and the heat generated in diagrams below. In Fig. 5.1 the operation time is illustrated, showing a decline for all experiments with higher temperatures. While little changes of time for the reduction experiments are noted, especially for the reduction with ammonia, the oxidation times show a strong decrease. A change from 20 min between 500°C and 900°C is noted. The results of the experiments conducted by García Labiano [23], could not show the same influence of the temperature on the operation time.

In contrast, his experiments showcased a more decisive influence of the temperature on the operation time for the reduction with H_2. The temperature in this work showed a higher impact on the oxidation reaction. It must be noted that different concentrations were used for the reduction reaction, and experiments were made in a TGA with a tiny amount of OC.

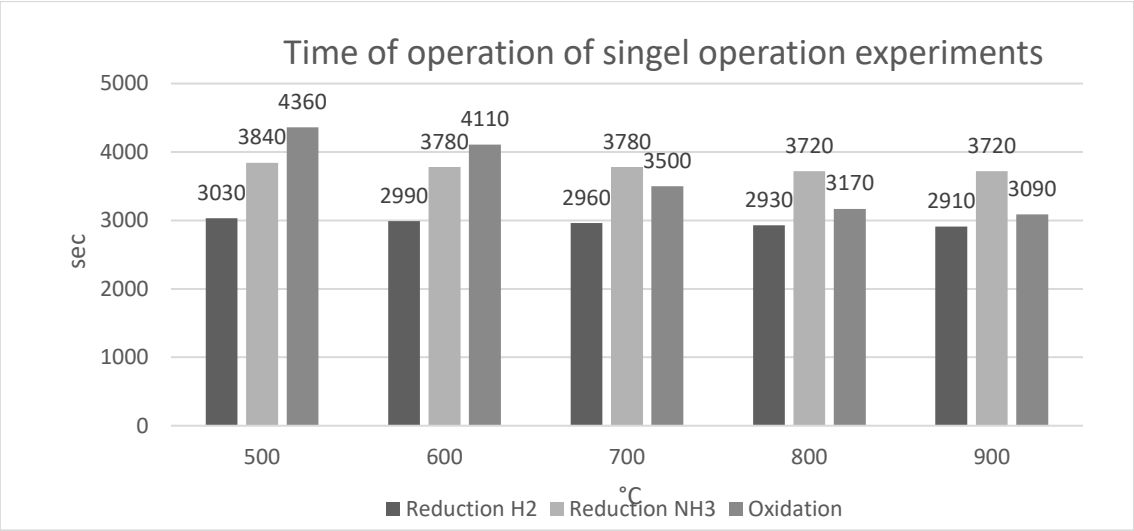

Figure 5.1: Comparison of operation time of single run experiments

The mean temperature difference, depicted in Fig. 5.2, was measured over the reactor's whole length at t_{end}. It showed a temperature change during the reduction of ~94°C and oxidation ~ 140 °C. This correlates very well with the reaction enthalpies. Surprisingly, the temperature difference decreased for the oxidation at higher temperatures, while the reduction reaction showed an increase in dT with the rise of temperature.

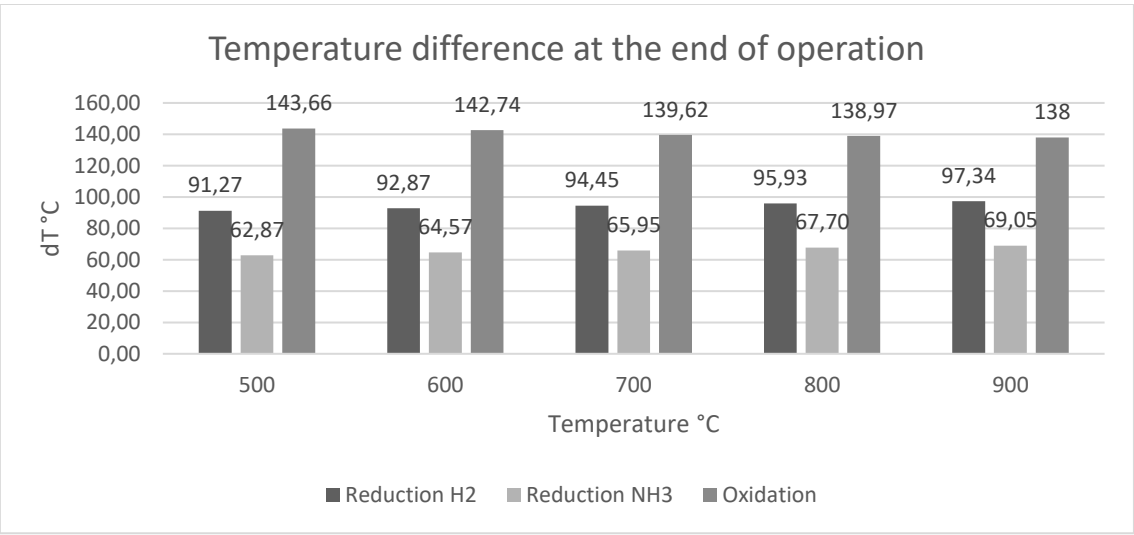

Figure 5.2 : Comparison of the temperature difference at t_{end} for single run experiments

The heat generated, illustrated in Figure 5.3 for the reduction with ammonia (7 watts), is half of the heat generated by the reduction with hydrogen (13 watts) and showed a slight increase with higher temperatures. While a substantial increase in heat generated could be noted for the oxidation (~5 watts), this can be attributed mainly to the reduction of the operation time.

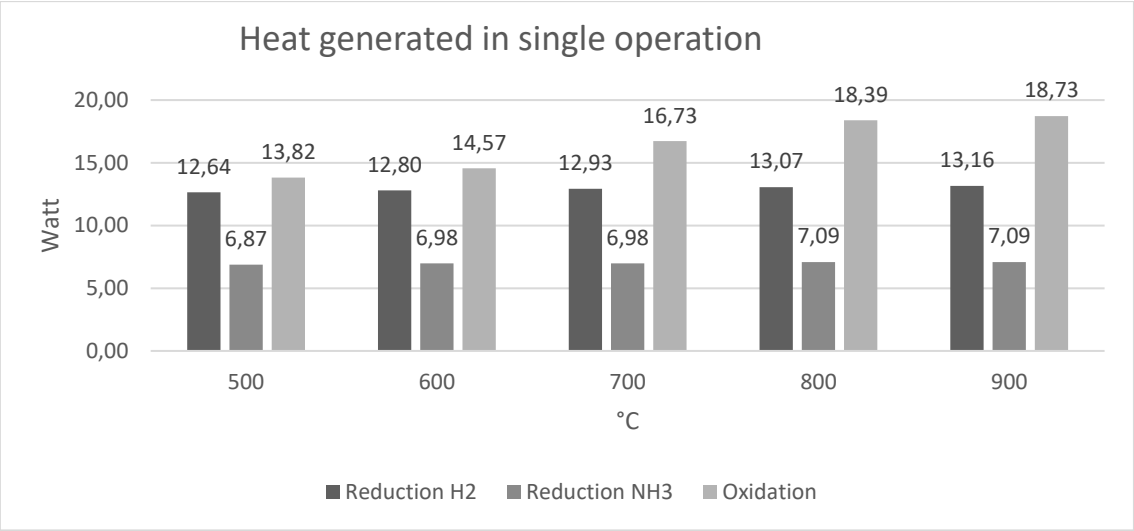

Figure 5.3: Comparison of the heat generated for different temperatures fuels/air

5.5. Cyclic operation

The cyclic operation is vital for a good understanding of efficiency. In a single operation, the OC does not convert fully. This leads to a loss of heat in the reactor. Two approaches are considered; in the first scenario, the fuel and air are injected from the same side, while in the second scenario, the air and fuel are injected from the opposite side. Both cyclic operations left a part of the OC unused during the oxidation reaction and showed advantages and disadvantages.

16.77 watts are extracted during oxidation from the reactor, and 15.89 watts during reduction to maintain it isothermally. The heat gets extracted continuously over the whole length of the reactor. The same entry parameters were used for both experiments to allow a fair comparison.

Same side

Table 5.4: Summary of the cycles with injection from the same side including duration, T_{mean} ,T_{max} ,T_{min}

	1. cycle	2. cycle	3. cycle	4. cycle	5. cycle	6. cycle	7. cycle	8. cycle	9. cycle	10. cycle
max. Tox [°C]	825.6	806.1	797.5	789.9	786.1	783.1	781.7	780.6	779.1	778.5
max. Tred [°C]	788.7	763.7	753.2	754.0	753.0	758.5	755.3	751.3	755.3	752.1
min.Tox [°C]	582.4	594.9	604.0	609.5	610.7	610.0	607.6	605.2	603.2	600.4
min.Tred [°C]	619.0	633.8	643.7	644.7	641.2	638.9	637.5	636.4	635.3	634.8
mean T oxi [°C]	698.1	696.8	694.7	692.1	689.5	687.0	684.9	683.0	681.1	679.8
mean T red [°C]	690.6	690.2	689.2	687.2	684.8	682.3	680.0	678.1	676.2	674.6
t [s]	6410	6360	6370	6360	6360	6350	6340	6350	6350	6330
t [min]	106.8	106.0	106.2	106.0	106.0	105.8	105.7	105.8	105.8	105.5

Opposite side

Table 5.5: Summary of the cycles with injection from the opposite side including duration, T_{mean} ,T_{max} ,T_{min}

	1. cycle	2. cycle	3. cycle	4. cycle	5. cycle	6. cycle	7. cycle	8. cycle	9. cycle	10. cycle
max. Tox [°C]	836.8	822.4	812.7	809.2	805.7	801.8	800.4	795.7	794.7	794.1
max. Tred [°C]	788.7	797.9	802.4	804.3	807.2	807.0	808.6	809.7	808.2	807.0
min.Tox [°C]	573.0	578.3	582.2	583.9	585.5	585.5	586.5	586.6	584.8	583.2
min.Tred [°C]	619.0	599.0	589.9	585.1	581.5	578.9	576.2	572.5	570.4	570.5
mean T oxi [°C]	698.7	698.0	696.9	695.6	694.1	692.6	691.0	689.3	687.8	686.5
mean T red [°C]	690.6	690.1	689.2	688.1	686.9	685.7	684.5	682.9	681.1	679.6
t [s]	6410.0	6410.0	6420.0	6430.0	6430.0	6430.0	6420.0	6420.0	6440.0	6440.0
t [min]	106.8	106.8	107.0	107.2	107.2	107.2	107.0	107.0	107.3	107.3

The mean temperatures after oxidation of the two different approaches of each cycle are compared in Figure 5.4. Scenario 2 seems to have a more balanced utilization of the OC. Moreover, it generates more heat than scenario 1 though the difference is not substantial (7 °C after 10 cycles). The degree of oxidation is very similar for both experiments.

Moreover, the OC is worn down faster in scenario one, where the OC gets heated up and cooled down twice as much. This further favor scenario two, since the OC is a valuable material, and its lifetime should be kept as long as possible. The main advantage of scenario one are the lower construction costs. Hence the additional piping and control system increase the construction costs significantly for scenario 2. The economic analysis is not part of this work, but an injection from opposite sides seems favorable from a technical perspective.

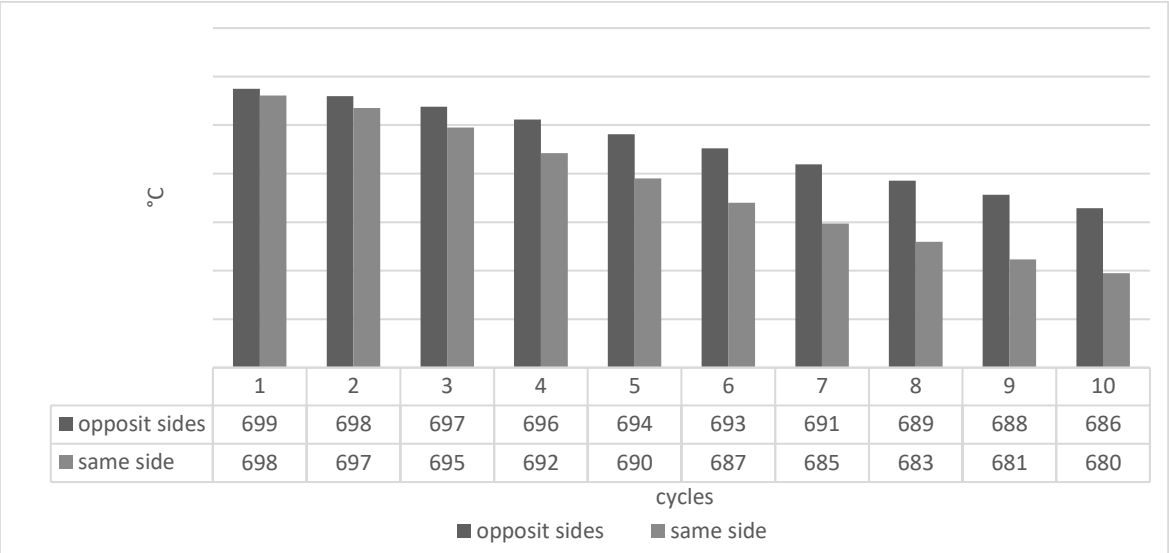

	1	2	3	4	5	6	7	8	9	10
opposit sides	699	698	697	696	694	693	691	689	688	686
same side	698	697	695	692	690	687	685	683	681	680

Figure 5.4: T_{mean} after oxidation of each cycle of the 2 different approaches (1. Injection same side 2. Injection opposite sides)

6. Conclusion

For the present thesis, a mathematical simulation of a fixed bed CLC reactor was tested with a copper-based OC. The influence of the operating temperature in a fixed bed CLC reactor using H_2 for reduction and O_2 for oxidation was observed. The usage of ammonia to reduce the reactor poses a new idea and was also investigated at different temperatures. The experiments started in connection with the project Ammonia2HeatStorage. This thesis presents the first results of the model. The simulation tests H_2 and ammonia as fuel and air for oxidation in a single operation. To create a more profound knowledge of the process, cyclic operations with H_2/air were conducted. The model was available at the Institute for chemical and energy engineering at the BOKU. It was adjusted and used for this thesis.

These results allow suggestions for practical tests but must be proven first since ideal conditions are assumed. The results can be summarized as follows:

- The reduction process with 100 vol% H_2 resulted in a good breakthrough curve and showed excellent usage of the OC for all temperatures, with conversion rates up to 100%.
- The temperature showed little influence on the reaction dynamics. A small reduction of the operation time could be observed, and additional heat was generated. The degree of oxidation remained the same for all temperatures.
- This leads to the conclusion that it is not reasonable to run the CLC reactor at high temperatures since the gas and the reactor must be heated up at desired temperatures resulting in much higher energy input.
- For the oxidation reaction, the temperature showed a significant influence on the reaction time; this also results in higher heat output. The degree of oxidation remained similar for all experiments leaving a small part of OC at the reactor end unused.
- Therefore, it could be meaningful to operate at higher temperatures, although it must be cleared how much additional energy is necessary to heat the air and reactor.
- Furthermore, higher temperatures lead to more chemical/physical stress opposed on the OC, although it proved its stability over more cycles in prior experiments conducted by Labiano and Abad [23,24]. The attrition and sintering processes rise at high temperatures reducing the lifetime of the OC.

A closer look was given to the reduction reaction of ammonia since it was never tested before.

- Ammonia showed good conversion of the OC, reducing the reactor entirely, taking about 10 min (total 1h) more than the reduction with H_2. However, the fuel ratio counts only 50 vol% as NH_3 was provided in a 50:50 molar mixture with water vapor.
- The temperature rose during the reaction also in the front part where the decomposition happened. The influence of the endotherm reaction was thought clearly visible. The reactor showed a decrease to the initial temperature at the front

part. Nevertheless, the rear part's temperature rose similar to the experiments with H_2, resulting in a mean temperature rise of 66 °C over the whole reactor length. (700°C)

- The influence of the temperature resulted similarly to the influence observed for the reduction with H_2. Small improvements in the operation time and the heat output could be observed. It can be suggested to run it at lower temperatures starting at 600 °C since an improvement to 500 could be seen, and the decomposition of NH_3 is more likely.
- The heat output was half the amount (~6 watts) of the output with H_2.
- Since ammonia has a high market value as fertilizer and conventional production is very energy-demanding, it seems not meaningful to use ammonia as fuel.
- It presents though an alternative use of ammonia and can be used to store heat over long periods and contribute to a sustainable supply mix of heat/energy.

The cyclic experiments give a first impression of the energy output under continuous operation. The degree of oxidation and the oxygen carrier usage showed an excellent conversion rate for both experiments. However, scenario 2 (injection of fuel and air from opposite sides) generated more heat than scenario 1 (injection of fuel and air from the same sides) under the same conditions. The OC usage was more uniform for scenario 2 and left the assumption of a longer lifetime of the OC. This must be verified through practical experiments. Looking only at the reactor performance a better working system for scenario 2 is predicted.

The lower construction costs strongly favor scenario 1. Since the additional piping and control system is connected with high costs, an economic analysis should provide information about which scenario is more economical considering heat generated, construction costs, and OC's lifetime.

List of Tables

List of Figures

Bibliography

(1) *Climate Change 2014: Synthesis Report*; Pachauri, R. K., Mayer, L., Intergovernmental Panel on Climate Change, Eds.; Intergovernmental Panel on Climate Change: Geneva, Switzerland, 2015.

(2) Tubiello, F. N.; Salvatore, M. Agriculture, Forestry and Other Land Use Emissions by Sources and Removals by Sinks. **2014**, 89.

(3) *Climate Change 2014: Mitigation of Climate Change: Working Group III Contribution to the Fifth Assessment Report of the Intergovernmental Panel on Climate Change*; Intergovernmental Panel on Climate Change, Edenhofer, O., Eds.; Cambridge University Press: New York, NY, 2014.

(4) Representative Concentration Pathway https://www.esrl.noaa.gov/gmd/ccgg/trends/mlo.html (accessed Jun 7, 2020).

(5) Blunden, J.; Arndt, D. S. State of the Climate in 2018. *Bull. Am. Meteorol. Soc.* **2019**, *100* (9), Si-S306. https://doi.org/10.1175/2019BAMSStateoftheClimate.1.

(6) Globale Allmende https://globale-allmende.de/Klima/ipcc/prognosen (accessed Jun 7, 2020).

(7) https://climate.nasa.gov/evidence/ https://climate.nasa.gov/evidence/ (accessed Jun 5, 2020).

(8) UNFCCC https://unfccc.int/process-and-meetings/the-paris-agreement/what-is-the-paris-agreement (accessed Jun 16, 2020).

(9) Tsupari, E.; Tähtinen, M.; Kärki, J. Feasibility of Solid Fuel CLC Plant Investment in the Future Energy Systems Including High Share of Solar and Wind. *Energy Procedia* **2014**, *63*, 7508–7516. https://doi.org/10.1016/j.egypro.2014.11.787.

(10) IEA https://www.iea.org/about/mission (accessed Oct 1, 2020).

(11) Science Communication Unit. *Nitrogen Pollution and the European Enviroment*; Science Communication Unit, University of the West of England (UWE), Bristol, 2013.

(12) Suddick, E. C.; Whitney, P.; Townsend, A. R.; Davidson, E. A. The Role of Nitrogen in Climate Change and the Impacts of Nitrogen–Climate Interactions in the United States: Foreword to Thematic Issue. *Biogeochemistry* **2013**, *114* (1–3), 1–10. https://doi.org/10.1007/s10533-012-9795-z.

(13) Erisman, J. W.; van Grinsven, H.; Grizzetti, B.; Bouraoui, F.; Powlson, D.; Sutton, M. A.; Bleeker, A.; Reis, S. The European Nitrogen Problem in a Global Perspective. In *The European Nitrogen Assessment*; Sutton, M. A., Howard, C. M., Erisman, J. W., Billen, G., Bleeker, A., Grennfelt, P., van Grinsven, H., Grizzetti, B., Eds.; Cambridge University Press: Cambridge, 2011; pp 9–31. https://doi.org/10.1017/CBO9780511976988.005.

(14) Wu, S.; Zhou, C.; Doroodchi, E.; Nellore, R.; Moghtaderi, B. A Review on High-Temperature Thermochemical Energy Storage Based on Metal Oxides Redox Cycle. *Energy Convers. Manag.* **2018**, *168*, 421–453. https://doi.org/10.1016/j.enconman.2018.05.017.

(15) Platzer, C.; Christoph, B.; Tahir, A. J.; Buchmaier, J.; Klein, P.; Mayr, B.; Koschikowski, J.; Gampmayer, R. En-RecoTreat „Innovative Membrandestillation zur Wertstoff- und Energierückgewinnung in der kommunalen Abwasserbehandlung“. **2016**, 59.

(16) AEE - Institut für Nachhaltige Technologien (AEE INTEC). Entwicklung eines Langzeitspeichersystems durch die Technologiekombination CLC und „grünem“ Ammoniak mittels MembrandestillationEntwicklung eines Langzeitspeichersystems durch die Technologiekombination CLC und „grünem“ Ammoniak mittels Membrandestillation. September 1, 2017.

(17) Zerobin, F. Steam and Power Generation via Chemical Looping Combustion of Natural Gas. PhD thesis, University of Natural Resources and Life Sciences, Vienna, 2018.

(18) Lyon, R. K.; Cole, J. A. Unmixed Combustion: An Alternative to Fire. *Combust. Flame* **2000**, *121* (1), 249–261. https://doi.org/10.1016/S0010-2180(99)00136-4.

(19) Adanez, J.; Abad, A.; Garcia-Labiano, F.; Gayan, P.; de Diego, L. F. Progress in Chemical-Looping Combustion and Reforming Technologies. *Prog. Energy Combust. Sci.* **2012**, *38* (2), 215–282. https://doi.org/10.1016/j.pecs.2011.09.001.
(20) Abanades, J. C.; Arias, B.; Lyngfelt, A.; Mattisson, T.; Wiley, D. E.; Li, H.; Ho, M. T.; Mangano, E.; Brandani, S. Emerging CO2 Capture Systems. *Int. J. Greenh. Gas Control* **2015**, *40*, 126–166. https://doi.org/10.1016/j.ijggc.2015.04.018.
(21) Chen, C.; Bollas, G. M. Optimal Design of Combined Cycle Power Plants with Fixed-bed Chemical-looping Combustion Reactors. *AIChE J.* **2019**, *65* (7), e16516. https://doi.org/10.1002/aic.16516.
(22) Proell Tobias. Innovative Fuel Conversion with CO2 Capture Using Dual Fluidized Bed Systems. Habilitation, Technische Universität Wien, Wien, 2011.
(23) García-Labiano, F.; de Diego, L. F.; Adánez, J.; Abad, A.; Gayán, P. Reduction and Oxidation Kinetics of a Copper-Based Oxygen Carrier Prepared by Impregnation for Chemical-Looping Combustion. *Ind. Eng. Chem. Res.* **2004**, *43* (26), 8168–8177. https://doi.org/10.1021/ie0493311.
(24) Abad, A.; García-Labiano, F.; de Diego, L. F.; Gayán, P.; Adánez, J. Reduction Kinetics of Cu-, Ni-, and Fe-Based Oxygen Carriers Using Syngas (CO + H_2) for Chemical-Looping Combustion. *Energy Fuels* **2007**, *21* (4), 1843–1853. https://doi.org/10.1021/ef070025k.
(25) Hill, A. Development of Low Temperature Catalysts for an Integrated Ammonia PEM Fuel Cell. PHD, University of Bath, 2014.
(26) Ishida, M.; Zheng, D.; Akehata, T. Evaluation of a Chemical-Looping-Combustion Power-Generation System by Graphic Exergy Analysis. *Energy* **1987**, *12* (2), 147–154. https://doi.org/10.1016/0360-5442(87)90119-8.
(27) Mattisson, T.; Keller, M.; Linderholm, C.; Moldenhauer, P.; Rydén, M.; Leion, H.; Lyngfelt, A. Chemical-Looping Technologies Using Circulating Fluidized Bed Systems: Status of Development. *Fuel Process. Technol.* **2018**, *172*, 1–12. https://doi.org/10.1016/j.fuproc.2017.11.016.
(28) Nandy, A.; Loha, C.; Gu, S.; Sarkar, P.; Karmakar, M. K.; Chatterjee, P. K. Present Status and Overview of Chemical Looping Combustion Technology. *Renew. Sustain. Energy Rev.* **2016**, *59*, 597–619. https://doi.org/10.1016/j.rser.2016.01.003.
(29) Idziak, K.; Czakiert, T.; Krzywanski, J.; Zylka, A.; Kozlowska, M.; Nowak, W. Safety and Environmental Reasons for the Use of Ni-, Co-, Cu-, Mn- and Fe-Based Oxygen Carriers in CLC/CLOU Applications: An Overview. *Fuel* **2020**, *268*, 117245. https://doi.org/10.1016/j.fuel.2020.117245.
(30) Mattisson, T.; Lyngfelt, A.; Leion, H. Chemical-Looping with Oxygen Uncoupling for Combustion of Solid Fuels. *Int. J. Greenh. Gas Control* **2009**, *3* (1), 11–19. https://doi.org/10.1016/j.ijggc.2008.06.002.
(31) Tian, Q.; Che, L.; Ding, B.; Wang, Q.; Su, Q. Performance of a Cu-Fe-Based Oxygen Carrier Combined with a Ni-Based Oxygen Carrier in a Chemical-Looping Combustion Process Based on Fixed-Bed Reactors: Original Research Article: Performance of a Cu-Fe-Based Oxygen Carrier Combined with a Ni-Based Oxygen Carrier. *Greenh. Gases Sci. Technol.* **2018**, *8* (3), 542–556. https://doi.org/10.1002/ghg.1763.
(32) Noorman, S.; van Sint Annaland, M.; Kuipers. Packed Bed Reactor Technology for Chemical-Looping Combustion. *Ind. Eng. Chem. Res.* **2007**, *46* (12), 4212–4220. https://doi.org/10.1021/ie061178i.
(33) Liu, X.; Zhang, H.; Hong, H. Reduction Kinetics of Fe-Based Oxygen Carriers Using Syngas in a Honeycomb Fixed-Bed Reactor for Chemical-Looping Combustion. *J. Therm. Sci.* **2020**, *29* (1), 13–24. https://doi.org/10.1007/s11630-020-1255-9.
(34) Spallina, V.; Romano, M. C.; Chiesa, P.; Gallucci, F.; van Sint Annaland, M.; Lozza, G. Integration of Coal Gasification and Packed Bed CLC for High Efficiency and Near-Zero Emission Power Generation. *Int. J. Greenh. Gas Control* **2014**, *27*, 28–41. https://doi.org/10.1016/j.ijggc.2014.04.029.

(35) Gallucci, F.; Hamers, H. P.; van Zanten, M.; van Sint Annaland, M. Experimental Demonstration of Chemical-Looping Combustion of Syngas in Packed Bed Reactors with Ilmenite. *Chem. Eng. J.* **2015**, *274*, 156–168. https://doi.org/10.1016/j.cej.2015.03.081.
(36) Noorman, S.; van Sint Annaland, M.; Kuipers, J. A. M. Experimental Validation of Packed Bed Chemical-Looping Combustion. *Chem. Eng. Sci.* **2010**, *65* (1), 92–97. https://doi.org/10.1016/j.ces.2009.02.004.
(37) Hamers, H. P.; Gallucci, F.; Cobden, P. D.; Kimball, E.; van Sint Annaland, M. A Novel Reactor Configuration for Packed Bed Chemical-Looping Combustion of Syngas. *Int. J. Greenh. Gas Control* **2013**, *16*, 1–12. https://doi.org/10.1016/j.ijggc.2013.02.021.
(38) Lucio, M.; Ricardez-Sandoval, L. A. Dynamic Modelling and Optimal Control Strategies for Chemical-Looping Combustion in an Industrial-Scale Packed Bed Reactor. *Fuel* **2020**, *262*, 116544. https://doi.org/10.1016/j.fuel.2019.116544.
(39) Lyngfeld, A.; Anthony, B.; Fennell, P. *Calcium and Chemical Looping Technology for Power Generation and Carbon Dioxide (CO2) Capture*, 1.; Elsevier Science, 2015.
(40) Pröll, T. Fundamentals of Chemical Looping Combustion and Introduction to CLC Reactor Design. In *Calcium and Chemical Looping Technology for Power Generation and Carbon Dioxide (CO2) Capture*; Elsevier, 2015; pp 197–219. https://doi.org/10.1016/B978-0-85709-243-4.00010-0.
(41) Moldenhauer, P.; Rydén, M.; Lyngfelt, A. Testing of Minerals and Industrial By-Products as Oxygen Carriers for Chemical-Looping Combustion in a Circulating Fluidized-Bed 300W Laboratory Reactor. *Fuel* **2012**, *93*, 351–363. https://doi.org/10.1016/j.fuel.2011.11.009.
(42) Ishida, M.; Jin, H.; Okamoto, T. A Fundamental Study of a New Kind of Medium Material for Chemical-Looping Combustion. *Energy Fuels* **1996**, *10* (4), 958–963. https://doi.org/10.1021/ef950173n.
(43) Zhao, H.; Mei, D.; Ma, J.; Zheng, C. Comparison of Preparation Methods for Iron-Alumina Oxygen Carrier and Its Reduction Kinetics with Hydrogen in Chemical Looping Combustion: PREPARATION AND REDUCTION KINETICS OF Fe-Al OXYGEN CARRIER. *Asia-Pac. J. Chem. Eng.* **2014**, n/a-n/a. https://doi.org/10.1002/apj.1791.
(44) Fan, L.-S.; Li, F. Chemical Looping Technology and Its Fossil Energy Conversion Applications. *Ind. Eng. Chem. Res.* **2010**, *49* (21), 10200–10211. https://doi.org/10.1021/ie1005542.
(45) Ortiz, M.; Gallucci, F.; Snijkers, F.; Van Noyen, J.; Louradour, E.; Tournigant, D.; van Sint Annaland, M. Development and Testing of Ilmenite Granules for Packed Bed Chemical-Looping Combustion. *Chem. Eng. J.* **2014**, *245*, 228–240. https://doi.org/10.1016/j.cej.2014.02.030.
(46) Han, L.; Zhou, Z.; Bollas, G. M. Heterogeneous Modeling of Chemical-Looping Combustion. Part 1: Reactor Model. *Chem. Eng. Sci.* **2013**, *104*, 233–249. https://doi.org/10.1016/j.ces.2013.09.021.
(47) Cho, P.; Mattisson, T.; Lyngfelt, A. Comparison of Iron-, Nickel-, Copper- and Manganese-Based Oxygen Carriers for Chemical-Looping Combustion. *Fuel* **2004**, *83* (9), 1215–1225. https://doi.org/10.1016/j.fuel.2003.11.013.
(48) Encyclopædia Britannica. Copper https://www.britannica.com/science/copper (accessed Sep 1, 2020).
(49) Sedghkerdar, M. H.; Karami, D.; Mahinpey, N. Reduction and Oxidation Kinetics of Solid Fuel Chemical Looping Combustion over a Core-Shell Structured Nickel-Based Oxygen Carrier: Application of a Developed Grain Size Distribution Model. *Fuel* **2020**, *274*, 117838. https://doi.org/10.1016/j.fuel.2020.117838.
(50) Jerndal, E.; Mattisson, T.; Lyngfelt, A. Thermal Analysis of Chemical-Looping Combustion. *Carbon Capture Storage* **2006**, *84* (9), 795–806. https://doi.org/10.1205/cherd05020.
(51) de Diego, L. F.; Gayán, P.; García-Labiano, F.; Celaya, J.; Abad, A.; Adánez, J. Impregnated CuO/Al2O3 Oxygen Carriers for Chemical-Looping Combustion: Avoiding Fluidized Bed Agglomeration. *Energy Fuels* **2005**, *19* (5), 1850–1856. https://doi.org/10.1021/ef050052f.

(52) Valera-Medina, A.; Xiao, H.; Owen-Jones, M.; David, W. I. F.; Bowen, P. J. Ammonia for Power. *Prog. Energy Combust. Sci.* **2018**, *69*, 63–102. https://doi.org/10.1016/j.pecs.2018.07.001.
(53) Lan, R.; Irvine, J. T. S.; Tao, S. Ammonia and Related Chemicals as Potential Indirect Hydrogen Storage Materials. *Int. J. Hydrog. Energy* **2012**, *37* (2), 1482–1494. https://doi.org/10.1016/j.ijhydene.2011.10.004.
(54) *Hydrogen and Fuel Cell*; Töpler, J., Lehmann, J., Eds.; Springer Berlin Heidelberg: Berlin, Heidelberg, 2016. https://doi.org/10.1007/978-3-662-44972-1.
(55) Yoshitsugu, K. A Green Ammonia Economy https://nh3fuelassociation.org/wp-content/uploads/2013/10/nh3fcx-yoshitsugu-kojima.pdf (accessed Oct 10, 2020).
(56) Wang, W.; Herreros, J. M.; Tsolakis, A.; York, A. P. E. Ammonia as Hydrogen Carrier for Transportation; Investigation of the Ammonia Exhaust Gas Fuel Reforming. *Int. J. Hydrog. Energy* **2013**, *38* (23), 9907–9917. https://doi.org/10.1016/j.ijhydene.2013.05.144.
(57) Zamfirescu, C.; Dincer, I. Using Ammonia as a Sustainable Fuel. *J. Power Sources* **2008**, *185* (1), 459–465. https://doi.org/10.1016/j.jpowsour.2008.02.097.
(58) *Ammonia*; Appl, M., Ed.; Wiley-VCH Verlag GmbH: Weinheim, Germany, 1999. https://doi.org/10.1002/9783527613885.fmatter.
(59) Li, C.; Wang, T.; Gong, J. Alternative Strategies Toward Sustainable Ammonia Synthesis. *Trans. Tianjin Univ.* **2020**, *26* (2), 67–91. https://doi.org/10.1007/s12209-020-00243-x.
(60) Guo, J.; Chen, P. Catalyst: NH3 as an Energy Carrier. *Chem* **2017**, *3* (5), 709–712. https://doi.org/10.1016/j.chempr.2017.10.004.
(61) Chisalita, D.-A.; Petrescu, L.; Cormos, C.-C. Environmental Evaluation of European Ammonia Production Considering Various Hydrogen Supply Chains. *Renew. Sustain. Energy Rev.* **2020**, *130*, 109964. https://doi.org/10.1016/j.rser.2020.109964.
(62) Fernández-Nava, Y.; Marañón, E.; Soons, J.; Castrillón, L. Denitrification of High Nitrate Concentration Wastewater Using Alternative Carbon Sources. *J. Hazard. Mater.* **2010**, *173* (1–3), 682–688. https://doi.org/10.1016/j.jhazmat.2009.08.140.
(63) Baltrusaitis, J. Sustainable Ammonia Production. *ACS Sustain. Chem. Eng.* **2017**, *5* (11), 9527–9527. https://doi.org/10.1021/acssuschemeng.7b03719.
(64) Deublein, D.; Steinhauser, A. *Biogas from Waste and Renewable Resources*; Wiley-VCH Verlag GmbH & Co. KGaA: Weinheim, Germany, 2008. https://doi.org/10.1002/9783527621705.
(65) Gandiglio, M.; Lanzini, A.; Soto, A.; Leone, P.; Santarelli, M. Enhancing the Energy Efficiency of Wastewater Treatment Plants through Co-Digestion and Fuel Cell Systems. *Front. Environ. Sci.* **2017**, *5*, 70. https://doi.org/10.3389/fenvs.2017.00070.
(66) DLG-Ausschuss für Ackerbau; DLG-Ausschuss für Pflanzenernährung; Dr.Lorenz, F.; Dr.Baumgärtel, G. *Gärreste Im Ackerbau Effizient Nutzen*; DLG Fachzentrum Landwirtschaft, 2017; p 24.
(67) Lawson, K. W.; Lloyd, D. R. Membrane Distillation. *Univ. Tex.* **1996**, No. 124 (1997), 1–25.
(68) Rasmuson, A.; Andersson, B.; Olsson, L.; Andersson, R. *Mathematical Modeling in Chemical Engineering*; Cambridge University Press: Cambridge, 2014. https://doi.org/10.1017/CBO9781107279124.
(69) Sanford Gordon and Bonnie J. McBride. Computer Program for Calculation of Complex Chemical Equilibrium Compositions, Rocket Performance, Incident and R Efleaed Shocks, and Chapman-Jouguet Detonations. NASA Lewis Research Center March 1976.
(70) Gordon, S.; Mc.Bride, B. J. Computer Program for Calculation of Complex Chemical Equilibrium Compositions and Applications. Nasa October 1994.
(71) Poirier, D. R.; Geiger, G. H. Fick's Law and Diffusivity of Materials. In *Transport Phenomena in Materials Processing*; Poirier, D. R., Geiger, G. H., Eds.; Springer International Publishing: Cham, 2016; pp 419–461. https://doi.org/10.1007/978-3-319-48090-9_12.
(72) Pröll, T. Applied Modelling in Process Engineering and Energy Technology, Lecture Notes, TU Vienna, 2016.

(73) Kemmetmüller, S.; Kugi, A. *Modellbildung - SS 2018*; Vorlesung und Übung; Vienna University of Technology: Vienna, 2018; p 263.
(74) Zerobin, F. Evaluation of a CuO/Al2O3 oxygencarrier for Chemical Looping Combustion. Masterthesis, Vienna University of Technology, 2013.

Ich erkläre eidesstattlich, dass ich die Arbeit selbständig angefertigt habe. Es wurden keine anderen als die angegebenen Hilfsmittel benutzt. Die aus fremden Quellen direkt oder indirekt übernommenen Formulierungen und Gedanken sind als solche kenntlich gemacht. Diese schriftliche Arbeit wurde noch an keiner Stelle vorgelegt.

Datum: Unterschrift:

_____ _____